Inaugural - Dissertation

zur
Erlangung der Doktorwürde
der
Naturwissenschaftlich-Mathematischen
Gesamtfakultät
der
Ruprecht-Karls-Universität
Heidelberg

vorgelegt von
Diplom-Mathematikerin Susanne Krömker
aus Osnabrück

Tag der mündlichen Prüfung: 18.12.1997

Model and Analysis of Heterogeneous Catalysis with Phase Transition

Gutachter: Prof. Dr. Dr. h.c. Willi Jäger
Prof. Dr. Georg Bock

Contents

1 Introduction

The present work is motivated by observations of spatio-temporal patterns, mainly in chemistry, but also in biology. Most of these patterns are far from being chaotic; instead they have a complex periodicity in space and time.

In the experiments chemical reaction fronts can be observed in situ as they propagate across a catalytically active metal surface. Spirals, traveling waves and standing waves are formed by the adsorbed reactants.
A mathematical model for such a reaction has to take into account as well the complex kinetic processes and the spatial coupling.
Since catalytic reactions at low pressure are considered to be isothermal, the temperature is a free parameter of the experiment. As well the partial pressures of the reactants can be regulated. But the various kinetic parameters are often not identical with those accessible by experiment. Some of them are known precisely from the literature, others are hardly measureable and vary by orders.
In a mathematical model the parameters can be varied continuously within these ranges, paying attention to their functional dependence on the free parameters of the experiment.

Heterogeneous Catalysis means that the reacting species and the catalyst do not have the same phase such that the e.g. gas phase reactants first have to be adsorbed at the catalyst surface and then react to the desired product. Depending on how strong the reactants are bound to the surface of the catalyst, the diffusion coefficients for the various species may differ by orders.
It is a known fact that diffusion not only smoothens the concentration gradients which are given by the initial data or result from the reaction kinetic processes. Diffusion is also able to induce instabilities which give rise to stable inhomogeneous steady or time-periodic solutions.
The conditions for such a bifurcation are rather restrictive but can be checked by only considering the kinetic part. This yields a method for finding critical parameters of the reaction-diffusion system. Numerical simulations which are carried out in the neighborhood of these critical parameters develop the same phenomena as observed in the experiment.

1.1 Survey of the Content

This work concentrates on reaction-diffusion models which consist of two and three differential equations modeling concentrations of the reactants and the catalytic activity of the surface.
In order to explain spatio-temporal structures and the process of self-organization a spatial operator such as the Laplacian describes the mobility, or surface diffusion, of a single species. The kinetic behavior is modeled with ordinary differential equations having polynomial nonlinearities up to third order.

The question is how to distinguish the reaction-diffusion system from a system without spatial coupling where the processes at each place are independent from each other. To answer this question the kinetic parameters are chosen in a range where any temporal periodicity can be excluded. These parameter ranges are found with standard methods for systems of ordinary differential equations, such as bifurcation theory, singular perturbation, unfolding of singularities, asymptotic analysis of planar and nonautonomous systems.

The detailed modeling of a heterogeneous surface reaction and the possibilities of simplification are given in CHAPTER 2.
The oscillations observed in the reaction rate are ascribed to a *phase transition* of the catalytically active platinum surface, known as *reconstruction* of the surface.
Slightly different models are proposed mainly for low-index platinum surfaces.
The result of a comparison of the different models is that the crucial nonlinearity is posed by the quadratic order of one of the elementary reaction processes. The cubic order of another process does not play an important role.
This work proposes to model the *hysteresis* in the phase transition. The advantage is a parametrical dependency controling the strength of the hysteresis, which differs a lot between the various surfaces. With this slight change in the model, it is possible to handle the Pt(100) case as well as the Pt(110) case within the same model. It may therefore serve for a combined surface of polycrystalline platinum foils which are dominated by patches of these two well defined surface structures.

The kinetic parts of these models are analyzed in CHAPTER 3 with the methods of singular perturbation and unfolding of the singularities.
It is known from the experiment that the adsorbed concentrations of the reactants, i.e. oxygen and carbon monoxide, are strictly anticorrelated. Asymptotic analysis reduces the number of equations and yields a system of two variables, one is the adsorbed carbon monoxide and the other is the catalytic activity of the surface. Qualitative changes of the dynamics can be traced out with functions of the parameters. This was done in order to control the kinetic part before turning the system into a partial differential system and solving the initial value problem by numerical methods.

CHAPTER 4 shows the results of numerical investigations for the reaction-diffusion system in one and two spatial dimensions. Spatio-temporally periodic structures need both a nonlinear phenomenon that accounts for sustained oscillations and a mechanism that synchronizes the oscillators which are thought of as being spread at random all over the domain. The spatio-temporal attractors are obtained for a system which stems from the previous model and is mainly a single reaction-diffusion equation coupled with an ordinary differential equation.
The initial value problem of the reaction-diffusion system is solved for Neumann boundary values on one- and two-dimensional grids with numerical methods for straightforward but time-implicit integration. Particularly for two-dimensional computations the data leads to animation sequences of spatio-temporal patterns which are in good agreement with the observed phenomena in diverse experiments. In these numerical experiments several

initial values are tested; they vary from simple cross gradient profiles to randomly chosen values about the critical constant solutions. In either case the self-organization leads to qualitatively similar solutions.

Although this setting of the problem already reveals a great variety of spatio-temporal solutions, it is not possible to bifurcate such an attractor from an asymptotically stable constant equilibrium.

CHAPTER 5 investigates whether it is possible to use a single diffusion coefficient as bifurcation parameter for a space-dependent supercritical Hopf bifurcation, the so called *wave bifurcation*.
This diffusion-induced bifurcation to spatio-temporal solutions which are periodic in space and time can be decided by a change in sign of the highest but one Hurwitz determinant. A third differential equation is required. The kinetic part of the three equations has to fulfill a number of conditions in order to destabilize the constant equilibrium by introducing a diffusion term with a large diffusion coefficient in a single equation. This is formulated in detail in THEOREM 5.5 for a system of a single reaction-diffusion equation coupled with two ordinary differential equations.
In the commonly known Turing bifurcation the constant solution is destabilized to a steady but nonconstant one. The rule in the case of *activator-inhibitor* systems, i.e. the inhibitor has to diffuse faster, has an analogon in the case of the wave bifurcation. For a bifurcating spatio-temporally periodic solution it is necessary (but not sufficient) that the purely kinetic subsystem, i.e. the part of the system that does not contain a diffusion operator, is *stabilizing*. Thereby the bifurcation to either a steady nonconstant solution or a standing wave exclude each other (see REMARK 5.5).
For systems of any size the number of conditions which have to be fulfilled for a wave bifurcation increases in a way that a formulation of conditions is not convenient anymore. The restriction on a single reaction-diffusion equation coupled with at least two ordinary differential equations gives exactly six conditions which solely concern the kinetic part.

The conditions on the kinetic system imposed in CHAPTER 5 can be used to construct dynamical systems of a form that will exhibit a certain observed behavior like standing waves. Examples for the wave bifurcation are given in CHAPTER 6 where heterogeneous autocatalytic models are constructed.
The surface reconstruction mechanism which is described in detail in CHAPTER 2 has an autocatalytic effect on the adsorption process, and it is possible to build a model which bifurcates in a constant solution to a standing wave solution. The diffusion coefficient serves as bifurcation parameter.
Furthermore the suggested models can be tested for their capability of revealing such solutions. This was successful for an autocatalytic model recently suggested by ZHABOTINSKY et al. [46]. The nonlinear coupling is ascribed to the autocatalytic effect of a reactant and is responsible for boundedness of the solution.
The periodic attractors were first known from biological applications. In chemistry they were introduced much later by Belousov and Zhabotinsky. Therefore it is quite natural to look for biological systems exhibiting a similar behavior. This is done in CHAPTER 7

where the developed method of CHAPTER 5 is applied to a model for microbial growth. It shows that this modified *Monod model* reveals sustained oscillations in the presence of mobility for cells with a low-consuming metabolism. These periodic solutions can be excluded for each parameter constellation of the spatially not coupled chemostat system.

To improve the text in readability, the theorems which are only citations are put into APPENDIX A. Related systems to the topic are listed in APPENDIX B, and a summary of notations can be found in APPENDIX C.

1.2 Computational Tools

To perform the algebraic transformations of the semi-phenomenological models introduced by the experimentalists the computer algebra program *Maple V* is used. By these transformations the simpler models are related directly to the free parameters of the experiments, e.g. partial pressures of reactants and temperature.
The computer algebra program is also used to solve the stationary problem, since in contrast to iterative methods, for instance a Newton method, it uses Gröbner bases for the description of the solution manifold and is able to find multiple zeros. For small systems which have a lot of parameters it is the appropriate method of finding all existing equilibria simultaneously with their dependency on the specific parameters.

For the initial value problem, the discretized system of ordinary differential equations is solved with the LSODE package (see HINDMARSH [23]), using numerical estimates of the Jacobian matrix. This program offers an implicit method for time discretization, originally developed for stiff problems of ordinary differential equations. As maximal step size a time step of $t = 0.01$ is used. The error tolerances are 1×10^{-8} relative and 1×10^{-12} absolute. The spatial discretization then is adjusted according to the relative size of the spatial parameters.
For spatio-temporal solutions the reacting fronts propagate across the whole domain and there is no need for adaptive grid refinement. Using an equidistant cartesian grid suits the problem and no further efforts are made to improve the simple discretization scheme.

The graphics are realized with the program *cnom2.0* especially developed for animation sequences of systems of differential equations (see KRÖMKER [32]). Although nowadays there exists a variety of such programs for various hardware platforms this was not so at the time this investigation started.

2 Catalytic Reactions on Metal Surfaces

2.1 Heterogeneous Catalytic Reactions

The prototype of kinetic oscillations in chemistry is the Belousov-Zhapotinsky reaction, resulting in the widely studied Field-Noyes equations (see EXAMPLE B.3). Since it is a homogeneous catalytic reaction taking place in the liquid phase, it can be modeled under stirring conditions. This is not possible in the case of heterogeneous catalysis, the form of catalysis in which the catalyst and the reaction mixture have different phases. Since most catalytic reactions are heterogeneous as, for example, fluid and gas phase reactions on metal surfaces, they are of great importance.

The kinetic process of heterogeneous catalysis comprises the adsorption of the reactants, the reaction and desorption. Apart from the reactants, the amount of free adsorption sites on the surface and the phase transitions have to be modeled. In many cases an oscillatory behavior of the concentrations (coverages) on the surface is observed. What emerges are interesting spatio-temporal patterns such as traveling reaction fronts, standing waves, target patterns, spiral waves or turbulent patterns.

To improve the understanding of the effects of transport towards the surface, the dynamics of the reaction process at the surface, and the desorption of the product, basic studies of small reaction systems are necessary. One of the best understood mechanisms is the oxidation of carbon monoxide on platinum, which is last not least due to the fundamental investigations of Ertl and his group at the *Fritz-Haber Institut der Max-Planck-Gesellschaft, Berlin*.

In this chapter the present models are introduced and first attempts are made to improve the setting. The catalytically active surface with the adsorbed coverages of reacting species has to be understood as a reaction-diffusion system of at least two or three equations. The difficulty lies in understanding the effect of parameters responsible for a change of the dynamical behavior. A more detailed analysis is carried out in CHAPTER 3.
These equations may serve as boundary conditions for a future model which takes into account a more detailed interaction of the gas phase with the surfaces species.

2.2 Oxidation of Carbon Monoxide on Platinum

The catalytic oxidation of CO on a platinum single crystal surface may serve as an example for a catalytic surface reaction. It is well established that this reaction proceeds via a Langmuir-Hinshelwood mechanism where $*$ denotes a free adsorption site and has different meaning for the two adsorbates.

$$\begin{aligned} CO + * &\rightleftharpoons CO_{ad} \\ O_2 + * &\rightarrow 2\, O_{ad} \\ O_{ad} + CO_{ad} &\rightarrow CO_2 + 2* \end{aligned}$$

On palladium surfaces, this reaction also takes place, and it shows oscillatory character as well, but for different regimes of partial pressure and, as shown experimentally, with different mechanisms. Whereas the Pt surfaces reconstruct their topmost atomic layer, Pd does not show a reconstruction but tends to build oxids and incorporates atomic oxygen in deeper atomic layers.

2.2.1 Experimental Tools

The work function $\Delta\phi$ of a metal is defined as the energy difference between the Fermi level and the vacuum level. It is changed upon adsorption by the nonzero dipole moment of each adsorbate complex. Adsorbed oxygen has a much higher dipole moment than adsorbed CO and the changes in work function mainly reflect changes in the oxygen coverage. Since up to now spatio-temporal oscillations have only been observed at low pressure, this ensures strictly isothermal conditions. The experiment takes place in a gradient-free flow reactor. That means that the partial pressure of each reactant is kept constant, including counterregulation of oscillations in the partial pressure of CO of about 1%. Regions of oscillation are found by fixing the temperature and the partial pressure for oxygen and then gradually increasing the partial pressure for CO. The work function $\Delta\phi$ is proportional to the oxygen coverage. It parallels the reaction rate since adsorption of oxygen is rate limiting. A sharp decrease of the work function indicates the transition from an oxygen-covered to a CO-covered surface. In this parameter range spontaneous oscillations can be observed.

Spatially resolving experimental tools used on or especially developed for heterogeneous catalytic processes are briefly listed here.

LEED (Low Energy Electron Diffraction) was first used to reveal the lattice of the surface. In a scanning LEED technique the beam typically has a diameter of $\sim$0.5mm and scans the sample so that the traveling reaction fronts are resolved.

The PEEM (Photo Electron Emission Microscopy, developed by Engel et al. [12]) is a more direct and spatially better resolving tool. It uses the dipole moment of the adsorbed species, has a spatial resolution of $\sim 0.2\mu$m and a temporal resolution of 20ms. Adsorbed oxygen appears dark in these pictures, CO is lighter grey and the free surface nearly white. Subsurface oxygen appears extremely light due to the fact that it reverses the dipole of the above layer. The whole sample has a typical size of 0.5cm^2 rectangular surface area and a thickness of about one millimeter. A visual field of 600μm can be viewed in situ and recorded on a video tape in order to digitize the data with a frame grabber for further analysis. Examples of PEEM images are shown in Figures 2.1, 2.2 and 2.10 to 2.12.

Both LEED and PEEM techniques can only be used in a UHV-chamber restricting the experiment to regimes of partial pressure less than 10^{-4}mbar.

Via the work function measurement the overall reaction rate oscillations can be detected

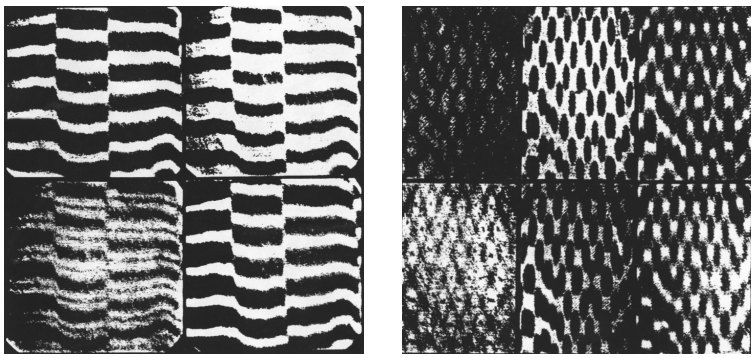

FIG. 2.1: Left: Standing-wave-type patterns on a $0.3\times0.3\,\mathrm{mm}^2$ surface area accompanying rapid harmonic temporal oscillations with a period duration of $\tau=1.4$s. $T=550$K, $p_{\mathrm{CO}}=1.75\times10^{-4}$mbar and $p_{\mathrm{O}_2}=4.1\times10^{-4}$mbar, $t=0$, 0.08, 0.12, and 0.46s (after [26]). Right: Standing-wave patterns on a $0.2\times0.3\,\mathrm{mm}^2$ surface area associated with regular temporal oscillations with a period duration of $\tau=2.8$s. $T=544$K, $p_{\mathrm{CO}}=1.2\times10^{-4}$mbar and $p_{\mathrm{O}_2}=3.1\times10^{-4}$mbar, $t=0$, 0.6, 0.8, 1.4, 2.0, and 2.2s (after [26]).

for even higher pressures. At the moment new experimental tools [1] are being developed to close the so-called pressure gap between UHV and atmospheric conditions.

2.3 Modeling the Kinetic Process at the Surface

Throughout this work and according to all citations on the matter, u stands for adsorbed $\mathrm{CO}_{\mathrm{ad}}$ concentration and v stands for adsorbed oxygen.

Adsorption of CO is assumed to depend linearly on the partial pressure of carbon monoxide p_{CO}. It is only weakly affected by the presence of adsorbed oxygen. Its coefficient is modeled with a function $f_{\mathrm{ad}}(\mathrm{CO})$ depending on the adsorption rate known from kinetic gas theory, the sticking coefficient, that is the probability of CO to get adsorbed at the place where it first hits the surface, and a precursor effect modeling the effectively available surface sites for adsorption.
The coefficients for the desorption k_d and the recombination k_r are temperature dependent and can be modeled with Arrhenius kinetic $k_i=k_i^0 e^{-E_{a_i}/RT}$.

$$\dot{u} = f_{\mathrm{ad}}(\mathrm{CO})p_{\mathrm{CO}} - k_d u - k_r uv$$

O_2 adsorption is a dissociative chemisorption process and needs a fairly large ensemble of neighboring unoccupied surface atoms, which means that adsorbed CO acts as an inhibitor for this process. On the other hand the oxygen coverage does not inhibit CO adsorption, and this phenomenon is called *asymmetric inhibition* of adsorption.

[1] EMSI (Ellipso-Microscopy for Surface Imaging) for example is pressure independent and is used in combination with RAM since both techniques work with different angles of observation so that the effects of these angles can be computed and kept out of the result [43].

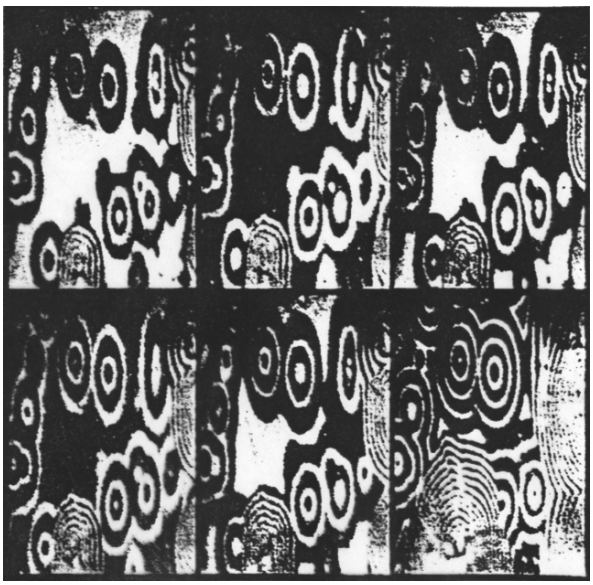

FIG. 2.2: Sequence of target patterns on a $0.2 \times 0.3\,\mathrm{mm}^2$ section of the Pt(110) surface at $T = 427\,\mathrm{K}$, $p_{\mathrm{CO}} = 3 \times 10^{-5}\,\mathrm{mbar}$ and $p_{\mathrm{O}_2} = 3.2 \times 10^{-4}\,\mathrm{mbar}$. The time interval between the first five images is 4.1s; the time interval between the last two images is 30s (after [26]).

The quadratic dependency of oxygen adsorption on the amount of free surface sites is due to the fact that the elementary reaction with the surface is of second order. So the adsorption coefficient is a function $f_{\mathrm{ad}}(\mathrm{O})$ of the adsorption rate, the sticking probability and a quadratic term modeling the amount of available surface sites. The latter is the main difference to the adsorption process of carbon monoxide.

Desorption of O may be neglected since its coefficient for the requested temperature is orders smaller than the other parameters.

$$\dot{v} = f_{\mathrm{ad}}(\mathrm{O}) p_{\mathrm{O}_2} - k_r u v$$

When modeling the system with two equations for each reactant species, only bistability but no oscillations occur. This can be explained by the strict anticorrelation of both quantities as is done in [7] (see also the survey by ERTL [14]).

The reconstruction model for low pressure on platinum foils serves as an explanation for the observed oscillations. Recently subsurface oxygen was suggested as a source for oscillatory behavior in the case of palladium and platinum at higher pressures, too.

2.3.1 Reconstruction of the Surface

A reconstruction of the topmost layer of metal atoms has been found to be responsible for the dynamic process on platinum at low pressure. Variations in the overall reaction rate are due to periodic structural changes in the surface which modify the catalytic

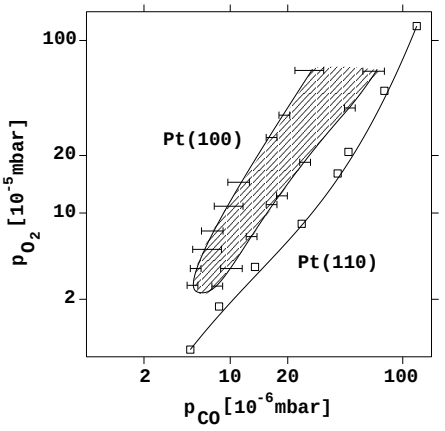

FIG. 2.3: Existence diagram for the occurence of kinetic oscillations on Pt(100) and Pt(110) at a fixed temperature of $T = 480$K. The narrow existence region for oscillations on Pt(110) is represented by a single line (after [13]).

activity. This can be explained as follows: The crystal structure of platinum is a cubic face centered lattice in the bulk. If a single crystal is cut in a way to yield a Pt(111) surface, the Miller indices indicate that the bulk-like lattice is represented at the surface by a quasi-hexagonal structure. This surface is already at its minimum free energy. No reconstruction takes place in this case.

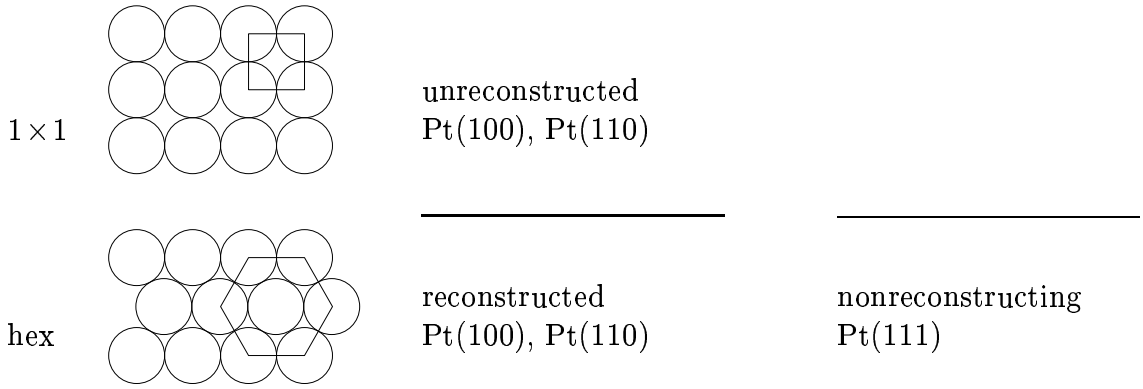

FIG. 2.4: Schematic 1×1 and hexagonal surface structure for low-index planes of Pt. In the absence of adsorbates, the hex structure has minimal free surface energy. Pt(111) does not reconstruct, since it already has a hexagonal surface.

In contrast to this situation, Pt(100) and Pt(110) undergo a reconstruction. Their bulk-like termination results in a 1×1 structure which is not stable and reconstructs to a

quasi-hexagonal structure (simply denoted as "hex"). This is because of the absence of any outer forces from one side of the surface. Apparently the reconstructed surface represents a state of minimum free energy lower than the bulk-like 1×1 surface. In FIGURE 2.4 the two phases are assigned to the low-index Pt surfaces.

The reconstruction is lifted in the presence of an adequate adsorbate. The adsorption energy is added to the surface free energy, causing a switching of the stability of the two phases, since the adsorption energy on the unreconstructed phase is substantially higher than on the hex phase.

In the Pt(100) case, CO can be adsorbed on either surface structure, but oxygen adsorption is almost impossible on the reconstructed phase. On Pt(110) this is not as drastic, but in either case the CO coverage can be regarded as a pace-maker for the reaction. At first glance this contrasts with the observation that adsorbed CO forms dense adlayers and thereby inhibits the adsorption of oxygen. Large CO coverage will always be associated with a low reaction rate. But this putative contradiction can be explained with the bistability of the system: There is another branch of stable solutions for small CO coverage with a high reaction rate. Oscillations are detected inbetween these branches.

The dependency on the phase transition is mostly apparent in the sticking coefficient for oxygen. It differs for the two phases and is substantially higher on the part of the surface where the reconstruction is lifted.

The adsorbed CO molecules have a measurable mobility. This accounts for a more complicated than a linear dependency on the free surface sites in the adsorption term of carbon monoxide, known as precursor effect. The surface diffusion occurs again as a separate term, and in this strictly isothermal model it is responsible for spatial self-organization. In contrast oxygen has a higher activation energy for the adsorption process. Hence, it is strongly bound to the place on the surface where it first hits. Surface diffusion for oxygen can be neglected for the temperatures in consideration.

The reaction of CO_{ad} and atomic O_{ad} is comparably fast and carbon dioxide immediately leaves the surface. If the adsorbate coverage falls below a certain threshold, the metal surface again reconstructs to the hex phase.

The reconstruction mechanism is also relevant for polycrystalline platinum as used in technical applications. The polycrystalline surface is composed of patches of low-index planes of Pt on a thin platinum foil or on some inert substrate. Contrary to a former opinion, Pt(111) patches only occupy about $\sim10\%$ of the surface area, while the rest is occupied by $\sim50\%$ of Pt(110) and $\sim40\%$ of Pt(100).

FIGURE 2.3 shows the oscillatory regions in a diagram of p_{CO} versus temperature for both Pt(100) and Pt(110). Oscillations on Pt(100) are very irregular, showing up in a smeared range of 10^{-5} to 10^{-4}mbar and 400 – 550K at a fixed partial pressure for oxygen (always about an order of magnitude higher) with periods of one to several minutes. In contrast the oscillatory region of Pt(110) is a sharp line and oscillations are very regular. Periods range from about one second to one hour. Fast oscillations with a medium amplitude

occur for $T > 530$K, slow oscillations with a period > 1min and large amplitudes occur for $T < 490$K. These large oscillations are often superimposed by fast small amplitude ones. The experimental observations with PEEM also reveal a much greater variety of spatio-temporal patterns in the Pt(110) case (see the diagrams and figures in [40]).

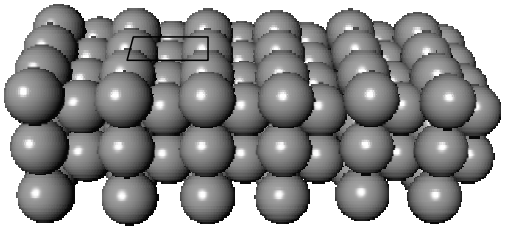

FIG. 2.5: Ball model of unreconstructed Pt(110) surface. The square on top indicates the 1×1 structure. It looks similar to the Pt(100) unreconstructed surface but has bigger spaces between the atomic centers.

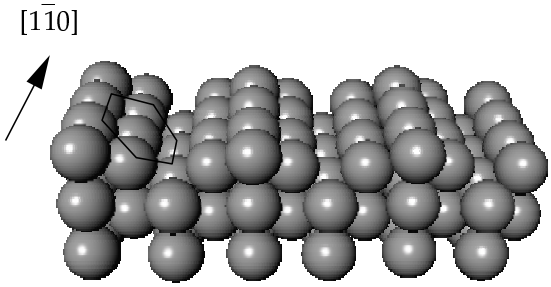

FIG. 2.6: Pt(110) reconstructs to a 1×2-surface which has a missing row structure. Its quasi-hexagonal surface is found at the flanks of the rows in the [1$\bar{1}$0] direction as marked with the hexagon.

The sticking coefficient for oxygen on Pt(100) is substantially higher on the 1×1 phase, where it is about 0.1, than on the hex phase, where it is about $10^{-4}-10^{-3}$. Adsorption of oxygen on the hex phase - and therefore the equation for a O_{ad} species on this phase - is neglectable.
This is not true for Pt(110), where the sticking coefficient is about 0.6 on the 1×1 phase, and about $0.3-0.4$ on the 1×2 or so-called missing row phase (see FIGURE 2.6).

It should be mentioned that experimental conditions are favorable for faceting, a process which is possible on Pt(110) surfaces and is initiated by the periodic structural transformation (see [40]). The effect of faceting is that it facilitates the donation of metal electrons into the antibinding $2\pi^*$-orbital of the O_2 molecule, causing a shift to a higher reaction rate, that is, a higher catalytic activity of the surface. In KRISCHER et al. [30] mixed mode oscillations are explained with faceting, but the qualitative aspect of oscillatory behavior itself is not linked with this phenomenon. Therefore it will not be taken into account here.

2.3.1.1 The Pt(100) Model

The first mathematical model describing the process on Pt(100) was published by IMBIHL et al. [24] in 1985 and is given here in a way slightly corrected by the author [25]. The indices a and b indicate the 1×1 and hex phase of the surface respectively, dealing with different species whether the reactants are bound on one or the other fraction of the surface. A higher desorption coefficient on the hex phase accounts for the weaker bonds of CO_{ad} on this phase. A parameter k_3 introduces the trapping, that is an increase of u_a

which is proportional to the amount of u_b and the fraction of 1×1 phase a, and is due to the higher adsorption energy on this phase.

There is no equation for v_b in the model, reflecting a sticking probability of almost zero for oxygen on the hex phase. Therefore reaction takes place with only the reactant bound on a, the fraction of the surface area present as 1×1 phase (the fraction of hex phase then being $b=1-a$). The switching of phases is modeled as a piecewise linear function which can be seen easily when replacing the condition $c<1$ by $c' := u_a/U_{\min} + v_a/V_{\min} < a$; then the term $-k_8 a(1-c)$ simplifies to $-k_8(a-c')$ and this term is negative for a positive parameter k_8.

$$
\begin{aligned}
\dot{u}_a &= k_1 p_{\mathrm{CO}} a - k_2 u_a + k_3 a u_b - k_4 u_a v_a / a \\
\dot{u}_b &= k_1 p_{\mathrm{CO}} (1-a) - k_6 u_b - k_3 a u_b \\
\dot{v}_a &= k_7 a p_{\mathrm{O}_2} \left\{ [1 - 2u_a/a - 5v_a/3a]^2 + \gamma\,[1 - 5v_a/3a]^2 \right\} - k_4 u_a v_a / a
\end{aligned}
$$

$$
\dot{a} = \begin{cases}
\dfrac{\dot{u}_a}{U_{\max}} & \text{for} \quad \dot{u}_a > 0 \quad \text{and} \quad \dfrac{u_a}{a U_{\max}} > 1 \\
-k_8 a (1-c) & \text{for} \quad c := \dfrac{u_a}{a U_{\min}} + \dfrac{v_a}{a V_{\min}} < 1 \\
0 & \text{otherwise}
\end{cases}
$$

The same paper reports on the measured and calculated hysteresis in the adsorption of CO in a heating/cooling cycle monitoring the hysteresis of hex reconstruction, too. The latter can be ascribed to the existence of nucleation barriers in the formation of the new phase.

Discussion

The term $\gamma[1-5v_a/3a]^2$ takes into account the existence of defects in the CO adlayer which are needed so that oxygen adsorption is not blocked. Without this term no oscillations were obtained in the simulations. The prefactor γ, however, cannot be determined experimentally and is only fitted in to gain the experimentally observed results with the above model.

Division by a yields abnormal singularities especially when introducing a surface diffusion term for CO in the first equation; in [24] this term has the form $k_5 \Delta u_a / a$.

In computer simulations the waves always have to be triggered from that side of the spatial domain which is given the higher values for sticking coefficients and defects. This is another reason to scrap this rather complicated model or at least simplify it to a model which also reproduces the qualitative features.

Explanation	Parameter	Value at 480 K
CO Adsorption	k_1	2.205×10^5 MLs^{-1}mbar^{-1}
CO Desorption$_{1\times1}$	k_2	9×10^{-3} s^{-1}
CO Trapping	k_3	1.5 s^{-1}
Reaction	k_4	$10^3 - 10^5$ MLs^{-1}
CO Diffusion$_{1\times1}$	k_5	$10^{-5} - 10^{-3}$ cm^{2}s^{-1}
CO Desorption$_{hex}$	k_6	11 s^{-1}
O_2 Adsorption$_{1\times1}$	k_7	3.75×10^5 MLs^{-1}mbar^{-1}
Phase transition	k_8	$0.4 - 2.0$ s^{-1}
Crit. CO_{ad} coverage	$U_{\min}$	0.32
Crit. O_{ad} coverage	$V_{\min}$	0.4
Growing condition	$U_{\max}$	0.5 ± 0.1

Tab. 2.1: Kinetic parameters for the Pt(100) model as reported in [24]. ML stands for monolayer since the adsorbate concentration is thought of as a single layer of molecules.

A Simplification of the Model

Here is a first heuristic simplification of the model:

$$\begin{aligned} \dot{u} &= \rho(1-u-v) - \lambda' uv \\ \dot{v} &= \sigma' a(1-u-v)^2 - \lambda' uv \\ \dot{a} &= \begin{cases} \kappa'(1-a) & \text{if} \quad c \geq 1 \\ -\kappa' a & \text{if} \quad c < 1 \end{cases} \end{aligned}$$

The adsorption of carbon monoxide depends linearly on the amount of free surface sites $(1-u-v)$ whereas oxygen adsorption takes place only on the unreconstructed phase and its main feature is the quadratic dependency on the amount of free surface sites.
The catalytic activity depends on a critical coverage $c = (u+v)/0.4$. Above c the activity is growing, below it is shrinking. Assuming a correlation to the fraction of 1×1 phase a, this quantity is modeled as a linear differential equation which switches at c from a positive to a negative coefficient of the linear term in a. The phase transition is almost decoupled from the quantities u and v.

As far as the locations of fixed points are concerned, this sketch has a reflection symmetry at a plane where u equals v, but the flow itself has no such symmetry. This can be seen easily when computing the linear stability behavior of these fixed points.
The experimentally observed asymmetric inhibition in the adsorption processes, namely that preadsorbed CO blocks oxygen adsorption but not vice versa, is an outcome of the dynamical behavior of the model. It has a locally stable CO-covered state, whereas the oxygen-covered state is unstable, comparable to the observations in experiments. There is another almost oxygen-covered state that also appears locally stable, but it does not

block the reaction since the CO coverage does not vanish completely. Hence, it is not a physically implausible "adsorbing state".

An improvement of this model is achieved by changing the switch from a piecewise linear but discontinuous function to a continuous one. The discontinuity of height κ' is smoothened with a monotone function depending on u and v in an ε-neighborhood of $c=1$. There are at most four (symmetric) fixed points located in this neighborhood which are now accessible to bifurcation theory.

A detailed bifurcation analysis is done in KRÖMKER [31]. For a brief discussion of this model see also SECTION 3.1.

2.3.1.2 The Pt(110) Model

The model developed by KRISCHER [29], too, is an ordinary differential system that is derived from a system for reactant coverages showing bistability.

$$\begin{aligned} \dot{u} &= k_u p_{\mathrm{CO}} s_u (1-(u/u_s)^q) - k_d u - k_r uv &&= f_1(u,v) \\ \dot{v} &= k_v p_{\mathrm{O}_2} (s_{v_1} w + s_{v_2}(1-w))(1-(u/u_s)-(v/v_s))^2 - k_r uv &&= f_2(u,v) \end{aligned}$$

The adsorption of CO is modeled as a product of the adsorption rate k_u, the partial pressure of CO (a free parameter in the experiment), the sticking probability s_u, and the total amount of available surface sites. The latter is modeled with a precursor effect, described after GASSER and SMITH [18], where u_s is the saturation coverage. The mobility parameter q in the precursor kinetic is reported to be $q=3\pm0.5$. Most authors agree in a sticking probability and a saturation coverage equal to unity (measured in monolayers ML). The coefficients for desorption and reaction are modeled with Arrhenius kinetic (see TABLE 2.2).

A first step towards understanding local behavior of dynamical systems can be made by analyzing the shape of null clines. A null cline is the zero set of a single equation. In planar systems, these null clines are simply curves, and the intersections of the curves for both equations are the fixed points of the system.

Multiple solutions as in the case of bistability typically arise from an s-shaped null cline. However, the cubic term in the adsorption of CO is not responsible for this shape of the null cline $f_1(u,v)=0$. Rather it stems from the quadratic term in the adsorption of oxygen which enters the first equation through the reaction part. In detail this adsorption term is $k_v s_v (1-u/u_s-v/v_s)^2$ where k_v is the adsorption rate and v_s is the saturation coverage for oxygen. As long as w is kept constant, $s_v := (s_{v_1} w + s_{v_2}(1-w))$ is just a sticking coefficient for oxygen.

The stable equilibria, representing branches of high and low reaction rate, undergo saddle-node bifurcations, and this is the only type of bifurcation occuring in this planar system. Neither the unstable saddle(s) nor the stable nodes can get oscillatory. No stable limit cycle can occur (with an argument used in SECTION 7.1.2) because for each time periodic

solution $\varphi(t) := \Big(u(t), v(t)\Big)$ with $\varphi(0) = \varphi(T)$ the integrated divergence $\int_0^T \partial_u f_1(u,v) + \partial_v f_2(u,v)\, dt$ is always negative. That means that each limit cycle has to be stable, which is not possible in this planar system because of the Poincaré-Bendixson theory.

The system becomes oscillatory with an additional equation for the reconstruction w.

$$\dot{w} = k_w(f(u) - w)$$

The switch in this equation is modeled with a function f that is nondecreasing and differentiable. It is zero for $u \leq 0.2$ and one for $u \geq 0.5$. As recently reported in [15], the preexponential factor k_w^0 in the Arrhenius equation for k_w may be greater by an order than in TABLE 2.2.

Explanation	Parameter	Value	Energy E_a	Value at 540 K
CO adsorption				
hitting rate	k_u	3.135×10^5 s^{-1}mbar^{-1}		
sticking coefficient	s_u	1		
saturation coverage	u_s	1		
mobility parameter	q	3.5 ± 0.5		
CO desorption	k_d^0	2×10^{16} s^{-1}	159098 J/mol	8.157 s^{-1}
Reaction	k_r^0	3×10^6 s^{-1}	41868 J/mol	267.454 s^{-1}
O_2 adsorption				
hitting rate	k_v	5.858×10^5 s^{-1}mbar^{-1}		
sticking coefficient$_{1\times2}$	s_{v_1}	0.4		
sticking coefficient$_{1\times1}$	s_{v_2}	0.6		
saturation coverage	v_s	0.8		
Phase transition	k_w^0	10^2 s^{-1}	29308 J/mol	0.146 s^{-1}

Tab. 2.2: Kinetic parameters as reported in [30]; Arrhenius kinetic yields $k_i = k_i^0 e^{-E_{a_i}/RT}$.

This model of KRISCHER et al. [30] is also used by FLACKE et al. [15] and BÄR et al. [5] who turn the system into a reaction-diffusion system by adding a Fick-type surface diffusion for the CO equation. Spirals can be detected numerically in a range of parameters which is in quite good agreement with the experiments [40].

In the work on traveling waves of FLACKE et al. [15], the typical shapes of null clines of this system are shown.
With a more or less heuristic argument the oxygen equation is turned from a differential equation to an algebraic equation by simply setting the temporal derivative to zero. It can now be solved for the oxygen coverage and incorporated into the first equation.
This so called adiabatic elimination (without change in entropy) yields a system of two equations.

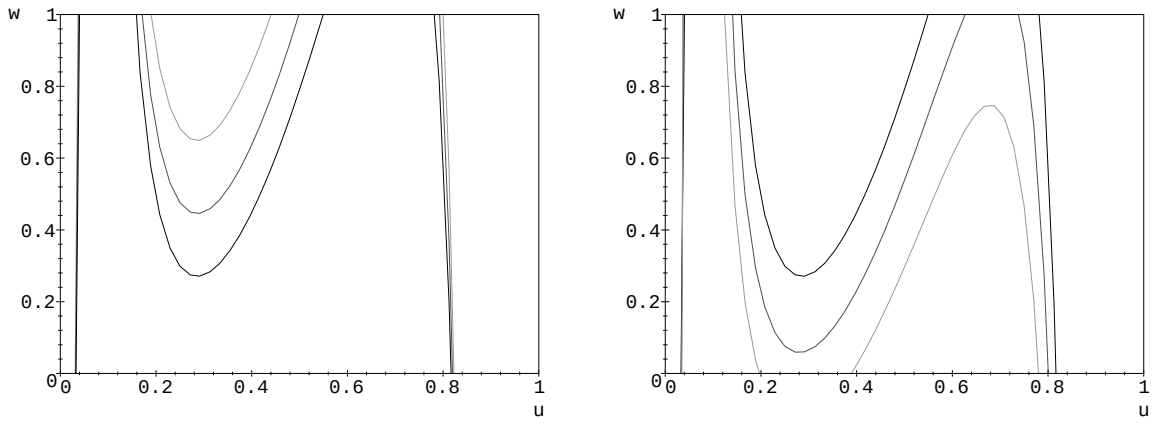

FIG. 2.7: Typical null clines for the u-equation shown as implicit functions $n_i(u)=w$. The solid line in both pictures corresponds to $p_{\mathrm{CO}}=4\times10^{-5}$ mbar and $p_{\mathrm{O}}=1.4\times10^{-4}$ mbar, respectively. The temperature is fixed at 538K. On the left solely the partial pressure of oxygen is decreased in three steps from the solid line to the lighter lines, and on the right solely the partial pressure of CO is decreased, fixing the oxygen pressure.

A more formal analysis argues with a variable transformation and then an expansion in terms of powers of a small parameter. This leads to a comparable system of two equations but with the possibility to estimate and explain the regions of validity of the model (see CHAPTER 3).

The precursor kinetic needs a closer look, since it is a nonlinear effect that might cause a global behavior of the flow not evident in the local analysis. The mobility of adsorbed CO is responsible for a deviation of the linear dependency of adsorption on the amount of free surface sites. Any exponent $q>1$ substantially increases the term of effective free sites for small coverages, so that the dependency of adsorption on the preadsorbed species is the lower the smaller the coverages are. However, the exponent can be set at $q=1$ without qualitatively changing the results on adsorption of mixed gases, as is reported in KRISCHER et al. [30].

With the equation for oxygen already eliminated adiabatically, the solution curve for $f_1(u,v(u,w),w)=0$ is plotted in FIGURE 2.7. Further algebraic investigations show that the shape of the curve is not essentially influenced by the exponent q. As a function of w it is a fraction of polynomials, and the numerator as well as the denominator polynomial are of degree $n:=\max\{4,2q\}$. Increasing q mainly affects the general shape for $u>1$, and since u is a concentration, this is physically not relevant (see FIGURE 2.8 on the facing page).

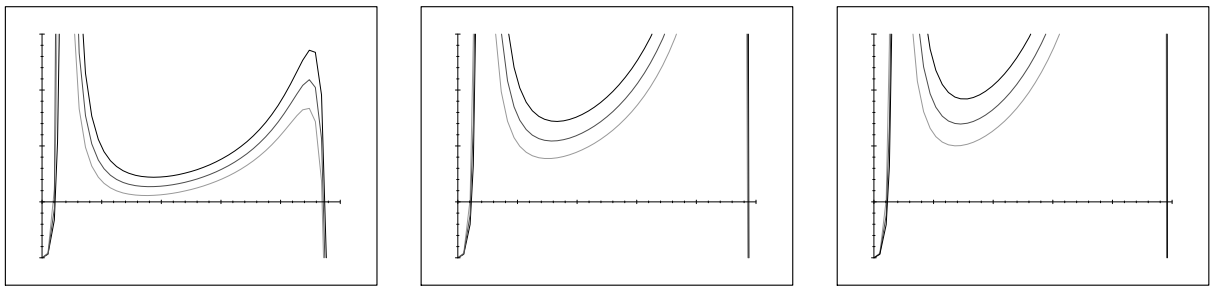

FIG. 2.8: From left to right are shown null clines of the u-equation on $w \in (0,1)$; the mobility parameter changes from $q=1$ to $q=2$ to $q=3$. The partial pressure of CO is decreased in three steps from the solid line to the lighter lines. The temperature is fixed at 500K. The sticking coefficient rather resembles the Pt(100) case, therefore the partial pressure for CO is almost halvened in comparison with FIGURE 2.7.

Only a rough sketch of this s-shaped null cline of the u-equation survives in the following model:

$$\begin{aligned} \dot{u} &= -k_0(u-u_1)(u-u_2(w))(u-u_3) + D\Delta u \\ \dot{w} &= k_w(f(u)-w) \end{aligned}$$

with u_1 and u_3 being constants, and $u_2(w)$ a linear function. After appropriate scaling it remains a system of the form:

$$\begin{aligned} \dot{u} &= -\frac{1}{\varepsilon}u(u-1)\left(u - \frac{w+b}{a}\right) + \Delta u \\ \dot{w} &= f(u) - w \end{aligned}$$

The shape of the null clines reminds of a Fitz-Hugh–Nagumo system (see EXAMPLE B.2).

Discussion

The switch can be improved to an analytic function as is done in [41]. But the zero set of the w-equation always remains a function of u as long as f is a function of u. Multiple solutions for w at a fixed value of u (which introduces hysteresis in the phase transition) are not possible with this model.

2.3.2 Hysteresis in the Phase Transition

The phase transition is the crucial feature of the process, and its dynamical modeling is more or less heuristic. In the KRISCHER model the cubic nonlinearity in the equation for the reconstruction process is only used to yield a C^1-function for the switch and is later improved to an analytic function in [41]. These models all have in common that the null cline is a monotone increasing function of u. The reconstruction process, however, involves half of the metal atoms of the topmost layer (in the case of Pt(110) it can also

involve deeper layers). An s-shaped null cline is ascribed to the existence of nucleation barriers. The so-modeled phase transition not only causes reaction rate changes but also oscillations of coverages. The coverages themselves can be modeled as simple as possible and still all other basic observations such as a poisoned state of a CO-covered surface and the quadratic dependency of oxygen adsorption on free surface sites are reproduced in the following model.

$$\begin{aligned} \dot{u} &= 1 - u - \sigma a(1-u)^2 \\ \dot{a} &= \kappa(u - h(a,\beta)) \end{aligned}$$

Here the greek letters are parameters that can be assigned a physical meaning, so that for example σ is a function of oxygen adsorption rate normalized by the rate of CO adsorption. The function $h(a,\beta)$ is a cubic polynomial, and its graph is fitted in a unit square (see FIGURE 2.9) such that for all values of β its turning point is at (0.5,0.5), passing through (0.0,0.0) and (1.0,1.0). The parameter β is a measure to control the humps.
Take for example

$$h(a,\beta) := \beta a^3 - \frac{3\beta}{2}a^2 + \left(1 + \frac{\beta}{2}\right)a$$

to satisfy the above requirements.
Analysis of this model for a wide range of positive parameters is done in SECTION 3.2.

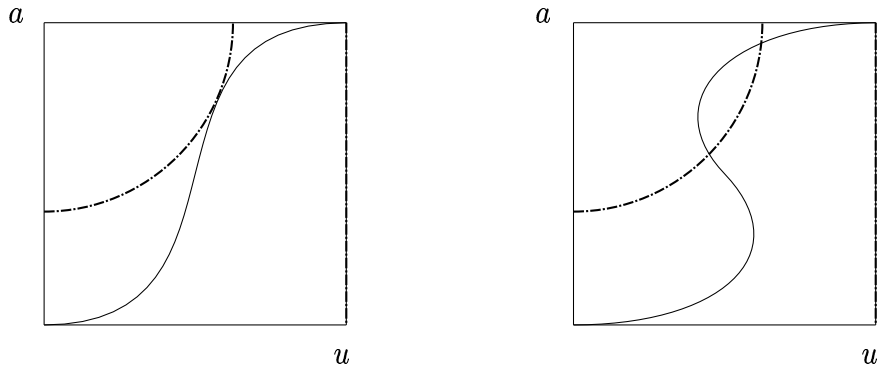

FIG. 2.9: The hysteretic behavior of the phase transition is modeled so that its null cline is a cubic polynomial $h := h(a,\beta)$ shown as solid s-shaped line. It depends on a with a control parameter β for the humps. Left: $\beta < 4$. Right: $\beta > 4$. The dash-dotted lines resemble the null clines of the u-equation.

2.3.3 Comparison of the Models

The models for CO oxidation on single crystal Pt(100) and Pt(110) surfaces differ in the process of adsorption caused by the different reconstruction processes. Therefore it is sensible to pay a closer look to the equation for the fraction of unreconstructed surface.

According to the expected nucleation barriers in first order phase transitions, an s-shaped null cline should be used to model the equation for the reconstruction process. It is convenient to form this differential equation out of a cubic polynomial depending solely on the fraction of 1×1 phase. If then for the sake of simplicity it depends linearly on the adsorbate(s), the null cline traces the shape of the cubic polynomial.

Aiming at a better understanding of the overall process not just on a single crystal but also on polycrystalline material, the simplified models should not differ much in the shape (or number) of equations. Rather they should contain only a parametric dependency for the different reconstruction mechanisms which is able to explain the observed features.

In the present work a parameter β monotonically controls the extreme points of the cubic polynomial h. Thereby the model ranges from no hysteresis for small β, which might be appropriate for Pt(100), up to strong hysteresis in the case of Pt(110), and it is usable for any combined material.

2.4 Spatial Self-Organization

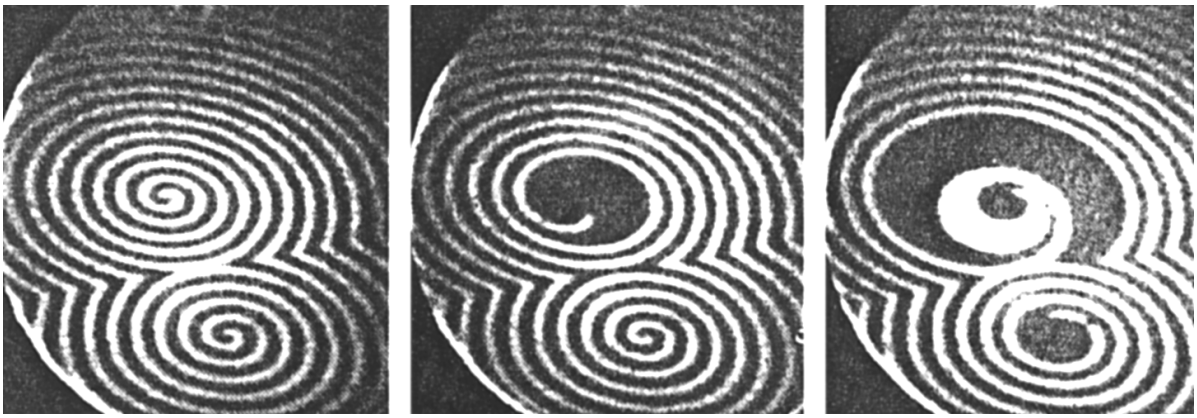

FIG. 2.10: Sequence of PEEM images at $p_{CO}=5.6\times10^{-5}$mbar, $p_{O_2}=4.0\times10^{-4}$mbar, and $T=483$K after a periodic forcing of the catalyst temperature; the section is $173\times173\mu m^2$ (after [6]).

In heterogeneous catalysis the spatial self-organization needs a closer look since it cannot be achieved by stirring as in the homogeneous case. Many of the experimental methods only measure mean values since they are not capable of resolving spatial structures. Nevertheless these mean values oscillate. Self-organization of a process with initial conditions randomly distributed over the surface area has to be proposed to explain such effective correlations.

Possible mechanisms for the coupling of the various oscillators are thermal coupling, mass transfer, and concentration changes in the gas phase. Thermal coupling will not be considered here, since it occurs mainly at high pressure where local temperature gradients

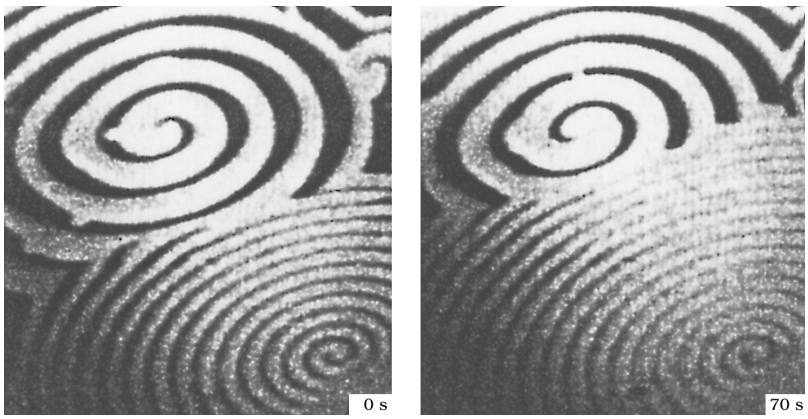

FIG. 2.11: Coexistence of two spirals with different rotation period and wavelength a 448K, $p_{CO} = 4.3 \times 10^{-5}$mbar and $p_{O_2} = 4 \times 10^{-4}$mbar. The long-wavelength spiral rotates with a period of $T = 25.3$ s around an elliptical core of $\sim 17 \times 9 \mu$m. The short-wavelength spiral rotates with a period of $T = 12.8$s around an elliptical core of $\sim 8 \times 5 \mu$m (after [40]).

of more than 150 K have been observed. Temperature then enters into the coefficients for desorption and reaction and the heat equation has to be solved, too.

At low pressure, ensuring isothermal conditions, mass transfer and gas phase coupling are more appropriate.

Mass transfer means a surface diffusion of the adsorbates. Since oxygen is strongly bound to the surface, its diffusion can be neglected. In contrast CO has a certain mobility that is higher in the direction of the missing row than perpendicular to it. Target patterns and spirals therefore appear elongated in the $(1\bar{1}0)$ direction (see FIGURE 2.6).

Since the anisotropy is assumed not to be coverage dependent, it can be scaled out with appropriate space coordinates

$$D\Delta u = D_1 \frac{\partial^2 u}{\partial x^2} + D_2 \frac{\partial^2 u}{\partial y^2}$$

setting $\hat{x} = \sqrt{x/D_1}$ and $\hat{y} = \sqrt{y/D_2}$.

For gas phase coupling at very low pressure LEVINE and ZOU [34] use the assumption that the partial pressures in the gas phase are proportional to the average coverages on the surface. This assumption uses the fact of instantaneous equilibration in the gas phase: The gas pressure at any fixed point in space reacts to the change in total concentration, since in the gas horizontal gradients disappear on a much faster time scale. Now the partial pressures are modified to become

$$p_{CO}(1 + \alpha' \bar{u} - \alpha \bar{v}) \qquad \text{and} \qquad p_{O_2}(1 + \beta \bar{u} - \beta' \bar{v})$$

with positive parameters α, α' and β, β' and

$$\bar{u} \equiv \frac{1}{L} \int u \, dx, \qquad \bar{v} \equiv \frac{1}{L} \int v \, dx$$

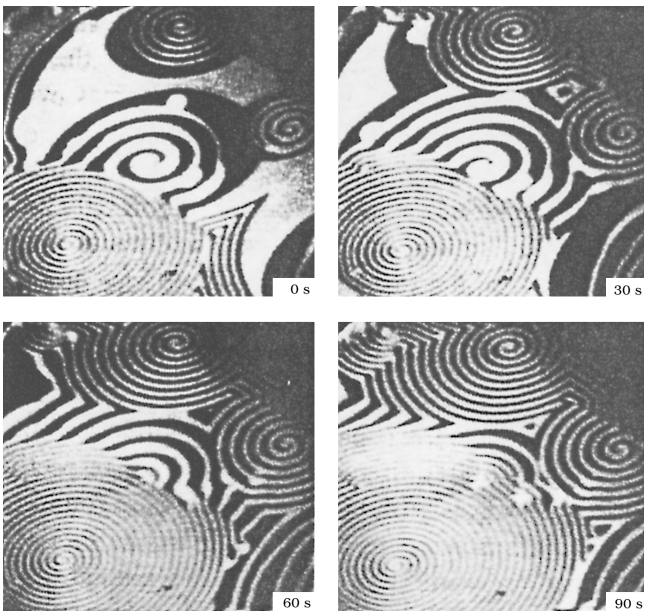

FIG. 2.12: Temporal evolution of a population of spirals with strongly differing rotation periods and wavelengths at $T = 448\text{K}$, $p_{\text{CO}} = 4.3 \times 10^{-5}\text{mbar}$ and $p_{\text{O}_2} = 4 \times 10^{-4}\text{mbar}$. The core size of the central spiral with large wavelength is $\sim 25 \times 14\mu\text{m}$. The spiral annihilating the latter rotates around a core of about $5 \times 3\mu\text{m}$ (after [40]).

where L is the measure of the (one-dimensional) space domain. In this context the asymmetric inhibition of the adsorption process is modeled by a slight enhancement of the partial pressure through a greater CO coverage and a reduction of the effective partial pressures by a greater oxygen coverage. Recall that asymmetric inhibition means that a dense adlayer of CO blocks the adsorption of oxygen. Thereby it locally increases the partial pressure particularly of oxygen. In contrast a great oxygen coverage still allows for the adsorption of CO molecules. The locally effective partial pressure of CO is thereby decreased.
For convenience LEVINE and ZOU [34] only investigated the case of nonzero $\alpha = \beta$ and of the other parameters equal to zero. That causes a self-induced parametric resonance due to the fact that both coverages are anticorrelated. As a result of their analysis of the amplitude equations this resonance broadened the region for the *modulated standing waves* (constant oscillations superimposed by nonconstant standing waves). Nevertheless, the qualitative behavior does not change when introducing such a coupling.

At higher pressure more complicated models for pressure and velocities have to be applied. First computational results for catalytic methan conversion have been achieved in the group of Warnatz. They investigate hysteresis in ignition-extinction processes with detailed chemical reaction mechanisms incorporated in the Navier-Stokes equations. The simulations are compared to experiments with a counter flow reactor (see [8]). So far the surface is a single point boundary condition that does not oscillate. A combination of temporally oscillating boundary conditions in one or two dimensions with gas phase dynamics still has to be done. Possibly the pressure gap can be closed by simulations parallel to closing it in experiments.

3 Treating Nonlinear Kinetics

3.1 Kinetic Equations without Hysteresis

The model of this section is described in IMBIHL et al. [24], where a local analysis is done, too, for the obvious fixed points of the equation. Here a more complete local and also global analysis is carried out.
In a first approximation a Hamiltonian system can be detected for a certain parameter constellation. The unfolding of a Takens-Bogdanov point, which is of course a local argument, reveals the global behavior of the flow for a wide range of parameters.
The concentration of adsorbed CO on the surface is described by u, the concentration of adsorbed oxygen is described by v, and a means an averaged amount of 1×1 structure supporting the reaction in so far as oxygen can only be adsorbed on this part of the surface since the O_2 molecules have to be dissociated. This resembles more or less the Pt(100) case.
The adsorption coefficient of CO is called ρ, the reaction rate of CO_2 is λ', σ' is the adsorption rate of oxygen and κ' is a coefficient modeling the velocity of changes in the surface structure.
The threshold concentration c separating the growing from the shrinking averaged surface structure is modeled by $c=(u+v)/0.4$. The third equation is coupled with the u and v-equation only by this threshold.

$$\begin{aligned} \dot{u} &= \rho(1-u-v)-\lambda' uv && (3.1)\\ \dot{v} &= \sigma' a(1-u-v)^2-\lambda' uv && (3.2)\\ \dot{a} &= \begin{cases} \kappa'(1-a) & \text{if} \quad c\geq 1 \\ -\kappa' a & \text{if} \quad c<1 \end{cases} && (3.3) \end{aligned}$$

The equations can be scaled with $t\to t/\rho$ so that it yields for $\lambda=\lambda'/\rho$, $\sigma=\sigma'/\rho$ and $\kappa=\kappa'/\rho$

$$\begin{aligned} \dot{u} &= 1-u-v-\lambda uv \\ \dot{v} &= \sigma a(1-u-v)^2-\lambda uv && (3.4)\\ \dot{a} &= \kappa(g(u,v,\varepsilon)-a). \end{aligned}$$

The discontinuity of the right-hand side of EQUATION (3.3) is smoothened with the function $g:=g(u,v,\varepsilon)$ so that the flow becomes differentiable. The conditions on g are as follows.

Definition 3.1 *The function $g:=g(c,\varepsilon)\in C^\infty$ is called a* smoothening function *of the jump of height 1 at c^* if*

(1) *it is monotone and ranges in $[0,1]\subset\mathbb{R}$,*

(2) $g\equiv 0$ if $c<c^*-\varepsilon$, $g\equiv 1$ if $c\geq c^*+\varepsilon$,

(3) *g behaves well when perturbed with a Poincaré series.*

As an example g can be realized with the flat function g_0 in the following way:

$$g(c,\varepsilon) := \frac{g_0(c-(1-\varepsilon))}{g_0(c-(1-\varepsilon))+g_0(1+\varepsilon-c)} \quad \text{with} \quad g_0(x) := \begin{cases} e^{\frac{1}{x}} & \text{if} \quad x>0 \\ 0 & \text{if} \quad x\leq 0 \end{cases}$$

Its derivative again is a C^∞ function converging to a δ distribution for $\varepsilon \to 0$.
The vector field of the system of differential equations yields a flow ϕ on $\Omega = \mathrm{P} \cup U_\epsilon$ where x is a solution vector $x=(u,v,a)^t$, P is the prisma $\mathrm{P} := \{x \in [0,1]^3 \mid \ u+v \leq 1\}$, and $U_\epsilon = \{x \in \mathbb{R}^3 \mid \ |x-\hat{x}| < \epsilon,\ \hat{x} \in \partial\mathrm{P}\}$ a small open neighborhood.

Remark 3.1 *The closed set $\mathrm{P} \subset \Omega$ is positively invariant.*

This can be shown easily, since the vector field on ∂P points into the prisma P.
Dynamical systems generated by more than two differential equations may exhibit chaotic behavior. But in this case it can be shown that as a first approximation, the dynamics can be described as a planar system. The parameter λ is very large in comparison to the other parameters of the system (see TABLE 2.1). Transforming with $v=\epsilon\tilde{v}$, $\epsilon = 1/\lambda$ yields the following system

$$\begin{aligned} \dot{u} &= 1-u-\epsilon\tilde{v}-u\tilde{v} \\ \epsilon\dot{\tilde{v}} &= \sigma a(1-u-\epsilon\tilde{v})^2 - u\tilde{v} \ . \\ \dot{a} &= \kappa(g(u,\epsilon\tilde{v},\varepsilon)-a) \end{aligned} \tag{3.5}$$

Rename $\tilde{v}=v$ and consider the vector x an asymptotic expansion of Poincaré type:

$$x = \sum_{m=0}^{\infty} \epsilon^m x_m = x_0 + \epsilon x_1 + o(\epsilon) \quad \text{with} \quad \epsilon < x_{im} < 1, \ {\scriptstyle i=1,2,3,\ m=0,1,2,\ldots}$$

Differentiate and get

$$\begin{aligned} \dot{u}_0 + \epsilon\dot{u}_1 &= 1-u_0-\epsilon u_1-\epsilon v_0-(u_0+\epsilon u_1)(v_0+\epsilon v_1)+o(\epsilon) \\ \epsilon\dot{v}_0+\epsilon^2\dot{v}_1 &= \sigma(a_0+\epsilon a_1)(1-u_0-\epsilon u_1-\epsilon v_0)^2-(u_0+\epsilon u_1)(v_0+\epsilon v_1)+o(\epsilon) \\ \dot{a}_0+\epsilon\dot{a}_1 &= \kappa(g-a_0+\epsilon a_1)+o(\epsilon) \end{aligned}$$

such that a comparison of coefficients yields the following system for ϵ^0

$$\dot{u}_0 = 1-u_0-u_0v_0 \tag{3.6}$$
$$0 = \sigma a_0(1-u_0)^2-u_0v_0 \tag{3.7}$$
$$\dot{a}_0 = \kappa(g(u_0,0,\varepsilon)-a_0). \tag{3.8}$$

The system for ϵ^0 resembles a system for $\lambda \to \infty$.
The term $u_0 v_0$ in the first equation can be replaced by $\sigma a_0 (1-u)^2$, resulting from the second, algebraic, equation. A planar system remains as a first approximation.

$$\begin{aligned} \dot{u}_0 &= 1 - u_0 - \sigma a_0 (1-u_0)^2 \\ \dot{a}_0 &= \kappa (g(u_0, \varepsilon) - a_0) \end{aligned} \tag{3.9}$$

Remark 3.2 *The asymptotic expansion is singular for* $u_0 = 0$.

That can be seen when solving EQUATION (3.7) for v_0

$$v_0 = \frac{\sigma a (1-u_0)^2}{u_0} \qquad \text{for} \quad u_0 \neq 0.$$

A consequence of this singularity is that the planar system defined on the unit square is no longer positively invariant: The vector field at $u_0 = 0$, $a_0 > 1/\sigma$ points out of the unit square. But the fixed points of the system are away from $u_0 = 0$; the local analysis of the planar system can be carried out without thinking about the uniform validity of the expansion in the whole domain.

3.1.1 The Hamiltonian System

There are at most three fixed points or equilibria for the planar SYSTEM (3.9). The obvious one that exists and is stable for all parameters is $E_1 = (1,1)$. The fixed points E_2 and E_3 develop out of a saddle-node bifurcation when the convex graph of the hyperbola $1/\sigma(1-u)$ penetrates the monotone smoothening function g. These two fixed points are of interest for the local analysis.
The linearization at $E_2 = E_3$ might as well have a double zero eigenvalue with a matrix in Jordan normal form $\begin{pmatrix} 0 & 1 \\ 0 & 0 \end{pmatrix}$.
With THEOREM A.3 the higher order terms can be put into a Poincaré-Birkhoff Normal Form where they appear as homogeneous polynomials. The successive steps of the transformation are derived in a constructive way as described in the proof. The universal unfolding of the double zero eigenvalue follows the form of BOGDANOV [3]. The transformation needed to put a vector field into normal form is formal, but it cannot be determined how precisely the dynamical behavior of the normal form represents the behavior of the nontransformed equations.
The chosen complementary space $\mathcal{G}_2$ of ad $\mathrm{L}(\mathcal{H}_2)$ in $\mathcal{H}_2$ (the space of homogeneous polynomials of second order (and two variables)) is spanned by the vectors

$$\mathcal{G}_2 = \mathrm{span}\left\{ \begin{pmatrix} 0 \\ x^2 \end{pmatrix}, \begin{pmatrix} 0 \\ xy \end{pmatrix} \right\}, \quad \mathcal{H}_2 = \mathrm{ad}\ \mathrm{L}(\mathcal{H}_2) \oplus \mathcal{G}_2.$$

A normal form for the nonlinearities up to terms of second order looks as follows

$$\begin{aligned} \dot{x} &= y \\ \dot{y} &= k_1 x^2 + k_2 xy. \end{aligned} \tag{3.10}$$

Note that for SYSTEM (3.9) the transformation of the quadratic part doesn't bring in additional errors since it turned out that $(I+DP)^{-1}=I-DP$ in this special case.
Let a^* be the second coordinate of E_3. The transformation is done with a Taylor expansion of the vector field where E_3 is shifted to zero. The transformation

$$\begin{aligned} u_0 &:= x - C - \sigma a^* (x-C)^2 \\ a_0 &:= \sigma (a^*)^2 (x - y - C) \end{aligned}$$

with

$$C := \left(1 - \frac{\sigma_c}{\sigma}\right) \frac{\sigma (a^*)^2}{2g'\sigma a^* - g''}$$

results in SYSTEM (3.11). There is no term according to the basis vector $\begin{pmatrix} 0 \\ xy \end{pmatrix}$ of $\mathcal{G}_2$.

$$\begin{aligned} \dot{x} &= y \\ \dot{y} &= c_1 + (1-\kappa)y + \left(\frac{\kappa g'}{a^*} - \frac{\kappa g''}{2\sigma (a^*)^2}\right) x^2 \end{aligned} \tag{3.11}$$

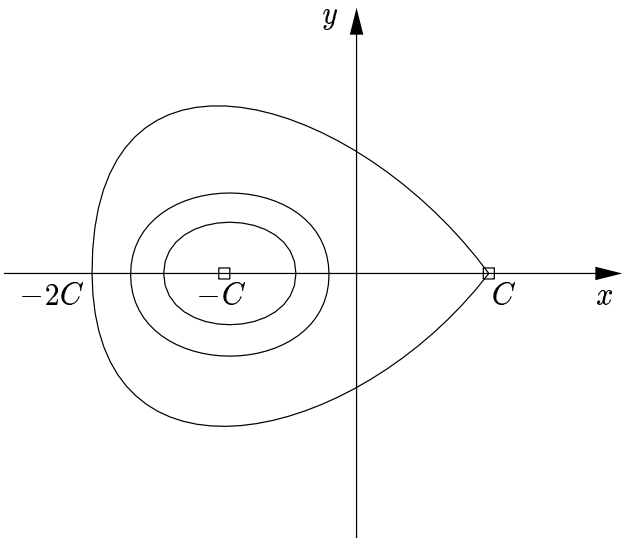

FIG. 3.1: The Hamiltonian system in the kinetic equations for the coordinates x and y.

The constant term takes the form

$$c_1 = C\kappa\left(\frac{\sigma_c}{\sigma} - 1\right) + C^2\kappa\left(\frac{g'}{a^*} - \frac{g''}{2\sigma(a^*)^2}\right)$$

such that for $\sigma = \sigma_c$ the expression for C and in consequence c_1 is zero. If in addition $\kappa = \kappa_c = 1$, the linearization in zero has a double zero eigenvalue and is in Jordan normal. For $\kappa = 1$ the SYSTEM (3.11) is an integrable Hamiltonian system with Hamilton function

$$H(x,y) = \frac{y^2}{2} - c_1 x - c_3\frac{x^3}{3} \tag{3.12}$$

and a coefficient $c_3 = \kappa\left(\frac{g'}{a^*} - \frac{g''}{2\sigma(a^*)^2}\right)$.

The Ljapunov center theorem (see THEOREM A.4) can be applied, showing that there is a branch of noncritical periodic orbits, even for the perturbed vector field $f(\kappa;x,y) = J\nabla H + (1-\kappa)(0,y)^t$.
H is a Ljapunov function for the flow φ induced by the vector field f for $\kappa > 1$ since then

$$\dot{H}(x,y) = \nabla H \cdot f(\kappa;x,y) = \nabla H \cdot J\nabla H + (1-\kappa)|(0,y^2)| = (1-\kappa)y^2,$$

such that $\dot{H}(x,y) < 0$ for all $y \neq 0$ in an appropriate neighborhood. $\dot{H}(x,y) > 0$ for $\kappa < 1$ showing that this bifurcation is transcritical. There are no noncritical periodic orbits in a neighborhood of zero for $\kappa \neq 1$. Parameterizing the branch of solutions with $s \in (-\varepsilon,\varepsilon)$ yields $\kappa(s) \equiv 1$. It means that in the bifurcation diagram the periodic solution branches perpendicular off the zero solution.
Denoting the homoclinic orbit of the Hamiltonian system with $\Gamma(t) = (x^\Gamma, y^\Gamma)$ the Melnikov function (see APPENDIX A.1.1) for the perturbed system is

$$M(\kappa) = \int_{-\infty}^{\infty} (1-\kappa)(y^\Gamma)^2 \, dt$$

and $M(\kappa) \equiv 0$ again only if κ is critical. The trace of the Jacobian at the saddle is $1-\kappa$, indicating again a transcritical situation for the bifurcating periodic orbits of the saddle-loop.

Remember that here transformations up to second order do not bring on additional errors. Higher order terms in the normal form do not change the observations made here.
Numerical solutions of the nontransformed system also show a slightly deformed but qualitatively similar behavior (see FIGURE 3.2 on the next page).

3.2 Modeling Hysteresis

Systems with a coupling that only switches between two different reaction mechanisms might behave in the described nongeneric way. It is more realistic to model these switches

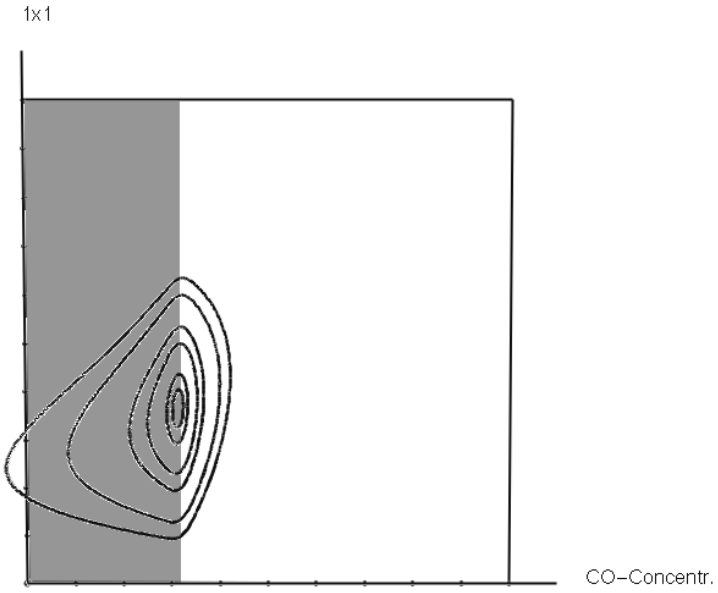

FIG. 3.2: The Hamiltonian system is valid not only in a small perturbation of the critical situation but also for parameters far away from the critical ones as shown here for $\sigma >> \sigma_c$ and $\kappa = \kappa_c = 1$. The area of decreasing catalytic activity ($\dot{a} < 0$) is marked grey.

with a hysteresis loop. Then the generic situation of the unfolding of a double zero eigenvalue appears in the system: The saddle-node, Hopf and saddle-loop bifurcation occur one after another in parameter space when continuously varying the parameters. It depends on the sign of the coefficients in the unfolding whether the limit cycle is stable or not. For the model described here, a stable limit cycle is detected for all bifurcation problems.
This result is obtained with a change in the third equation of SYSTEM (3.4). A cubic-like function $h := h(a,\beta)$ is introduced that has the following properties for each parameter β:

(1) $h : [0,1] \times \mathbb{R} \to \mathbb{R},\ h \in C^2$

(2) $h(0,\beta) = 0,\ h(1,\beta) = 1,\ h''(0.5,\beta) = 0$

(3) The graph of h is a subset of the closed unit square.

The parameter β is introduced to control the extreme points or humps of h. This is better shown in a special example that is constructed for the implementation of h. It is a cubic polynomial of the form

$$h(a,\beta) := \beta a^3 - \frac{3\beta}{2} a^2 + \left(1 + \frac{\beta}{2}\right) a \tag{3.13}$$

and its extreme points lie inside the unit square for $4 < \beta < 16$. Instead of the SYSTEM (3.4) the model to be discussed is

$$\begin{aligned} \dot{u} &= 1-u-v-\lambda uv \\ \dot{v} &= \sigma a(1-u-v)^2-\lambda uv \\ \dot{a} &= \kappa(u+v-h(a,\beta)). \end{aligned} \tag{3.14}$$

A formal expansion in terms of ε again leads to a planar system for terms of order ε^0 of the form

$$\begin{aligned} \dot{u} &= 1-u-\sigma a(1-u)^2 \\ \dot{a} &= \kappa(u-h(a,\beta)). \end{aligned} \tag{3.15}$$

This system, too, has at most three fixed points. Following the same method as in the previous section, namely, shifting the critical fixed point $E_3=(u^*,a^*)$ to zero and making a Taylor expansion results in

$$\begin{aligned} \dot{u} &= u-\frac{1}{\sigma(a^*)^2}a-\sigma a^* u^2+\frac{2}{a^*}ua-\sigma u^2 a \\ \dot{a} &= \kappa u-\kappa\sum_{k=1}^{\infty}\frac{1}{k!}h^{(k)}(a^*)a^k. \end{aligned}$$

The Jacobian at this equilibrium reads

$$A|_{E_3}=\begin{pmatrix} 1 & -\dfrac{1}{\sigma(a^*)^2} \\ \kappa & -\kappa h' \end{pmatrix}$$

and the eigenvalues are

$$\lambda_{1,2}(E_3)=\frac{1}{2}\left(1-\kappa h'\pm\sqrt{(1-\kappa h')^2+4\kappa\left(h'-\frac{1}{\sigma(a^*)^2}\right)}\right).$$

It is easy to deduce the critical parameters from the above eigenvalues: Either the term in front of the square root has to be zero, or the term under the root evaluates to zero. This is true for $\kappa_c=h'^{-1}$, or $\sigma_c=((a_{2=3})^2h')^{-1}$. In this system a Hopf bifurcation occurs for the critical parameter κ when $h'(a^*)\leq\dfrac{1}{\sigma(a^*)^2}$ (which is only possible for the node E_3), and the critical σ causes a saddle-node bifurcation at a limit point where $E_2=E_3$. If both parameters are critical, the linearization A is similar to a Jordan normal form with double zero eigenvalue.

$$A=\begin{pmatrix} 1 & -h' \\ h' & -1 \end{pmatrix}\Rightarrow S^{-1}AS=\begin{pmatrix} 1 & 0 \\ 1 & -h' \end{pmatrix}\begin{pmatrix} 1 & -h' \\ h'^{-1} & -1 \end{pmatrix}\begin{pmatrix} 1 & 0 \\ h'^{-1} & -h'^{-1} \end{pmatrix}=\begin{pmatrix} 0 & 1 \\ 0 & 0 \end{pmatrix}$$

The unfolding of the Takens-Bogdanov point then results in a system

$$\begin{aligned} \dot{x} &= y \\ \dot{y} &= -c_1 + c_2 y + c_3 x^2 - c_4 xy \end{aligned} \tag{3.16}$$

and the transformation needed is

$$\begin{aligned} u &:= x + \mathrm{C} - \sigma a^* (x - \mathrm{C})^2 \\ a &:= \sigma (a^*)^2 (x - y + C) \end{aligned}$$

with positive constants c_i, C, except for c_2 which is indefinite. Note that the transformation is a formal one derived from the comparison of coefficients for the successive linear and quadratic terms, neglecting terms of higher order. This makes it valid only in a small neighborhood of the fixed point. Nevertheless the transformation is sufficient in order to judge the stability of the bifurcating solutions. The coefficients of the system are functions of the parameters σ and κ that still have a physical meaning. [1]

$$c_1 := \frac{\frac{\kappa}{2}\left(h' - \frac{1}{\sigma(a^*)^2}\right)^2}{\frac{2}{a^*} + \sigma(a^*)^2 h''} \qquad c_2 := 1 - \kappa h' + \frac{\kappa\sigma(a^*)^2 h''\left(h' - \frac{1}{\sigma(a^*)^2}\right)}{\frac{2}{a^*} + \sigma(a^*)^2 h''}$$

$$c_3 := \frac{\kappa}{2}\left(\frac{2}{a^*} + \sigma(a^*)^2 h''\right) \qquad c_4 := \kappa\sigma(a^*)^2 h''$$

$$\mathrm{C} := \frac{\frac{1}{\sigma(a^*)^2} - h'}{\frac{2}{a^*} + \sigma(a^*)^2 h''}$$

The coordinates of the fixed points are $x_{1,2} = \pm\sqrt{\frac{c_1}{c_3}} =: \pm\mathrm{C}$, and $y_{1,2} = 0$. Note that C is positive since $h'(a^*) \leq \frac{1}{\sigma(a^*)^2}$. Then the Jacobian

$$A = \begin{pmatrix} 0 & 1 \\ \pm 2c_3\mathrm{C} & c_2 \mp c_4\mathrm{C} \end{pmatrix}$$

has the following eigenvalues indicating a saddle at $(+\mathrm{C}, 0)$ and a node at $(-\mathrm{C}, 0)$.

[1] For example σ is the coefficient of the adsorption term of oxygen, and this is proportional to the partial pressure of oxygen and reciprocal to the partial pressure of CO, both free parameters in the experiment. The other parameter κ is proportional to the rate of phase transition and therefore temperature-dependent, and (due to scaling) it is reciprocal to the partial pressure of CO, too. If the parameters are intended to be varied independently, the method of choice should be to vary oxygen pressure.

$$\lambda_{1,2}(+\mathrm{C},0) = \frac{1}{2}\Big(c_2 - c_4\mathrm{C} \pm \sqrt{(c_2 - c_4\mathrm{C})^2 + 8c_3\mathrm{C}}\Big) \qquad \text{Saddle}$$

$$\lambda_{1,2}(-\mathrm{C},0) = \frac{1}{2}\Big(c_2 + c_4\mathrm{C} \pm \sqrt{(c_2 + c_4\mathrm{C})^2 - 8c_3\mathrm{C}}\Big) \qquad \text{Node}$$

The transformation can be proved at the critical parameters: A saddle-node bifurcation occurs for $\mathrm{C}\equiv 0$ and this is the case for the critical $\sigma_c = ((a_{2=3})^2 h')^{-1}$. A Hopf bifurcation is possible for $c_2 = -c_4\mathrm{C} \Leftrightarrow 1-\kappa h' = 0 \Leftrightarrow \kappa = h'^{-1}$.

3.2.1 The Hopf Case

The resulting system now has a term according to the basis vector $\begin{pmatrix} 0 \\ xy \end{pmatrix}$ of $\mathcal{G}$ with a coefficient c_4. As a consequence the bifurcating branch of periodic solutions does not behave like in a linear (Hamiltonian) system but tends to one side. In order to compute the stability criterium (see THEOREM A.7) the SYSTEM (3.15) has to be described in the coordinates of the kernel. The complex eigenvectors b, $\bar{b}$ of the critical eigenvalues form a basis $\hat{e}_{1,2} = \left(\frac{1}{2}(b+\bar{b}), \frac{-i}{2}(b-\bar{b})\right)$ that is

$$\hat{e}_1 = \begin{pmatrix} h' \\ 1 \end{pmatrix}, \quad \hat{e}_2 = \begin{pmatrix} -h'\sqrt{(h'\sigma(a^*)^2)^{-1} - 1} \\ 0 \end{pmatrix}.$$

After the basis transformation, abbreviating $\sqrt{(h'\sigma(a^*)^2)^{-1} - 1} = \sqrt{}$, the system has the form

$$\dot{x} = -y\sqrt{} - \frac{1}{h'}\sum_{k=2}^{\infty}\frac{1}{k!}h^{(k)}(a^*)x^k$$

$$\dot{y} = x\sqrt{} + \frac{1}{h'\sqrt{}}\sum_{k=2}^{\infty}\frac{1}{k!}h^{(k)}(a^*)x^k$$

$$-\frac{\sigma a^* h'}{\sqrt{}}\big(x + y\sqrt{}\big)^2 + \frac{2}{a^*\sqrt{}}\big(x + y\sqrt{}\big)x - \frac{\sigma h'}{\sqrt{}}\big(x + y\sqrt{}\big)^2 x$$

which is the standard form of the Hopf bifurcation. The stability criterium computes to

$$\delta = \frac{1}{\sqrt{}}\left(\sqrt{}^2\left(\frac{-h'''}{h'}\right) - \left(\frac{h''}{h'}\right)^2 - 2\frac{h''}{h'a^*} - \frac{8\Big(1-(a^*)^2\Big)}{(a^*)^2}\right) < 0$$

which is negative since the function h modeling the hysteresis has positive h''', h'', and h' in E_3. Hence each term in the bracket is negative.
The Hopf bifurcation is supercritical for all positive parameters, the stable node loses its stability to the branch of periodic solutions.

3.2.2 Bifurcation from a Homoclinic Orbit

The parameter range where bifurcation from a homoclinic orbit takes place can be detected with Melnikov theory.
Return again to SYSTEM (3.16) with nonzero c_2 and c_4. It shall be regarded as a perturbation of a Hamiltonian system where these two coefficients are zero.

	Hamiltonian system		perturbation
$\dot{x}$	$= y$		
$\dot{y}$	$= -c_1 + c_3 x^2$	$+$	$c_2 y - c_4 x y$

The Hamilton function for this system is similar to EQUATION (3.12) with different coefficients. See also FIGURE 3.1.

$$H(x,y) = \frac{y^2}{2} + c_1 x - \frac{c_3 x^3}{3}$$

H is a first integral and its value at the saddle point $(+\mathrm{C},0)$ is the same as for the homoclinic orbit connected with the saddle and lying around the node $(-\mathrm{C},0)$.

$$H(+\mathrm{C},0) = c_1\mathrm{C} - \frac{c_3\mathrm{C}}{3} = \frac{2}{3}c_1\mathrm{C}$$

This value occurs again on the ordinate at $-2\mathrm{C}$.
For these parameters the homoclinic orbit can be written as follows.

$$\Gamma(t) = (x^\Gamma, y^\Gamma) = \left(\mathrm{C} - 3\mathrm{C}\,\mathrm{sech}^2(t), 3\mathrm{C}\sqrt{2c_3\mathrm{C}}\,\mathrm{sech}^2(t)\tanh(t)\right)$$

Since this is an autonomous perturbation the Melnikov function is time independent and computes to

$$\begin{aligned} M(c_2,c_4) &= \int_{-\infty}^{\infty} c_2\left(y^\Gamma\right)^2 - c_4 x^\Gamma\left(y^\Gamma\right)^2\,dt \\ &= \int_{-\infty}^{\infty} c_2\left(18c_3\mathrm{C}^3\mathrm{sech}^4(t)\tanh^2(t)\right) \\ &\qquad -c_4 18c_3\mathrm{C}^4\left(1-3\,\mathrm{sech}^2(t)\right)\mathrm{sech}^4(t)\,\tanh^2(t)\,dt. \end{aligned}$$

Whenever $M(c_2,c_4)\equiv 0$ the system has a homoclinic orbit. What has to be solved is

$$c_2 18c_3\mathrm{C}^3\int_{-\infty}^{\infty}\mathrm{sech}^4(t)\tanh^2(t)\,dt = c_4 18c_3\mathrm{C}^4\int_{-\infty}^{\infty}\left(1-3\,\mathrm{sech}^2(t)\right)\mathrm{sech}^4(t)\,\tanh^2(t)\,dt.$$

With $\mathrm{sech}^2(t) = 1-\tanh^2(t)$ and $\displaystyle\int_{-\infty}^{\infty}\mathrm{sech}^2(t)\tanh^k(t)\,dt = \left.\frac{\tanh^{k+1}(t)}{k+1}\right|_{-\infty}^{\infty} = \frac{2}{k+1}$

and dividing by $18c_3\mathrm{C}^3$ this evaluates to

$$7c_2 = -5c_4\mathrm{C}.$$

Whenever this condition is fulfilled, the homoclinic orbit is preserved in the perturbed Hamiltonian system. It is called the saddle-loop condition and with $c_2 = 1-\kappa h' - c_4\mathrm{C}$ it can be written implicitly as

$$SL(\sigma,\kappa,\beta) = 1 - \kappa h' - \frac{2c_4\mathrm{C}}{7} = 0.$$

The trace of the Jacobian at the saddle of the homoclinic orbit has to be negative to indicate that periodic orbits bifurcating from the saddle loop are stable (see THEOREM A.5). This is the case for the range of parameters inbetween the Hopf condition and the saddle-loop condition.

3.2.3 Inbetween Hopf and Saddle-Loop Conditions

The stable periodic orbit lies inbetween two manifolds in parameter space indicating the necessary conditions for Hopf bifurcation $Ho(\sigma,\kappa,\beta)$ and saddle-loop bifurcation $SL(\sigma,\kappa,\beta)$. At first glance $Ho(\sigma,\kappa,\beta)=1-\kappa h'$ seems not to be σ-dependent, but it is, due to the σ-dependency of the coordinates of E_3 that enter h'.

$$\begin{aligned} Ho(\sigma,\kappa,\beta) &= 1-\kappa h' &&= 0 \\ SL(\sigma,\kappa,\beta) &= 1-\kappa h' - \frac{2c_4\mathrm{C}}{7} &&= 0 \end{aligned}$$

These equations are identical for $c_4\mathrm{C}\equiv 0$. In the three-dimensional parameter space their two-dimensional manifolds touch each other at a curve for Hamiltonian systems, that is $c_2=c_4=0$, and a curve for B-points, that is $c_2=C=0$.
Sinse a^* is always positive and for positive parameters κ and σ the following expressions are equivalent:

$$c_4 = \kappa\sigma(a^*)^2 h'' = 0 \Leftrightarrow h'' = 0$$

$$\mathrm{C} = \frac{\frac{1}{\sigma a^*} - h'}{\frac{2}{a^*} + \sigma(a^*)^2 h''} = 0 \Leftrightarrow \frac{1}{\sigma a^*} - h' = 0$$

This result can be illustrated with the specified cubic polynomial (EQUATION (3.13)). The first case of Hamiltonian systems occurs for $h''=3\beta(2a^*-1)=0$, that is either $\beta=0$ (the polynomial $h(a,\beta)$ then degenerates to a linear function), or $a^*=0.5$ which is equivalent to $\sigma=4$.
The second case, when $\mathrm{C}=0$, represents the curve of B-points. The position of the manifolds in parameter space can be analyzed by implicit derivatives and sketched as in

FIGURE 3.3 on the following page. With respect to β, the saddle-loop manifold always lies above the Hopf manifold. The dynamic behavior for increasing σ is sketched in FIGURE 3.4 on the next page. At a critical value σ_c a saddle and a node emerge from a limit point, the stable node turns unstable when the Hopf condition is reached; a stable limit cycle bifurcates. Since the branch of limit cycles is not compact and cannot return to the same bifurcation point, it either is unbounded in period or returns to another Hopf point. As long as there are no turning points on the branch, the two values of σ that indicate homoclinic orbits mark a gap of limit cycles. Increasing κ leads to a merging of both homoclinic orbits and finally a penetration. But for κ in consideration here, there is a gap whithout periodic solutions.

This result is also checked with the bifurcation software AUTO of E. DOEDEL revealing no additional features of the nontransformed two and three variables system, ensuring that the transformation preserves the qualitative behavior not only in an approximative sense.

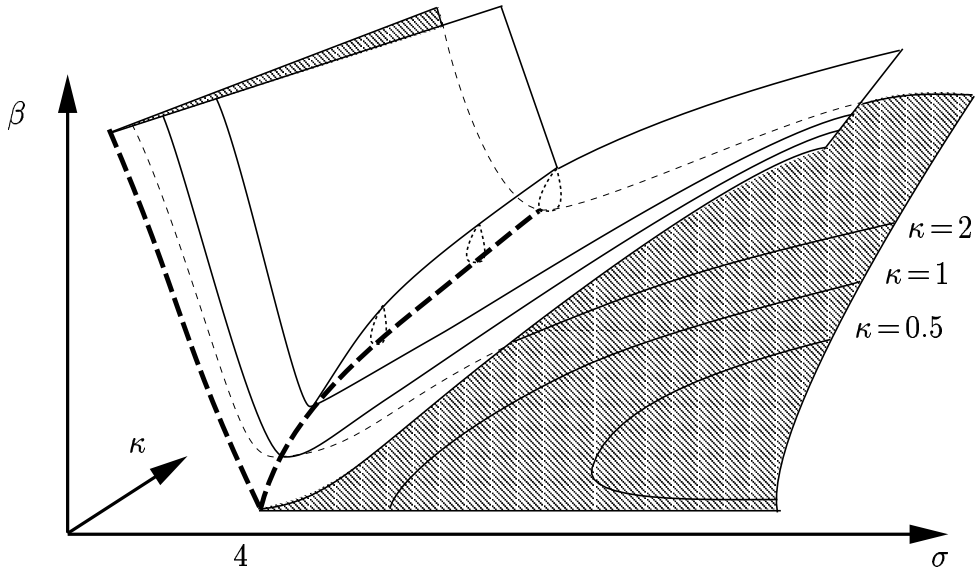

FIG. 3.3: The surfaces for Hopf condition (shaded) and saddle-loop condition (blank). The bold dashed lines mark the curve of B-points (to the left) and the curve of Hamiltonian systems. Stable limit cycles can be detected for parameters inbetween both manifolds.

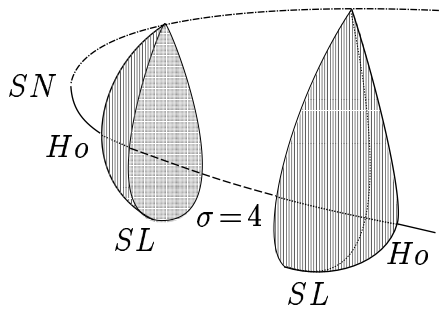

FIG. 3.4: A sketch of the dynamics. From left to right the parameter σ is increased. The solid part of the parabola indicates a stable fixed point, the dash-dotted line is the saddle and the dashed line the unstable node. SN denotes the saddle-node bifurcation. There are two Hopf bifurcation points Ho and two homoclinic orbits SL, and inbetween in either case a branch of stable periodic solutions.

4 Spatio-Temporally Oscillating Solutions

4.1 Adding a Fick-Type Diffusion Term

A stable equilibrium of a planar system can be destabilized to nonconstant steady solutions by a diffusion term, but not to time-periodic solutions (see CHAPTER 5). This is due to the fact that diffusion coefficients always diminishes the trace of the Jacobian. What happens in the neighborhood of unstable oscillatory constant solutions when diffusion is added is not accessible for the theory. Especially since Neumann boundary conditions are also accepted by constant but time-periodic solutions, the diffusion not necessarily introduces attractors to the system that are not already known from the kinetic system.

In the computational experiments of this chapter the kinetic system is therefore fixed to the situation that there is an unstable node and no periodic solution. The situation is as follows: Besides the asymptotically stable constant state E_1, there is a saddle E_2 and an unstable node E_3 which is oscillatory. There is no periodic solution for the kinetic system, and as a consequence E_1 is globally attractive. This global attractor is a so called poisoned state and corresponds to a situation where the whole surface is covered by a single reactant. This state should be avoided since no reaction takes place any more. The influence of the diffusion operator can then be seen whenever the solution is bounded away from the only attractor of the kinetic system.
The mobility of carbon monoxide on the surface is modeled with a Fick-type diffusion term solely in the first equation of SYSTEM (4.1). The nonlinearities always stem from the reaction kinetic.

$$\begin{array}{rcll} \dot{u} & = & d_1\Delta u & + \quad 1-u-\sigma a(1-u)^2 \\ \dot{a} & = & & \kappa(u-h(a,\beta)) \end{array} \tag{4.1}$$

Throughout this chapter the exact values for the kinetic parameters are $\sigma=4$, $\kappa=3$, and $\beta=5$. This fixes E_3 at (0.5,0.5).

4.1.1 Computational Setting

The reacting fronts propagate across the whole domain and there is no need for adaptive grid refinement. Using a rectangular equidistant grid suits the problem and no further efforts are made to improve the discretization scheme. In each time step only the nearest neighbors are used to compute the diffusion term. Homogeneous Neumann boundary conditions are implemented as reflections at the boundary. For a one-dimensional setting on a unit interval this comprehends the left and right neighbor grid point and at 0 and 1 twice the right and twice the left grid point. For a two-dimensional setting four nearest neighbors are used in a 5-star term for the diffusion operator.
The discretized system of ordinary differential equations is solved with the LSODE package (see HINDMARSH [23]), using numerical estimates of the Jacobian matrix. Time

discretization is done implicitly with a maximal step size of $t=0.01$. The error tolerances are 1×10^{-8} relative and 1×10^{-12} absolute. The size of the spatial grid then is adjusted according to the value of the diffusion coefficient such that the spatial wavelength is best resolved.

4.1.2 About the Graphics Realization

In the figures of this chapter the CO coverage is shown as colored surface. The color mapped to the surface represents the local fraction of the amount of catalytically active phase of the surface, the 1×1-phase. The color ranges from light green for the hex phase over blue and red to light yellow for a complete 1×1-phase.
For one-dimensional computations the spatio-temporal development is displayed as (x,t)-plot where the time axis is shown to the rear.
The results of simulations in two space dimensions are shown as snapshots of the time-periodic attractors. Animated sequences show the transient dynamical behavior before the attractors of similar waveforms are reached for various initial data. These evolutions can be displayed with the program *cnom2.0* (see KRÖMKER [32]).

4.2 Results in One Space Dimension

To guarantee the spatial step size h to be of the appropriate order of magnitude, i.e. $h^2\sim t$, the space discretization for e.g. d_1 about a hundredth is 100 gridpoints on a unit interval, such that $h^2={d_1}^{-1}(100)^{-2}\sim0.01$. This indeed is the coarsest grid, and finer grids are only used for even smaller diffusion coefficients.

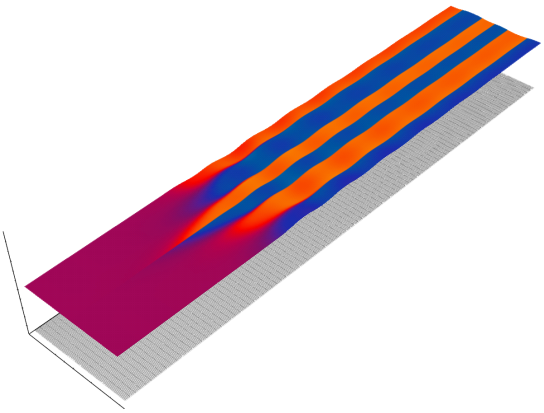

FIG. 4.1: There exist nonconstant steady states where the u-equation is continuous and close to its value at E_3, whereas the a-equation is discontinuous as marked by the abrupt color changes ($d_1=0.16$).

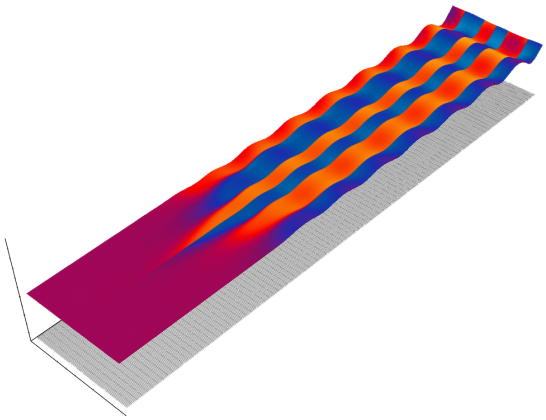

FIG. 4.2: No nonconstant steady states are found for diverse initial conditions at $d_1=0.14$. E_1 is globally attracting.

From FIGURE 4.1 to FIGURE 4.5 the diffusion coefficient for surface diffusion is diminished. The initial conditions are either small gradient, cross gradient, or the data is randomly distributed with a mean value at the unstable fixed point in request, that is E_3. Testing a small defect in the middle of the unit interval, the initial conditions are the same for both equations; they are constant above and below the critical E_3 with a small discontinuity of height 0.0001 at the middle of the unit interval.

The following observations can be made:
For a diffusion coefficient d_1 greater or equal to 0.16 steady patterns can be recognized, but their shapes strongly depend on the initial conditions. To resolve the interfaces correctly, adaptive regridding at the discontinuity has to be made. Here this has not been investigated further.
If the diffusion coefficient is close to 0.16, the upper and lower parts of the solutions are oscillatory but damped out to a discontinuous steady solution for the a-equation and a continuous solution for u (see FIGURE 4.1 on the facing page).
Diminishing the diffusion coefficient leads to an increase in oscillatory behavior; no steady nonconstant solution can be detected whenever these oscillations in the u-equation increase in amplitude after once the formation of clearly separated phases in space has been established (see FIGURE 4.2). Then again the CO-poisoned state is the only attractor to be found. From the point of view of asymptotic behavior the simulations do not differ from the kinetic equations.

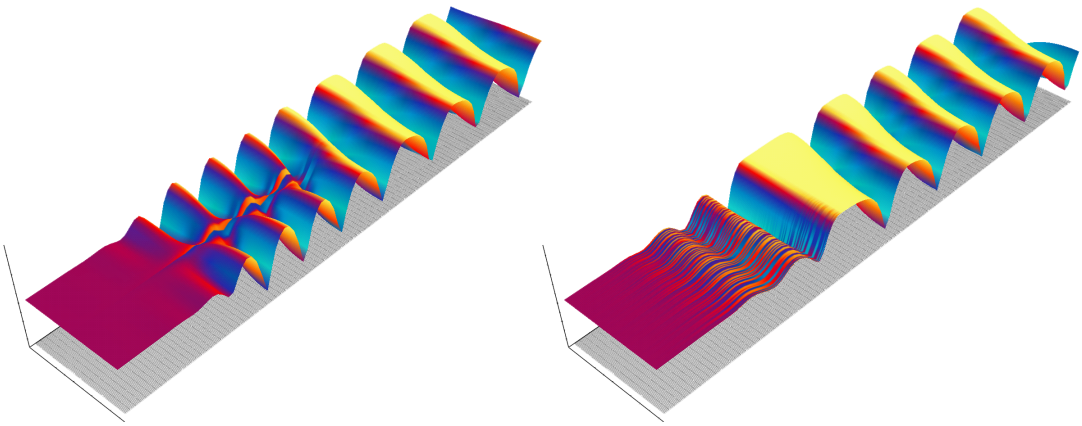

FIG. 4.3: A first mode standing wave for $d_1 = 0.03$. Left: Initial conditions are the same for both equations, they are constant above and below the critical E_3 with a small discontinuity of height 0.0001 at the middle of the unit interval. Right: Here the initial conditions are randomly distributed around E_3 with a maximal variance of 0.001. The same asymmetric waveform establishes itself.

For a diffusion coefficient $d_1 = 0.03$ a first mode standing wave establishes itself which is asymmetric insofar as its amplitude is larger at one side of the boundary than at the other (see FIGURE 4.3).

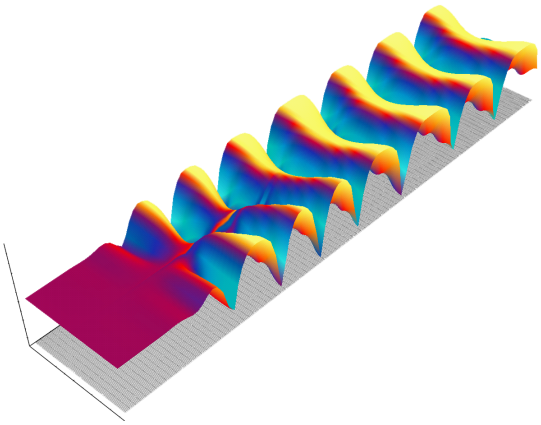

FIG. 4.4: A second mode standing wave for $d_1 = 0.01$. The initial conditions are the same as in the left part of FIGURE 4.3.

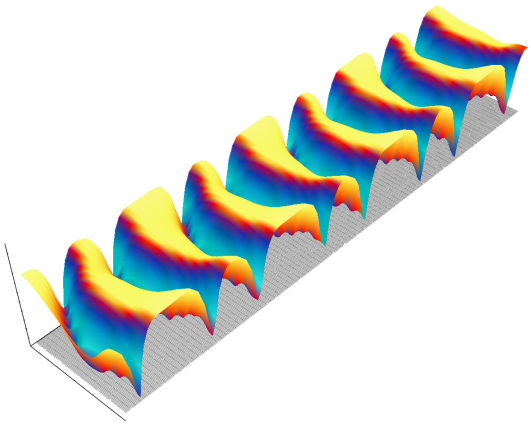

FIG. 4.5: Period doubling. Since it takes a much longer time until this attractor is established, the figure shows 500 time steps when the waveform is reached, comparable to the initial 500 steps of the previous figures ($d_1 = 0.005$).

Then there is a well-separated gap where the system behaves again like the kinetic system which has no other attractor than the CO-poisoned state.
For $0.013 > d_1 > 0.009$, however, there is again a spatio-temporal attractor of a now symmetric standing wave resembling a second mode oscillation. Again its amplitude is largest at the boundary and much smaller in the middle of the domain.
Further diminishing the diffusion coefficients leads to a period doubling for example at $d_1 = 0.005$ rather than to a higher spatial mode (see FIGURE 4.5). For even smaller d_1 (and increasing the number of gridpoints appropriately) this leads to unpredictable chaotic behavior, and finally there are no other attractors found than the constant E_1.

4.3 Results in Two Space Dimensions

For two-dimensional computations of temporally oscillating attractors animated sequences better show the temporal development. In order to interpret the figures on the following pages, imagine that light blue parts are moving upwards whereas light yellow parts move down. Periodicity comes into play because of the dynamics of the problem: When moving upwards, the color changes from blue to yellow. This behavior can already be observed in the (x,t)-plots of the one-dimensional computations and is a result of the nonlinear dynamic of the reaction. When the catalytic activity is high, the reaction rate is also high, and this diminishes the coverages of the adsorbed reactants. Below the threshold of critical coverages, the catalytic activity decreases, and the adsorption of the reactants predominates the loss by the reaction.

Thereby the curly patterns in FIGURES 4.9 to 4.12 are spiraling around their respective cores.
The missing row surface structure which causes an anisotropy of the diffusion can be scaled out, see SECTION 2.4. Target patterns and spirals which are elongated in the direction of the missing row appear circular in the new coordinates.
Due to the symmetry inherent in the problem setting, only one eighth of the following figures is computed, namely a triangle from the center of the displayed domain to one corner and the middle of an edge. For a better image presentation the reflection of the data is done by the graphics program.
The initial data is taken close to the unstable constant solution E_3 and is randomly distributed at level 0.5 with a maximal variance of 0.0001. The difference to the one-dimensional case lies in the a-equation: Various initial data are tested on their capability of revealing comparable attractors. They indeed have the same wavelength or develop spiraling cores of the same size in case that initially there are connected clusters above and below the critical a-coordinate of E_3. This corresponds to the idea of the catalytic activity stemming from a certain surface structure. Such structures must have a certain extension to be recognized.
The scenario remains the same as in the one-dimensional case in so far that diminishing the diffusion coefficient is reflected by a decrease of the wavelength. No period doubling is detected in two space dimensions, spiral cores arise instead.

Discussion

The kinetic parameters are fixed to the situation of a globally attracting fixed point E_1 in order to gain insight into the effects of the surface diffusion of a single reactant on the computed solution.
The diffusion is temperature dependent, and the lower the temperature is the smaller is the diffusion coefficient. This corresponds to the experimental observations described in CHAPTER 2 in so far that the standing wave patterns are detected for a much higher temperature [1] (about 550K, see FIGURE 2.1 on page 7) than the spirals (T=448K, compare FIGURE 2.12 on page 21).

The one-dimensional computations only give a first impression of the effect of a diffusion operator in the u-equation. Irregular behavior that begins as period doubling is found for small diffusion coefficients (or large domains) in this setting.
For the same diffusion coefficient in the two-dimensional case very regular periodic attractors are found. They correspond to higher modes of spatial wavelength.
Finally spatio-temporally periodic solutions coexist with an area where a constant (poisoned) solution is established. But it is not at all clear if this phenomenon depends on the discretization that turns the PDE problem into a finite dimensional system of ordinary differential equations.

[1] Temperature also changes the kinetic parameters but these are as well controlled by the partial pressure. The experimentalist will always adjust the partial pressures of the reactants to values for which the phenomenom is best observed.

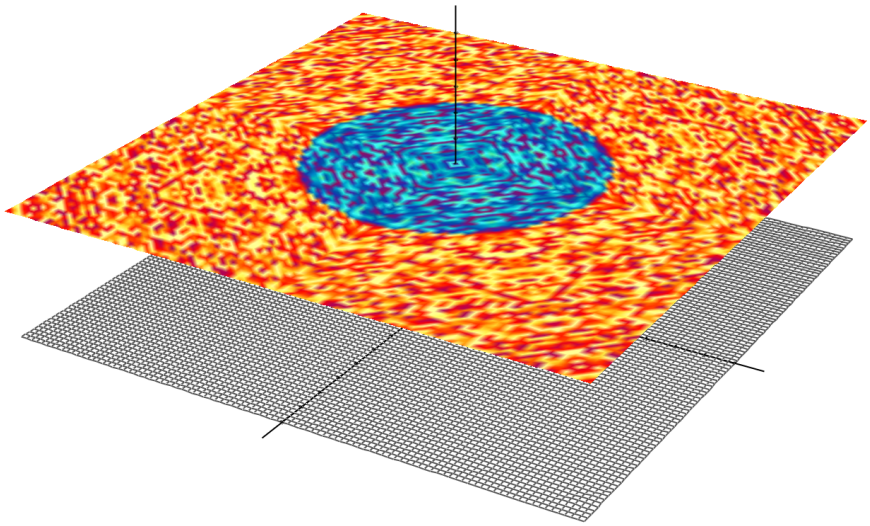

FIG. 4.6: Initial conditions for the following figures are all as shown here. The height above the grid represents the u-data which is randomly distributed at level 0.5 with a maximal variance of 0.0001. The initial data for the a-equation is shown in color. It is also randomly distributed with the same variance, but in the more blue colored area the data is below, outside the circle it is above 0.5 (the a-coordinate of E_3).

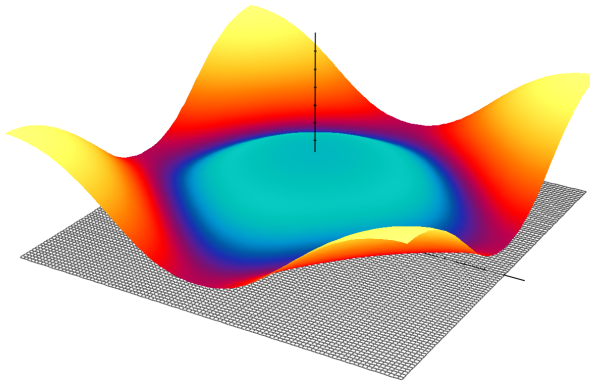

FIG. 4.7: Standing wave solutions are established for the same diffusion coefficients as in the one-dimensional case ($d_1 = 0.03$).

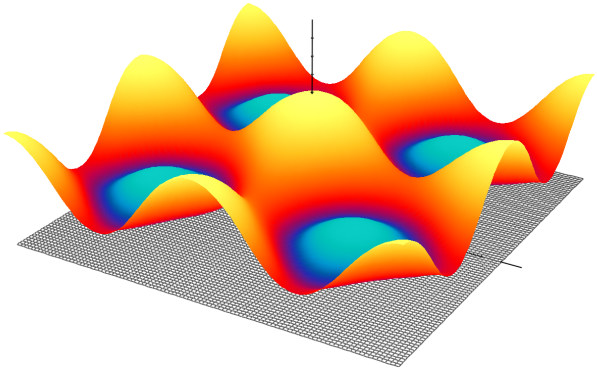

FIG. 4.8: The second mode standing wave solution clearly reveals the reflection process of the graphics representation ($d_1 = 0.01$).

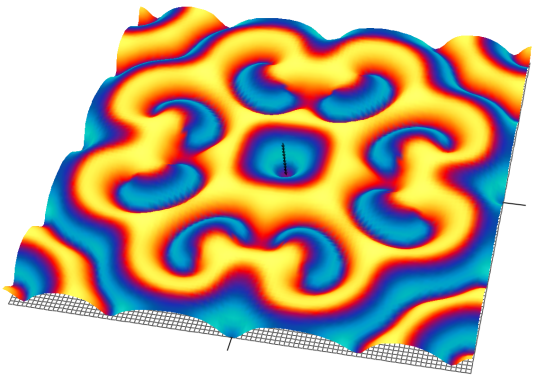

FIG. 4.9: The smaller the diffusion coefficient gets, the shorter is the wavelength. Spiral cores are established to fit the waves into the prescribed area with no flux boundary conditions ($d_1 = 0.001$).

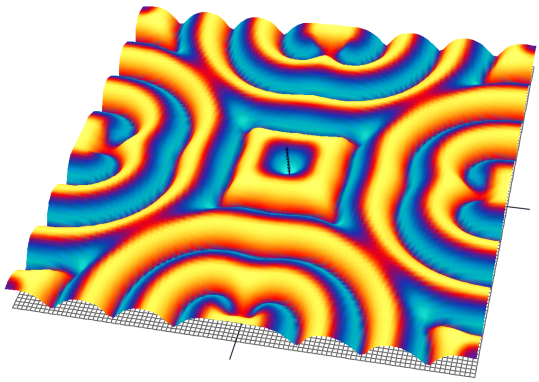

FIG. 4.10: The locations of the spiral cores depend on the initial data, the wavelength is determined by the diffusion coefficient ($d_1 = 0.0005$).

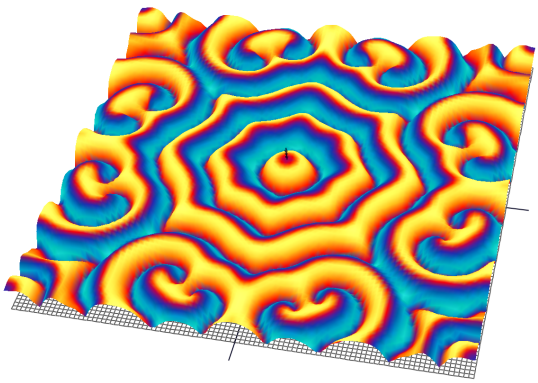

FIG. 4.11: Target and spiral patterns are formed as a result of no-flux boundary conditions ($d_1 = 0.0003$).

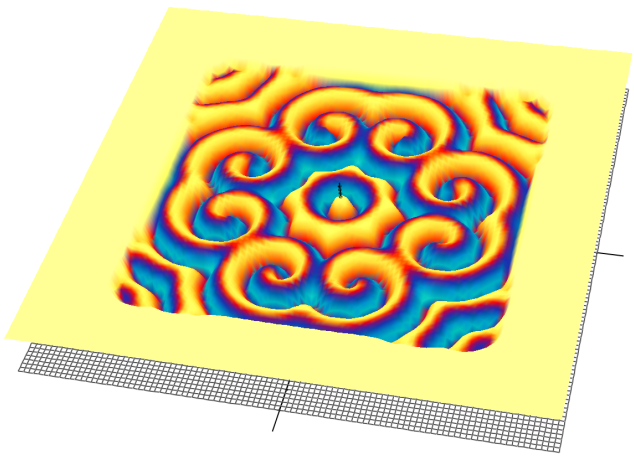

FIG. 4.12: Coexistence of a spiral pattern and an adsorbing state which is poisoned with adsorbed CO and thereby catalytically inactive ($d_1 = 0.0002$).

5 Diffusion-Induced Instabilities

5.1 The Turing Instability

Diffusion-induced instability or Turing instability means that for a reaction-diffusion system of at least two scalar equations there is a spatially constant steady solution which is asymptotically stable in the sense of linearized stability in the space of constant functions. Nevertheless, it is unstable to spatially inhomogeneous perturbations.
Therefore the quotient of the diffusion coefficients d_1 and d_2 has to lie beyond a critical value to be determined out of the eigenvalues of the system. Consider the system

$$\begin{aligned} \dot{u} &= d_1 \Delta u + f_1(u, v, \Lambda) \\ \dot{v} &= d_2 \Delta v + f_2(u, v, \Lambda) \end{aligned} \tag{5.1}$$

with periodic or homogeneous Dirichlet or Neumann boundary conditions and, for the sake of simplicity, on an interval of unit length.

$u(0,t) = u(1,t),$		$v(0,t) = v(1,t)$		Periodic boundary
$u(0,t) = u(1,t) = 0,$		$v(0,t) = v(1,t) = 0$		Dirichlet boundary
$u_x(0,t) = u_x(1,t) = 0,$		$v_x(0,t) = v_x(1,t) = 0$		Neumann boundary

The diffusion coefficients and the kinetic parameters Λ form the set of parameters. Without loss of generality assume the constant zero to be a solution for a fixed set of kinetic parameters. Otherwise the constant solution is shifted to zero. Let A denote the Jacobian of the kinetic equations

$$\begin{aligned} \dot{u} &= f_1(u, v) \\ \dot{v} &= f_2(u, v) \end{aligned} \quad ; \quad A|_{(0,0)} = \begin{pmatrix} \frac{\partial f_1}{\partial u} & \frac{\partial f_1}{\partial v} \\ \frac{\partial f_2}{\partial u} & \frac{\partial f_2}{\partial v} \end{pmatrix} = \begin{pmatrix} a_{11} & a_{12} \\ a_{21} & a_{22} \end{pmatrix}.$$

The general solution of the linear system is expressed as

$$(u(x,t), v(x,t)) = \sum_{m=-\infty}^{\infty} r_m e^{\lambda_m t} (\phi_m(x), \psi_m(x)),$$

$\{\lambda_m, (\phi_m(x), \psi_m(x))\} (m = 0, \pm 1, \pm 2, \cdots)$ are the eigenvalues and eigenfunctions of the following eigenvalue problem

$$\begin{aligned} \lambda \phi &= d_1 \phi_{xx} + a_{11} \phi + a_{12} \psi \\ \lambda \psi &= d_2 \psi_{xx} + a_{21} \phi + a_{22} \psi \end{aligned}$$

with the appropriate boundary conditions. The eigenfunctions of this system are of the form

$$\phi_m(x) = a_m e^{i\mu_m x},\ \psi_m(x) = b_m e^{i\mu_m x}$$

with $\mu_m = \pi m \quad (m = 0, \pm 1, \pm 2, \cdots)$, and the a_m, b_m are not independent of m. That means for $a_m = 1$ there is

$$b_m = \frac{d_1 {\mu_m}^2 - a_{11}}{|a_{12}|} .$$

Subject to homogeneous Dirichlet boundary conditions the set of eigenvalues of $-\Delta$ are $\{{\mu_m}^2{}_D = (\pi m)^2 \mid m = 1, 2, \cdots\}$. Subject to homogeneous Neumann boundary conditions the set of eigenvalues of $-\Delta$ are $\{{\mu_m}^2{}_N = (\pi m)^2 \mid m = 0, 1, 2, \cdots\}$. For periodic boundary conditions or the flux on S^1, that is the sphere, all these eigenvalues are double except that of zero.

Consider solely the kinetic system. The eigenvalues of a linearized planar system are the roots of the characteristic polynomial

$$\chi_A(\lambda) = \lambda^2 - \mathrm{tr}A\ \lambda + \mathrm{det}A = 0$$

over the real field with possibly complex conjugate solutions. Since it is required that the zero solution is asymptotically stable, the trace of A is negative while $\mathrm{det}A$ is positive. The linearization of the kinetic equations together with the Laplace operator is denoted by

$$\tilde{A}|_{(0,0)} = \begin{pmatrix} a_{11} - d_1 {\mu_m}^2 & a_{12} \\ a_{21} & a_{22} - d_2 {\mu_m}^2 \end{pmatrix} .$$

The trace is diminished $\mathrm{tr}\tilde{A} = \mathrm{tr}A - (d_1 + d_2){\mu_m}^2$ and the determinant is altered to $\mathrm{det}\tilde{A} = \mathrm{det}A - (a_{11}d_2 + a_{22}d_1){\mu_m}^2 + d_1 d_2 {\mu_m}^4$.
Since the eigenvalues ${\mu_m}^2$ of $-\Delta$ are always real positive scalars, and the diffusion coefficients are positive, $\mathrm{tr}\tilde{A} < \mathrm{tr}A < 0$.
The determinant $\mathrm{det}\tilde{A}$ is a quadratic polynomial in ${\mu_m}^2$ and may become negative although not for $d_1 = d_2 = \mathbf{d}$. Then $\mathrm{det}\tilde{A} = \mathrm{det}A - \mathrm{tr}A\ \mathbf{d}{\mu_m}^2 + \mathbf{d}^2 {\mu_m}^4$ is always positive for positive determinant and negative trace of A.

But for unequal diffusion coefficients there are two positive real roots of $\mathrm{det}\tilde{A} = 0$, namely,

$$\nu^{\pm} = \frac{1}{d_1 d_2}\left(a_{11}d_2 + a_{22}d_1 \pm \sqrt{(a_{11}d_2 + a_{22}d_1)^2 - 4\mathrm{det}A\ d_1 d_2}\right)$$

if and only if

$$a_{11}d_2 + a_{22}d_1 > 0$$

and

$$\mathcal{D} \equiv (a_{11}d_2 + a_{22}d_1)^2 - 4\det A\ d_1d_2 > 0.$$

Solving $\det\tilde{A}<0$, the roots $\nu^{\pm}$ give an upper and lower bound

$$\nu^- < {\mu_m}^2 < \nu^+$$

such that the following theorem holds.

Theorem 5.1 *Assume that the eigenvalue problem satisfies* $-\mathrm{tr}A>0$, $\det A>0$ *and* $\det\tilde{A}<0$. *Then the* m^{th} *eigenvalue* λ_m *has a positive real part if and only if the* m^{th} *spatial frequency* $\mu_m \equiv \pi m$ *satisfies the inequality* $\nu^- < {\mu_m}^2 < \nu^+$.

This shows that the spatially constant solution is unstable to perturbations with nonconstant functions of spatial frequency in the above interval.
In terms of bifurcation this means that a pair of diffusion coefficients (d_1,d_2) satisfies

$$\det\tilde{A}(\mu_m, d_1, d_2) = d_1d_2{\mu_m}^4 - (a_{11}d_2 + a_{22}d_1){\mu_m}^2 + \det A = 0.$$

This is the required degeneracy that does no longer allow to apply the Implicit Function Theorem. At such a point there are multiple solutions.
This equality yields a curve of critical parameters for every ${\mu_m}^2 \in \mathrm{spec}(-\Delta)$ in the parameter space $(d_1,d_2)\in\mathbb{R}^2_+$ of the form

$$d_2^*(\mu_m, d_1) = \frac{a_{22}d_1{\mu_m}^2 - \det A}{d_1{\mu_m}^4 - a_{11}{\mu_m}^2}.$$

The principal eigenvalue with respect to Neumann boundary conditions ${\mu_m}^2=0$ is not within the bounds $\nu^{\pm}$, so that perturbation with the corresponding eigenfunction $\mathbb{1}$ settles again to the constant solution.
For Neumann boundary conditions it is therefore not the principal eigenvalue but $\mu_1=\pi^2$ that will yield a nonconstant steady solution. Note that the corresponding eigenfunction changes sign. The solution for an appropriate initial value problem is always a layered solution with values above and below zero.
Consider d_1 to be fixed with $d_1 >> d_2$, then d_2 serves as the bifurcation parameter. For $d_2 < d_2^*$, the monolayered solution is stable whereas all other multilayered solutions remain unstable. The function $u(x,t)$ will stay close to the destabilized zero solution, but for the v-equation to be a bounded solution it is not sufficient to look at the linearization in an equilibrium but at the System (5.1). The function f_2 should be of sigmoidal shape.

The literature on the matter is vast; here only a few of those articles related to the topic of bifurcation, standing waves or applications to catalytic reactions are mentioned. See for example Maginu [35] who proves a stable stationary wave solution considering the "waveform", since it is not possible to localize the wave itself.

NISHIURA [39] investigates the case of recovering the stability of the branches for the different spatial modes from the singular shadow edge with singular perturbation theory. Further investigations with this method can be found in [16].
In all these settings the trivial solution is stable for zero mode perturbations.
KOPELL and HOWARD [28] consider the cases when the trivial solution is unstable and document numerical results of standing wave solutions for the Neumann case.

LAKOŠ and TERMAN [33] consider bifurcation from the constant zero solution to a positive nonconstant solution in the Dirichlet and Neumann case regardless of the asymptotic behavior of zero in the kinetic system. Their result is that there are no such steady solutions of only one sign for a reaction-diffusion system of two equations in the Neumann case. Their conclusion nevertheless has to be corrected: They refer to the mathematical models of isothermal catalytic processes as proposed by the group of ERTL. Since the experiment also shows steady nonconstant patterns as described in [26], they claim that applying their result to these models excludes such solutions. Therefore they demand a change of the spatial coupling from a simple (and linear) Fick-type surface diffusion to diffusion models for surfaces that are crowded with adsorbed species.
First of all, if zero is the constant solution from which nonconstant stationary solutions shall bifurcate, then the surface is far from being crowded. But indeed, all these models have multiple constant solutions, and in order to apply a local bifurcation theory it is more natural to choose a positive solution. So, secondly, if such a constant and positive solution is shifted to zero for convenience, it is not appropriate to look only for stationary nonconstant solutions lying above. Solutions with changing signs still mean positive concentrations when shifted back to the original problem.
So their argument dealing with the principal eigenvalue having an eigenfunction of one sign (Krein-Ruthman-Theorem) does not apply to exclude such steady state solutions in the Neumann case. Singular perturbation theory tells about how multi-layered solutions can be constructed and how they recover their stability (see for example NISHIURA [39] who investigated the case of recovering the stability from the singular shadow edge when varying the diffusion coefficients).
A last criticism considers the diagonal entries in the linearization of the kinetic equations. If both of them, a_{11} and a_{22}, are negative, it is impossible to arrange a change of sign of eigenvalues of the reaction-diffusion system by varying the diffusion coefficients d_1 or d_2 (see TABLE 5.1). The bifurcation set S in their article is empty then. So their proof can be essentially shortened since they need not to consider any of the cases where the set S is empty to prove their theorem 1.3.

5.2 Time-Periodic Turing Solution

With regard to the phenomena of spatio-temporal oscillations, it is quite natural to ask if there are bifurcations from a stable zero solution to periodical solutions.
In the Neumann case to get a spatial pattern one has to avoid the principal eigenvalue, which is zero, because it belongs to the eigenfunction that is the constant solution $\mathbb{1}$.

This is not so in the Dirichlet case, but anyhow, the trace of $\tilde{A}$ has to become zero to get a Hopf bifurcation for a two variables system. Then the real part of the eigenvalue crosses the imaginary axis. This is not possible for any pair (d_1,d_2) unless the trace of the linearization of the kinetic equations is nonnegative or at least zero. For $\mathrm{tr}A = 0$ there is the Hopf bifurcation for the purely kinetic system of ordinary differential equations already and one has to deal with oscillations of constant solutions.
Since most of the realistic models involve a lot of species for which kinetic equations can be imposed, it seems to be rather artificial to be restricted to planar systems. Increasing the number of equations frees from being limited to the case of $\mathrm{tr}A = 0$. The eigenvalue condition for the infinite dimensional case of the Hopf bifurcation (see CRANDALL and RABINOWITZ [10]) can then be verified for negative $\mathrm{tr}A$.
A wave bifurcation is a supercritical Hopf bifurcation from a stable steady constant solution to a stable periodic and nonconstant solution. The bifurcating solution in the case of Neumann boundary conditions then is a standing wave solution that is periodical in space and time. In a reaction-diffusion system there are a linear differential operator and a dynamic part that compete against each other. The constant solution is an equilibrium point of the kinetic system. The aim is to destabilize this solution by diffusion coefficients, as in the case of the classical *Turing Instability*, where a single eigenvalue becomes positive and the bifurcating solution is a nonconstant steady state. If the real part of a single pair of complex eigenvalues of the linearization of the whole system at this point crosses the imaginary axis and the bifurcation is supercritical, there exists a nonconstant time-periodic solution.
It is not possible to get a wave bifurcation for a two variables system (see TURING [45], and therein the cases e) and f): *e) Oscillatory case with a finite wave-length and f) Oscillatory case with extreme short wave-length, [...] possibilities [that] can only occur with three or more morphogens. [...] no attempt was made to develop formulae for these.*).
The attempt is now to give formal conditions for the dynamics that make it possible to arrange a destabilization of a constant solution for a three variables system. The main idea is to compare the Jacobian A of the kinetic system to the linearization $\tilde{A}$ of the PDE system at a constant solution.

5.3 Routh-Hurwitz Theory

The number of eigenvalues with positive real part of a linearization is the number of roots in the right half plane of its characteristic polynomial. This number can be computed with the help of the Routh-Hurwitz Theorem.

Theorem 5.2 (Routh-Hurwitz) *The number k of roots of the real polynomial $f(z) = a_0z^n+b_0z^{n-1}+a_1z^{n-2}+b_1z^{n-3}+\cdots \quad (a_0 \neq 0)$ which lie in the right half plane is given by the formula*

$$k = V\left(a_0, \Delta_1, \frac{\Delta_2}{\Delta_1}, \frac{\Delta_3}{\Delta_2}, \cdots, \frac{\Delta_n}{\Delta_{n-1}}\right)$$

or equivalently

$$k = V(a_0, \Delta_1, \Delta_3, \cdots) + V(1, \Delta_2, \Delta_4, \cdots)$$

with Δ_i, $i=1,\cdots,n$ *the successive principal minors of a square matrix* H *of order* n, *and* V *the number of changes of sign of adjacent members in a finite sequence* (GANTMACHER [17], p. 230).

For a system of N equations the characteristic polynomial is the sum of the symmetric functions $(-1)^i\sigma_i(\lambda)^{N-i}$ with alternating signs.

$$\chi_A(\lambda) = \lambda^N - \sigma_1\lambda^{N-1} + \cdots + (-1)^i\sigma_i\lambda^{N-i} + \cdots + (-1)^N\sigma_N\lambda^0 = 0.$$

The matrix H called *Hurwitz matrix* is filled according to the Hurwitz scheme with the coefficients of the characteristic polynomial. It is a square matrix of order N.

$$H = \begin{pmatrix} -\sigma_1 & -\sigma_3 & -\sigma_5 & \cdots & \cdots & 0 \\ 1 & \sigma_2 & \sigma_4 & \sigma_6 & \cdots & 0 \\ 0 & -\sigma_1 & -\sigma_3 & -\sigma_5 & \cdots & \\ 0 & 1 & \sigma_2 & \sigma_4 & \cdots & \cdot \\ 0 & 0 & -\sigma_1 & -\sigma_3 & \cdots & \cdot \\ 0 & 0 & 1 & \cdots & \cdots & \cdot \\ & \cdots & & \cdots & (-1)^{N-1}\sigma_{N-1} & 0 \\ & \cdots & & \cdots & (-1)^{N-2}\sigma_{N-2} & (-1)^N\sigma_N \end{pmatrix}$$

Their principale minors Δ_i, $i=1,\cdots,N$ are the so called *Hurwitz determinants*.

The Routh-Hurwitz Criterion. In order for all roots of the real polynomial $f(z) = z^N + \cdots$ $(a_0 = 1 > 0)$ to have negative real parts it is necessary and sufficient that the inequalities

$$\Delta_1 > 0, \Delta_2 > 0, \cdots, \Delta_N > 0$$

hold.

Theorem 5.3 *An odd number* k *of eigenvalues in the right half plane is equivalent to* $(-1)^N \det A < 0$.

Proof:

N even;

$$\begin{aligned} k = \quad & V(1,\Delta_1) + V(\Delta_1,\Delta_3) + \cdots + V(\Delta_{N-3},\Delta_{N-1}) \\ & + V(1,\Delta_2) + V(\Delta_2,\Delta_4) + \cdots + V(\Delta_{N-2},\Delta_N) \end{aligned}$$

N odd;

$$\begin{aligned} k = \quad & V(1,\Delta_1) + V(\Delta_1,\Delta_3) + \cdots + V(\Delta_{N-4},\Delta_{N-2}) + V(\Delta_{N-2},\Delta_N) \\ & + V(1,\Delta_2) + V(\Delta_2,\Delta_4) + \cdots + V(\Delta_{N-3},\Delta_{N-1}) \end{aligned}$$

$\Delta_N = \Delta_{N-1}(-1)^N \det A$ for all N. Let $(-1)^N \det A > 0$. Let $k=1$ and $\Delta_{-1}=1$ and $\Delta_0 = 1$. Then there is exactly one i with $V(\Delta_{i-2},\Delta_i)=1$ and $V(\Delta_{j-2},\Delta_j)=0$ for $j \neq i$ with $i,j \in \{1,\ldots,N\}$. In the first case let N and i be even numbers, then this is equivalent to $\Delta_j > 0$ for $j < i$ or j odd, and $\Delta_j < 0$ for $j \geq i$ and j even. Then $\Delta_N < 0 \Leftrightarrow \Delta_{N-1} < 0$. This contradicts $N-1$ odd and therefore $\Delta_{N-1} > 0$.
The other cases are similar and left to the reader. The case where k is even will not result in $\Delta_N < 0$ since changing sign twice is not recognized by the largest Hurwitz determinant. Δ_N and Δ_{N-1} are of the same sign and therefore $(-1)^N \det A > 0$. The case where k is odd can always be reduced to $k=1$. □

The idea behind the wave bifurcation uses Orlando's formula (see [17])

$$\Delta_{N-1} = (-1)^{\frac{N(N-1)}{2}} \prod_{i<k}^{1\ldots N} (\lambda_i + \lambda_k)$$

from which follows that $\Delta_{N-1}=0$ if and only if the sum of at least one pair of roots of the polynomial is zero. In particular this is true for a conjugate pair of pure imaginary roots. Together with the Routh-Hurwitz Theorem the case of a single pair of pure imaginary roots and all other roots with negative real part can be characterized by:

$$\begin{aligned} &\text{(a)} \quad \Delta_i > 0 \quad \text{for} \quad i = 1,\ldots,N-2 \\ &\text{(b)} \quad \Delta_{N-1} = 0 \\ &\text{(c)} \quad (-1)^N \det A > 0 \end{aligned} \tag{5.2}$$

The last inequality is needed to keep away from zero as a (multiple) root.

5.3.1 Application to Reaction-Diffusion Systems

The following notations are used: Let the tilde $\sim$ always denote the PDE system and let the index m indicate the respect to the appropriate mode via the eigenvalue ${\mu_m}^2$ of the negative Laplace operator with Neumann boundary conditions. If Ω is the unit interval, $-\Delta\xi_m = {\mu_m}^2 \xi_m$ results in $\xi_m = cos(\pi m x)$ the eigenfunction for the eigenvalue ${\mu_m}^2 = (\pi m)^2, m \in \mathbb{N}_0$. Claiming that all eigenfunctions of $\tilde{A}$ have the form $(c_1,c_2,c_3)^t \xi_m$ with coefficients $c_i \in \mathbb{R}$, they form three-dimensional functional subspaces of the solution space. The diffusion coefficients appear in the Jacobian as $d_{im} := d_i {\mu_m}^2$, $i = 1,\ldots,N$.

$$\tilde{A}(\mu_m) = A - D(\mu_m) = (a_{ij})_{i,j\in\{1,\ldots,N\}} - diag(d_{1m},\ldots,d_{Nm})$$

The trace of a submatrix of A consisting of the i_1 and i_2 column and row will be denoted as $\mathrm{tr}(A_{i_1 i_2})$. The minors with the same columns as rows will be abbreviated with $|A_{i_1 i_2}|$. For reaction-diffusion systems, the number of eigenvalues in the right half plane is the sum

$$\tilde{k} := \sum_{m=0}^{\infty} k_m,$$

where the nonnegative integer k_m belongs to the m^{th} spatial mode. Therefore one has to compute the Hurwitz determinants of all $\tilde{A}(\mu_m)$. The sum $\tilde{k}$ is zero if and only if the sign conditions are fulfilled for all m, that is $\tilde{\Delta}_i(\mu_m) > 0$, $i = 1,\ldots,N$ for all m, or, in short, $\tilde{\Delta}_i > 0$. If no special mode is explicitly indicated, this notation refers to all modes.

Theorem 5.4 *A constant steady state solution of a reaction-diffusion system that is stable against spatially constant perturbations and has equal diffusion coefficients cannot be destabilized when perturbed inhomogeneously.*

Proof:
This can be seen easily when comparing the characteristic polynomial of A with $\tilde{A} = A - D$ where D is a diagonal square matrix of order N with equal entries $D := diag(\mathbf{d},\ldots,\mathbf{d})$.

$$\begin{aligned} \chi_A(\lambda) &= \sum_{i=0}^{N} (-1)^i \sigma_i \lambda^{N-i} \\ \chi_{(A-D)}(\lambda) = \chi_A(\lambda + \mathbf{d}) &= \sum_{i=0}^{N} (-1)^i \sigma_i (\lambda + \mathbf{d})^{N-i} \end{aligned}$$

On condition that the roots z_i of $\chi_A(\lambda)$ all have negative real parts, the roots $\tilde{z}_i$ of $\chi_{(A-D)}(\lambda)$ are $\tilde{z}_i = z_i - \mathbf{d}$ and have more negative real parts. □

5.3.1.1 Planar Systems

The Hurwitz determinants for $N=2$ give simple conditions for stable nodes (see TABLE 5.1).

$$H = \begin{pmatrix} -\mathrm{tr}A & 0 \\ 1 & \det A \end{pmatrix}, \qquad \begin{aligned} \Delta_1 &= -\mathrm{tr}A &&> 0 \\ \Delta_2 &= -\mathrm{tr}A \det A &&> 0 \end{aligned}$$

Two variables reaction-diffusion systems with *activator-inhibitor* kinetic are widely studied (see for example [16]). The variable with positive diagonal entry in the Jacobian is called the activator, the variable with negative entry is the inhibitor. The necessary conditions on the kinetic equations to yield a Turing bifurcation are:

Conditions for Turing Bifurcation:

(c1) $-\mathrm{tr}A > 0$

(c2) $\det A > 0$

(c3) $a_{22} > 0$

Then an appropriate diffusion coefficient d_1 can make the term $a_{11}d_2+a_{22}d_1$ positive, although the trace $a_{11}+a_{22}$ is negative, and thereby change the sign of the determinant in the presence of spatial inhomogeneities. This is often abbreviated in the rule:

$$\frac{d_1}{d_2} > \frac{-a_{11}}{a_{22}} > 1 \qquad \Rightarrow \qquad \text{The inhibitor has to diffuse faster.}$$

Remark 5.1 (c1) *and* (c2) *guarantee a stable equilibrium,* (c3) *demands the presence of an activator, in the case of two variables systems just a positive diagonal entry in the linearization of the second equation, the* activator *equation.*

For a wave bifurcation, when $\tilde{k}$ increases by 2 and $\tilde{k}_m$ is even, THEOREM 5.3 shows that then $(-1)^N \det\tilde{A}(\mu_m)$ is positive. In two variables systems, the Hopf bifurcation can only be realized when the trace becomes positive. But in the regular as well as in the singular perturbation, that is $d_1 \to \infty$ or $d_2^{-1} \to \infty$, the trace is always diminished by a diffusion operator, so that $\mathrm{tr}A$ has to be nonnegative, contradicting the requirement of a stable equilibrium. The number of equations has to be increased to get a diffusion-induced supercritical Hopf bifurcation.

5.3.1.2 Systems of Three Equations

The eigenvalues of a system of three equations are the roots of

$$\chi_A(\lambda) = \lambda^3 - \mathrm{tr}A\ \lambda^2 + \sum_{1\le i<j\le 3} |A_{ij}|\ \lambda - \det A = 0.$$

and for $N{=}3$ the Hurwitz matrix is

$$H = \begin{pmatrix} -\mathrm{tr}A & -\det A & 0 \\ 1 & \sum|A_{ij}| & 0 \\ 0 & -\mathrm{tr}A & -\det A \end{pmatrix} = \begin{pmatrix} -\sigma_1 & -\sigma_3 & 0 \\ 1 & \sigma_2 & 0 \\ 0 & -\sigma_1 & -\sigma_3 \end{pmatrix}$$

with successive Hurwitz determinants to be computed using the coefficients $(-1)^i\sigma_i$, $i{=}1,2,3$ of the symmetric functions.

$$\begin{array}{rcll} \Delta_1 & = & -\mathrm{tr}A & = -\sigma_1 \\ \Delta_2 & = & -\mathrm{tr}A(\sum|A_{ij}|) + \det A & = -\sigma_1\sigma_2 + \sigma_3 \\ \Delta_3 & = & -\Delta_2\ \det A & = -(-\sigma_1\sigma_2 + \sigma_3)\sigma_3 \end{array}$$

All three eigenvalues have negative real parts if $\Delta_i > 0$ for $i{=}1,2,3$ (Routh-Hurwitz Criterion). This is equivalent to

$$\begin{array}{rcl} -\sigma_1 & > & 0 \\ -\sigma_1\sigma_2 + \sigma_3 & > & 0 \\ -\sigma_3 & > & 0\ . \end{array}$$

The conditions $-\sigma_1 > 0$ and $-\sigma_3 > 0$ are as easy to check as in the case of planar systems. The second Hurwitz determinant is critical at the surface $\sigma_1\sigma_2 = \sigma_3$ which is a hyperbolic paraboloid. For a kinetic system of three equations the number k computes as follows:

$$\begin{aligned} k = V\left(1, \Delta_1, \frac{\Delta_2}{\Delta_1}, \frac{\Delta_3}{\Delta_2}\right) &= V(1, \Delta_1, \Delta_3) + V(1, \Delta_2) \\ &= V(1, \Delta_1) + V(\Delta_1, \Delta_3) + V(1, \Delta_2) \end{aligned}$$

To illustrate the formal computations of k, the following figures give an impression where the regions of stable nodes are ($k=0$, shaded areas) and which lines or surfaces separate the regions for the various numbers of k in two and three variables systems. In contrast to FIGURE 5.1 the three variables system in FIGURE 5.2 shows the possibility of a linearization A having a negative trace and a determinant indicating an even number k, without necessarily being in the area of stable nodes.

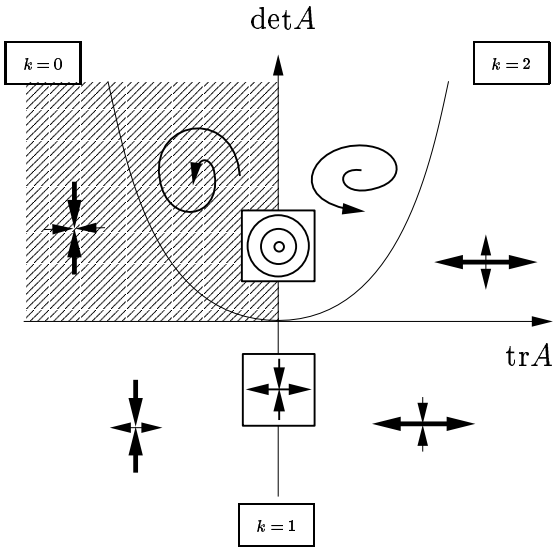

FIG. 5.1: For a two variables system a sign change of the trace results in an increase of k by 2.

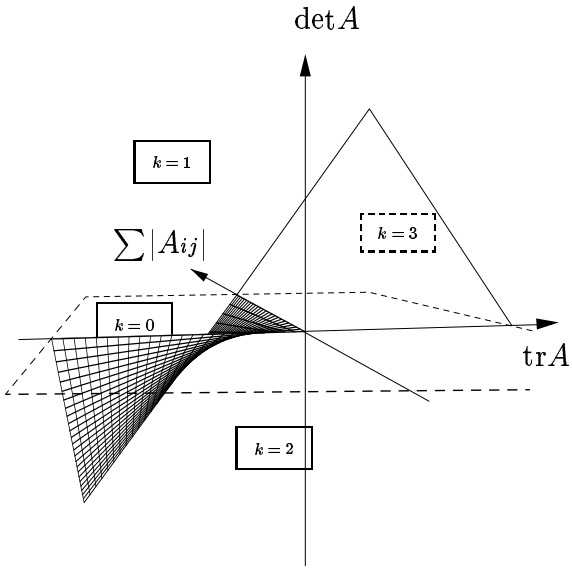

FIG. 5.2: For a three variables system the surface $\sigma_1\sigma_2 = \sigma_3$, $\sigma_2 > 0$, has to be crossed to increase k by 2.

Crossing the surface $\sigma_1\sigma_2 = \sigma_3$ has no effect on k for $\sigma_2 < 0$. Here only the sign of $\sigma_3 = \det A$ decides if k is one or two.

Qualitatively, the pictures do not change when considering $\tilde{A}(\mu_m)$ and $\tilde{k}_m$ instead of A and k, respectively.

If a single diffusion coefficient is able to induce a destabilization of the stable zero solution, then k is zero and at least one $\tilde{k}_m$ has become nonzero on varying this coefficient.

On condition that $-\mathrm{tr}A > 0$, $(V(1,\Delta_1) = 0)$ it yields $-\mathrm{tr}\tilde{A} > -\mathrm{tr}A > 0$, since diffusion only decreases the trace. Therefore $-\mathrm{tr}\tilde{A} = \tilde{\Delta}_1$ is always positive. Since $V(\tilde{\Delta}_1, \tilde{\Delta}_3) = 0$ is

equivalent to $(-\mathrm{tr}\tilde{A})(-\det\tilde{A})\tilde{\Delta}_2 > 0$, the expressions $-\det\tilde{A}$ and $\tilde{\Delta}_2$ have to be of the same sign in order not to change the sum $\tilde{k}$.
TABLE 5.2 on the facing page lists the various cases for $\tilde{k} \leq 2$, not considering the case of $\det\tilde{A}(\mu_j) < 0$ for exactly two modes $j = m$ and $j = n$. If a dependency on a special mode μ_m is indicated, for all other modes the same behavior as in the case of stable nodes is assumed.
What can be observed by now is that a change in sign of $\det\tilde{A}(\mu_m)$ for a single m gives exactly one positive real eigenvalue as well as in the two-dimensional case (see TABLE 5.1). In general a Turing bifurcation from a stable constant solution to a stable steady but nonconstant solution can be decided by the sign of the determinant.
Consider the case when $\tilde{k}$ increases by 2 in the system of three equations. This is equivalent to the question: Can diffusion change the sign of the second Hurwitz determinant without changing the sign of the first and third?
That means that $-\mathrm{tr}\tilde{A} > 0$ and $-\det\tilde{A} > 0$ for all m whereas

$$\tilde{\Delta}_2(\mu_m) \;=\; -\mathrm{tr}\tilde{A}(\mu_m) \sum_{1 \leq i < j \leq 3} |\tilde{A}(\mu_m)_{ij}| \;+\; \det\tilde{A}(\mu_m)$$

changes sign for a single m, but $\tilde{\Delta}_2 > 0$ for all $j \neq m$. If this is the case, generically two complex conjugate roots cross the imaginary axis and the equilibrium is no longer asymptotically stable. A critical diffusion coefficient leads to $\tilde{\Delta}_2(\mu_m, d_i^*) = 0$.

Remark 5.2 *The case of negative* $\mathrm{tr}A$ *and thereby negative* $\mathrm{tr}\tilde{A}$ *is assumed. Generically either* $\det\tilde{A}(\mu_m)$ *or* $\tilde{\Delta}_2(\mu_m)$ *changes sign first.*
In the case of a first change of sign of $\det\tilde{A}(\mu_m)$*, this is the usual Turing bifurcation to a steady state solution. If afterwards* $\tilde{\Delta}_2$ *changes sign, this can only happen for* $\sum|\tilde{A}(\mu_m)_{ij}| < 0$ *where it has no effect on* $\tilde{k}_m$*. If the sign of* $\det\tilde{A}(\mu_m)$ *changes back in this area, two positive (real) eigenvalues exist, which of course can meet and become a complex conjugate pair again. But such oscillating solutions do not necessarily give rise to a time-periodic solution.*
In case of $\tilde{\Delta}_2(\mu_m)$ *changing sign first while* $tr\tilde{A}$ *and* $det\tilde{A}$ *are negative, the number* $\tilde{k}$ *of eigenvalues in the right half plane increases by two so that there is a pair of pure imaginary eigenvalues.*

$\tilde{k}=0$	Stable Nodes		
	$V(1,\tilde{\Delta}_1) = 0$ $\wedge\ V(1,\tilde{\Delta}_2) = 0$	$\Leftrightarrow$	$-\mathrm{tr}\tilde{A} > 0$ $\wedge\ \det\tilde{A} > 0$

$\tilde{k}=1$	Turing Type Stationary Solution	$a_{22}>0$	
	$V(1,\tilde{\Delta}_1) = 0$ $\wedge\ V(1,\tilde{\Delta}_2(\mu_m)) = 1$	$\Leftrightarrow$	$-\mathrm{tr}\tilde{A} > 0$ $\wedge\ \det\tilde{A}(\mu_m) < 0$

Tab. 5.1: For two equations only a Turing type steady solution can bifurcate from the stable situation.

$\tilde{k}=0$	Stable Nodes		
	$V(1,\tilde{\Delta}_1) = 0$ $\wedge\ V(\tilde{\Delta}_1,\tilde{\Delta}_3) = 0$ $\wedge\ V(1,\tilde{\Delta}_2) = 0$	$\Leftrightarrow$	$-\mathrm{tr}\tilde{A} > 0$ $\wedge\ -\det\tilde{A} > 0$ $\wedge\ \tilde{\Delta}_2 > 0$

$\tilde{k}=1$	Turing Type Stationary Solution	$\lvert A_{23}\rvert<0$	
	$V(1,\tilde{\Delta}_1) = 0$ $\wedge\ V(\tilde{\Delta}_1,\tilde{\Delta}_3(\mu_m)) = 1$ $\wedge\ V(1,\tilde{\Delta}_2) = 0$	$\Leftrightarrow$	$-\mathrm{tr}\tilde{A} > 0$ $\wedge\ -\det\tilde{A}(\mu_m) < 0$ $\wedge\ \tilde{\Delta}_2 > 0$
or			
	$V(1,\tilde{\Delta}_1) = 0$ $\wedge\ V(\tilde{\Delta}_1,\tilde{\Delta}_3(\mu_m)) = 0$ $\wedge\ V(1,\tilde{\Delta}_2(\mu_m)) = 1$	$\Leftrightarrow$	$-\mathrm{tr}\tilde{A} > 0$ $\wedge\ -\det\tilde{A}(\mu_m) < 0$ $\wedge\ \tilde{\Delta}_2(\mu_m) < 0$

$\tilde{k}=2$	Turing Type Periodic Solution	$\lvert A_{23}\rvert>0$	
	$V(1,\tilde{\Delta}_1) = 0$ $\wedge\ V(\tilde{\Delta}_1,\tilde{\Delta}_3(\mu_m)) = 1$ $\wedge\ V(1,\tilde{\Delta}_2(\mu_m)) = 1$	$\Leftrightarrow$	$-\mathrm{tr}\tilde{A} > 0$ $\wedge\ -\det\tilde{A} > 0$ $\wedge\ \tilde{\Delta}_2(\mu_m) < 0$

Tab. 5.2: For three equations a diffusion-induced periodic solution is possible.

With Orlando's formula it is clear that the eigenvalue condition for the Hopf bifurcation in a three variables system depends on the second Hurwitz determinant.
It is quite easy to see that it is impossible to change the sign of $\tilde{\Delta}_2$ if every element on the diagonal of A is negative and none of the subminors is negative. And with THEOREM 5.4 a change of sign of $\tilde{\Delta}_2$ is also impossible if all diffusion coefficients are equal.
Under these assumptions $\tilde{\sigma}_3 = \det\tilde{A}$, too, cannot change sign, that is, the Turing bifurcation is also not possible.
In terms of σ_i and $\tilde{\sigma}_i$ the Hurwitz determinants of $\tilde{A}$ can be compared explicitly with those of A (d_i here abbreviates d_{im} since the equations refer to all m):

$$\begin{aligned}
\sigma_1 &= \mathrm{tr}A &&= a_{11} + a_{22} + a_{33} \\
\tilde{\sigma}_1 &= \mathrm{tr}\tilde{A} &&= \mathrm{tr}A - (d_1 + d_2 + d_3)
\end{aligned}$$

$$\begin{aligned}
\sigma_2 &= \textstyle\sum |A_{ij}| = &&(a_{11}a_{22} - a_{12}a_{21}) + (a_{11}a_{33} - a_{13}a_{31}) + (a_{22}a_{33} - a_{23}a_{32}) \\
\tilde{\sigma}_2 &= \textstyle\sum |\tilde{A}_{ij}| = &&\textstyle\sum |A_{ij}| - d_1(a_{22} + a_{33} - d_2) - d_2(a_{11} + a_{33} - d_3) - d_3(a_{11} + a_{22} - d_1)
\end{aligned}$$

$$\begin{aligned}
\sigma_3 &= \det A &&= a_{11}a_{22}a_{33} + a_{12}a_{23}a_{31} + a_{13}a_{21}a_{32} - a_{33}a_{12}a_{21} - a_{22}a_{13}a_{31} - a_{11}a_{23}a_{32} \\
\tilde{\sigma}_3 &= \det\tilde{A} &&= \det A - d_1|A_{23}| - d_2|A_{13}| - d_3|A_{12}| + \\
&&&\quad d_1d_2a_{33} + d_1d_3a_{22} + d_2d_3a_{11} - d_1d_2d_3
\end{aligned}$$

The terms of the second Hurwitz determinant $\tilde{\Delta}_2(\mu_m, d_1, d_2, d_3)$ which are not in Δ_2 can cause a change in sign.

$$\begin{aligned}
\tilde{\Delta}_2(\mu_m, d_1, d_2, d_3) = \quad & [2d_1d_2d_3 + (d_1)^2(d_2 + d_3) + (d_2)^2(d_1 + d_3) + (d_3)^2(d_1 + d_2)]\ (\mu_m{}^2)^3 \\
& -[\mathrm{tr}(A_{23})(d_1)^2 + \mathrm{tr}(A_{13})(d_2)^2 + \mathrm{tr}(A_{12})(d_3)^2 + \\
& \quad 2\mathrm{tr}A(d_1d_2 + d_1d_3 + d_2d_3)]\ (\mu_m{}^2)^2 \\
& +[(|A_{12}| + |A_{13}| + \mathrm{tr}(A_{23})\mathrm{tr}A)d_1 + \\
& \quad (|A_{12}| + |A_{23}| + \mathrm{tr}(A_{13})\mathrm{tr}A)d_2 + \\
& \quad (|A_{13}| + |A_{23}| + \mathrm{tr}(A_{12})\mathrm{tr}A)d_3]\ \mu_m{}^2 \\
& + \Delta_2
\end{aligned} \tag{5.3}$$

5.4 Wave Bifurcation in Case of $d_1 \neq 0$

The wave bifurcation cannot occur for systems with less than three equations. However, even in the case of three equations, a rule like that in the case of two equations and *activator-inhibitor kinetic* cannot be read off the Hurwitz determinant $\tilde{\Delta}_{N-1} = \tilde{\Delta}_2$ immediately. In order to derive conditions on the kinetic system that allow a wave bifurcation, consider some positive d_1 and a singular limit with $d_2 \to 0$ and $d_3 \to 0$. The formal limit

$$\begin{aligned}\lim_{\substack{d_2\to 0\\ d_3\to 0}} \tilde{\Delta}_2(\mu_m, d_1, d_2, d_3) &= \tilde{\Delta}_2(\mu_m, d_1, 0, 0)\\ &= -\mathrm{tr}(A_{23})(d_1{\mu_m}^2)^2 + (|A_{12}| + |A_{13}| + \mathrm{tr}(A_{23})\mathrm{tr}A)d_1{\mu_m}^2 + \Delta_2\end{aligned} \tag{5.4}$$

results in a parabola $\tilde{\Delta}_2(\mu_m, d_1, 0, 0) =: \tilde{\Delta}_2(d_1{\mu_m}^2)$ in d_1. The following conditions for a change in sign of $\tilde{\Delta}_2(d_1{\mu_m}^2)$ by the diffusion coefficient d_1 and the m^{th} spatial mode imply wave bifurcation.

Conditions for Wave Bifurcation:

(C1) $-\mathrm{tr}A > 0$

(C2) $\Delta_2 = -\mathrm{tr}A(\sum |A_{ij}|) + \det A > 0$

(C3) $-\det A > 0$

(C4) $-\mathrm{tr}(A_{23}) > 0$

(C5) $-(|A_{12}| + |A_{13}| + \mathrm{tr}(A_{23})\mathrm{tr}A) > 0$

(C6) $(|A_{12}| + |A_{13}| + \mathrm{tr}(A_{23})\mathrm{tr}A)^2 + 4\mathrm{tr}(A_{23})\Delta_2 > 0$

Remark 5.3 *The conditions* (C1) $-$ (C3) *guarantee a stable constant equilibrium of the kinetic system. The normed parabola to be discussed is*

$$\frac{1}{-\mathrm{tr}(A_{23})}\tilde{\Delta}_2(d_1{\mu_m}^2) = (d_1{\mu_m}^2)^2 - \frac{(|A_{12}| + |A_{13}| + \mathrm{tr}(A_{23})\mathrm{tr}A)}{\mathrm{tr}(A_{23})} d_1{\mu_m}^2 - \frac{\Delta_2}{\mathrm{tr}(A_{23})}.$$

This is the normed second Hurwitz determinant depending on the diffusion coefficient d_1 and the m^{th} spatial mode. (C4) *is needed for the right opening of the parabola,* (C5) *is needed for positive real parts of the roots and* (C6) *is sufficient for the existence of two real roots $\nu^{\pm} > 0$. For illustration purposes see* FIGURE *5.3 on page 58.*
Now the second Hurwitz determinant becomes negative for $d_1{\mu_m}^2$ in the open interval (ν^-, ν^+) and this results in complex eigenvalues for the Jacobian $\tilde{A}(\mu_m)$.
Note that all these conditions only concern the kinetic system.

Theorem 5.5 *Let X be an open subset of a real Banach space E. Consider a system of a parabolic and two ordinary differential equations and appropriate boundary conditions such that the right-hand side is $C^2(X^3 \times \mathbb{R}_+, E^3)$.*

$$\begin{aligned} u_{1_t} &= B(u_1, d_1) + g_1(u_1, u_2, u_3)\\ u_{2_t} &= g_2(u_1, u_2, u_3) \qquad \text{in } \Omega \times (0, \mathrm{T}^+)\\ u_{3_t} &= g_3(u_1, u_2, u_3)\end{aligned} \tag{5.5}$$

The spectrum of $-B(\,\cdot\,, d_1)$ is nonnegative, real, simple and discrete. Moreover, it depends strictly monotone on the parameter $d_1 \in \mathbb{R}_+$.

The kinetic system $g:=(g_1,g_2,g_3)$ *has an asymptotically stable constant equilibrium* $E^*=(u_1^*,u_2^*,u_3^*)$, *i.e.* (C1) – (C3) *are satisfied for the linearization* $A|_{E^*}$ *of* g, *and* $B(u_1^*,\cdot)=0$.

If the linearized kinetic system at the constant solution fulfills (C4) – (C6), *then there is a critical parameter* d_1^* *with*

$$\begin{aligned}\tilde{\Delta}_2(d_1^*{\mu_m}^2) &= 0 \quad \text{for } m\\ \tilde{\Delta}_2(d_1^*{\mu_l}^2) &> 0 \quad \text{for } l\neq m\end{aligned}$$

for a single $m\in\mathbb{N}$, *where* ${\mu_m}^2$ *denotes the* m^{th} *eigenvalue of* $-B$. *Furthermore,*

(i) $\{\pm i\omega\}$ *are simple eigenvalues of* $\tilde{A}$, *where* $\omega>0$,

(ii) *there are no eigenvalues of the form* $ik\omega$ *for* $k\in\mathbb{Z}\setminus\{\pm1\}$ *and*

(iii) $\partial_{d_1}\mathrm{Re}\rho(d_1^*)\neq0$, *where* $\rho(d_1)$ *is the unique continuation of the eigenvalue of* $\tilde{A}$ *for* d_1 *in a neighborhood of the critical* d_1^* *satisfying* $\rho(d_1^*)=i\omega$,

and the System (5.5) *has a unique one-parameter family of noncritical nonconstant periodic orbits in an appropriate neighborhood; precisely for* $u:=(u_1,u_2,u_3)$, *the minimal period* T *and the bifurcation parameter* d_1 *it yields*

$$(u(\cdot),T(\cdot),d_1(\cdot)) \in C^1((-\varepsilon,\varepsilon),V\times\mathbb{R}_+\times\mathbb{R}_+)$$

satisfying

$$(u(0),T(0),d_1(0)) = (E^*,\frac{2\pi}{\omega},d_1^*)$$

such that

$$\gamma(s) := \gamma(u(s))$$

is a noncritical nonconstant periodic orbit of System (5.5) *of period* $T(s)$ *passing through* $u(s)\in V$ *for* $0<s<\varepsilon$.

Proof:
The local existence of a bifurcating periodic solution follows from the Hopf bifurcation theorem in infinite dimensions of Crandall and Rabinowitz [10] which can be found in the Appendix A, Theorem A.6. For a slightly different formulation which is more coherent with the above notation, and a concrete stability criterion see Theorem A.7.

The constant solution E^* is a solution for all parameters d_1. Theorem 5.5 (i), i.e. the purely imaginary simple eigenvalues, results from the appropriate signs of an infinite set of Hurwitz determinants which satisfies the conditions (a), (b), and (c) of (5.2) for $N=3$ variables and for each value of the point spectrum. The purely imaginary eigenvalues

are simple because of the assumption that the spectrum of $-B$ only contains simple eigenvalues. Furthermore, $\tilde{\Delta}_2(d_1^* {\mu_m}^2) = 0$ at the critical parameter only for a single $m \in \mathbb{N}$.

$\tilde{\Delta}_1$ is positive for all modes, since a real positive spectrum of $-B$ only diminishes $\mathrm{tr}\tilde{A}$ compared with an already negative $\mathrm{tr}A$ of (C1).

It remains to prove that $-\det\tilde{A}(\mu_m, d_1, 0, 0) > 0$ (see FIGURE 5.2), which guarantees an even number of eigenvalues with positive real part. Consider the following limit:

$$\lim_{\substack{d_2 \to 0 \\ d_3 \to 0}} \Big(-\det\tilde{A}(\mu_m, d_1, d_2, d_3) \Big) =: -\det\tilde{A}(d_1 {\mu_m}^2) = |A_{23}| d_1 {\mu_m}^2 - \det A \qquad (5.6)$$

If $|A_{23}|$ is positive, then $-\det\tilde{A}(d_1 {\mu_m}^2) > -\det A > 0$ for all d_1 and all m, so that there is no change in sign of the determinant. The above conditions already imply that $|A_{23}|$ is positive, and this is proved in the following lemma.

Lemma 5.1 *Let A be such that* (C1) – (C5) *are fulfilled. Then $|A_{23}|$ is positive.*

Proof:

$$\begin{array}{rcl} (\mathrm{C5}) & \Rightarrow & |A_{12}| + |A_{13}| + \mathrm{tr}(A_{23})\mathrm{tr}A < 0 \\ & \Leftrightarrow & |A_{12}| + |A_{13}| < -\mathrm{tr}(A_{23})\mathrm{tr}A \overset{(\mathrm{C1})(\mathrm{C4})}{<} 0 \\ & \Rightarrow & |A_{12}| + |A_{13}| < 0 \end{array}$$

Assume $|A_{23}| \leq 0$, then

$$0 < \mathrm{tr}A\Big(|A_{12}| + |A_{13}| + |A_{23}| \Big) \overset{(\mathrm{C2})}{<} \det A \overset{(\mathrm{C3})}{<} 0$$

which is a contradiction. □

THEOREM 5.5 (ii), i.e. the nonresonance, follows from $\tilde{\Delta}_i(d_1^* {\mu_l}^2) > 0$ for $i = 1, 2, 3$ and all $l \neq m$ such that the rest of the spectrum of the right-hand side of SYSTEM (5.5) is bounded away from the imaginary axis.

In fact it even says more since $\mathrm{Re}\Big(\mathrm{spec}(\tilde{A}) \setminus \{\pm i\omega\}\Big) < 0$ which is a necessary condition for supercritical bifurcation. Now the stability criterion of THEOREM A.7 reduces to the evaluation of $\mathrm{sgn}(\delta)$.

THEOREM 5.5 (iii), i.e. the transversality condition of the Hopf theorem, follows from the assumption of strictly monotone dependence of $\mathrm{spec}(-B)$ on the parameter d_1.

The bifurcating periodic solution is nonconstant because the constant solution E^* is asymptotically stable. A certain mode m is destabilized when a pair of complex eigenvalues crosses the imaginary axis for critical d_1^*. The uniqueness statement of THEOREM A.7 now excludes a constant periodic solution in a neighborhood of (E^*, T^*, d_1^*).

This completes the proof. □

Remark 5.4 *Via cyclic changes of the indices* $i = 1, 2, 3$ *in* (C4) – (C6), THEOREM 5.5 *can be formulated for a spatial operator in the second or third equation.*

As an example for an operator $B(X \times \Lambda, E)$ *on a subset* X *of a real Banach space* E *and* $\Lambda \subset \mathbb{R}_+$ *serves the Laplace operator on bounded domains* Ω *with Neumann boundary conditions, multipied with a diffusion coefficient* d_1. *This operator fulfills the assumptions of the theorem and is used in the applications throughout* CHAPTER 6 *and* CHAPTER 7. *Attention has to be paid on the shape of the domains for dimensions greater than two. The destabilized mode might not be a simple eigenvalue of the operator.*

The following figure illustrates the picking of a single mode that becomes unstable.

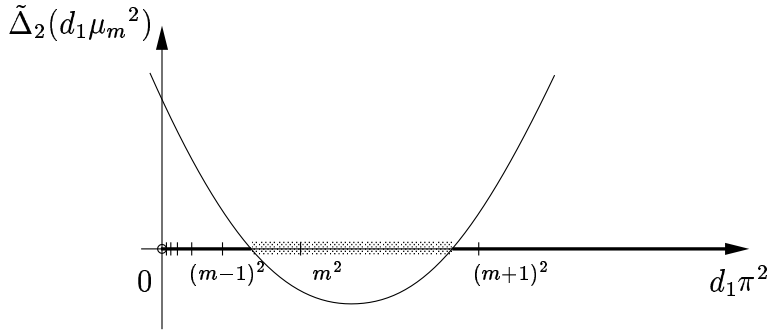

FIG. 5.3: The parabola $\tilde{\Delta}_2(d_1\mu_m{}^2)$ selects a single mode of oscillating solutions when the kinetic system is regularly perturbed with a diffusion operator in a single equation (here for the Laplace operator on a one-dimensional domain).

For the wave bifurcation $|A_{23}|$ has to be positive. But since EQUATION (5.4) might have no positive roots this is not sufficient. A simple computation shows that existence of positive roots can only be achieved if (C5) and (C6) are satisfied.

Nevertheless the positivity of $|A_{23}|$ can be used as a first check whether wave bifurcation is possible or not. A submatrix with only positive Hurwitz determinants (for a 2×2 matrix that means negative trace and positive determinant) will be called *stabilizing*. There are two different cases that can be distinguished for SYSTEM (5.5) at an asymptotically stable constant solution:

Remark 5.5 *If the constant steady solution satisfies* (C1) – (C3) *and* $|A_{23}| < 0$ *then there is a critical diffusion coefficent* d_1^* *for an appropriate mode* m *which causes a bifurcation to a Turing type stationary solution. The submatrix is* not stabilizing *in this case.*
A Turing type stationary solution can also be caused by a simultaneous change of sign of $\det\tilde{A}(\mu_m)$ *and* $\tilde{\Delta}_2(\mu_m)$ *(see* TABLE 5.2, $\tilde{k} = 1$*). For negative* $\mathrm{tr}\tilde{A}$ *it implies* $\sum|\tilde{A}_{ij}| = 0$. *In the limit of* $d_2 = d_3 = 0$ *the terms to become zero are* $-\det\tilde{A}(d_1\mu_m{}^2) = -\det A + d_1\mu_m{}^2|A_{23}|$ *and* $\sum|\tilde{A}(d_1\mu_m{}^2)_{ij}| = \sum|A_{ij}| - d_1\mu_m{}^2\mathrm{tr}(A_{23})$. *This means* $|A_{23}| < 0$ *and* $\mathrm{tr}(A_{23}) > 0$. *Again the submatrix is* not stabilizing.

If the constant steady solution satisfies (C1) – (C6)*, there are critical diffusion coefficents* d_1^* *causing a Hopf bifurcation. Conditions* (C4) *and* (C5) *imply* $\mathrm{tr}(A_{23}) < 0$ *and* $|A_{23}| > 0$. *This submatrix is* stabilizing.

The results of the computations on the stability at the equilibrium point can now be summarized.

Remark 5.6 *In a stable constant solution the sum* $\sum |A_{ij}|$ *is positive. For wave bifurcation at least one* $|A_{jk}|$ *has to be negative to satisfy* (C5)*. The spatial operator occurs in the* j^{th} *or* k^{th} *equation. The submatrix in which no spatial operator occurs is* stabilizing.

5.4.1 Estimation of Mode Selection

Further investigations of the wave bifurcation concern the biggest mode M that can be isolated. For one-dimensional domains Ω and the Laplace operator, this wavenumber is estimated by $\nu^{\pm}$, the roots of $\tilde{\Delta}_2(d_1 {\mu_m}^2)$ (see FIGURE 5.3). For all integers m less than M, a bifurcation to a wave solution with the appropriate wavenumber can be arranged either for shrinking or growing d_1. But for wavenumbers greater than M, at least two modes are within the unstable area. This does not mean that there is no such solution, but it strongly depends on the initial data which solution will survive.

Lemma 5.2 *The biggest wavenumber* M *for which only a single mode is destabilized in a one space dimensional system can be estimated by* $\mu^- := \dfrac{2\nu^-}{\nu^+ - \nu^-}$ *with*

$$\mu^- - 1 < M < \mu^- + \frac{1}{2}$$

where $\nu^{\pm}$ *are the roots of the parabola* $\tilde{\Delta}_2(d_1 {\mu_m}^2)$ *of* THEOREM 5.5.

Proof: Fix the left root ν^- at the M^{th} mode with the scaling factor $d_1\pi^2$.

$$d_1 \pi^2 M^2 = \nu^- \tag{5.7}$$

Maximizing the scaling factor gives the following inequalities. EQUATION (5.8) is needed to prevent getting a second mode in the unstable region, EQUATION (5.9) is introduced to make the interval (ν^-, ν^+) bigger than the previous spacing between two eigenvalues.

$$\nu^+ - \nu^- < d_1\pi^2((M+1)^2 - M^2) = d_1\pi^2(2M+1) \tag{5.8}$$

$$d_1\pi^2(M^2 - (M-1)^2) = d_1\pi^2(2M-1) < \nu^+ - \nu^- \tag{5.9}$$

Estimation from above is done with EQUATION (5.7) and EQUATION (5.8).

$$\frac{2M^2}{2\nu^-} = \frac{1}{d_1\pi^2} < \frac{2M+1}{\nu^+ - \nu^-}$$

$$\Rightarrow \quad \frac{2M^2}{2M+1} = M - \frac{M}{2M+1} < \frac{2\nu^-}{\nu^+ - \nu^-} = \mu^-$$

$$\Rightarrow \quad M - \frac{1}{2} < M - \frac{M}{2M+1} < \mu^- \quad \Rightarrow \quad M < \mu^- + \frac{1}{2}$$

For the estimation from below EQUATION (5.7) and EQUATION (5.9) are used.

$$\frac{2M-1}{\nu^+ - \nu^-} < \frac{1}{d_1\pi^2} = \frac{2M^2}{2\nu^-}$$

$$\Rightarrow \ \mu^- < \frac{2M^2}{2M-1} = \frac{M(2M-1)+M}{2M-1} = M + \frac{M}{2M-1} \leq M+1 \ \Rightarrow \ \mu^- - 1 < M$$

There are at most two integers within the bounds. It has to be checked if $\tilde{\Delta}_2$ always evaluates negative for both modes (then take the smaller one), or only for one of them. □

5.4.2 Considerations on Stability

Once the maximal M is found, the critical $d_{1_{M_r}}$ for which there is bifurcation to the standing wave solution for shrinking $d_1 < d_{1_{M_r}}$ can be calculated easily. In the same way a critical $d_{1_{M_l}}$ is calculated for $M-1$, and there is a bifurcation to a time-periodic solution for growing $d_1 > d_{1_{M_l}}$. The two possibilities correspond to the situations of either touching the square number with the right wing or with the left wing of the parabola. This yields the following sequence

$$\cdots \ d_{1_{M_l}} < d_{1_{M_r}} < d_{1_{(M-1)_l}} < d_{1_{(M-1)_r}} \ \cdots$$

and there is no mode destabilized within the open interval $(d_{1_{M_r}}, d_{1_{(M-1)_l}})$. So the mode destabilization is well separated up to the mode with the maximal number which can be estimated with LEMMA 5.2.

In contrast to the transcritical bifurcation the stability in case of a Hopf bifurcation has to be derived from third derivatives of the vector field at the bifurcation point.

THEOREM A.7 gives a concrete stability criterion which tells whether there is supercritical bifurcation or not. Only $\operatorname{sgn}(\delta)$ has to be determined since THEOREM 5.5 already implies $\operatorname{Re}\Big(\operatorname{spec}(\tilde{A}) \setminus \{\pm i\omega\}\Big) < 0$. If the right-hand side of SYSTEM (5.5) is at least C^3, then δ can be computed with the given formula. Note that neither $\pm i\omega$ nor the third root of $\chi(\tilde{A})$, which is always negative, do depend on ${\mu_m}^2$, but the basis of the kernel N does. Therefore $\operatorname{sgn}(\delta)$ might change for the same problem at each bifurcation point.

Nevertheless, straightforward integration in the neighborhood of a sequence of critical bifurcation parameters reveal a picture as sketched in FIGURE 5.4, where all branches appear supercritical.

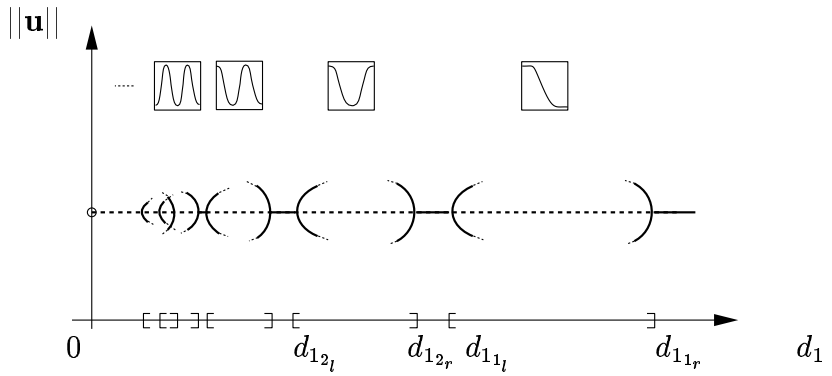

FIG. 5.4: The branches of periodic solutions are sketched as maximal amplitude of the solution in an appropriate norm versus the diffusion coeffcient d_1 as bifurcation parameter. The constant solution E^* is drawn as a solid line in case it is asymptotically stable, and as a dashed line if it is destabilized. The mode destabilization is well separated up to the mode with the maximal number that can be estimated with LEMMA 5.2.

5.5 Wave Bifurcation in Case of $d_1 = d_2 \neq d_3 = 0$

Return to EQUATION (5.3) and now consider the case where $d_1 = d_2 = \mathbf{d}$ and $d_3 = 0$. The second Hurwitz determinant is

$$\begin{aligned}\tilde{\Delta}_2(\mu_m, \mathbf{d}, \mathbf{d}, d_3) = \quad & [2\mathbf{d}^2 d_3 + \mathbf{d}^2(\mathbf{d} + d_3) + \mathbf{d}^2(\mathbf{d} + d_3) + 2{d_3}^2\mathbf{d}](\mu_m{}^2)^3 \\ & -[\mathbf{d}^2(\mathrm{tr}A + a_{33}) + {d_3}^2\mathrm{tr}(A_{12}) + \\ & \quad 2(\mathbf{d}^2 + 2\mathbf{d}d_3)\mathrm{tr}A](\mu_m{}^2)^2 \\ & +[\mathbf{d}(|A_{12}| + \textstyle\sum |A_{ij}| + (\mathrm{tr}A)^2 + a_{33}\mathrm{tr}A) + \\ & \quad d_3(|A_{13}| + |A_{23}| + (\mathrm{tr}(A_{12}))^2 + a_{33}\mathrm{tr}(A_{12}))]\mu_m{}^2 \\ & + \Delta_2\end{aligned}$$

and for $d_3 \to 0$

$$\begin{aligned}\tilde{\Delta}_2(\mu_m, \mathbf{d}, \mathbf{d}, 0) = \quad & 2(\mathbf{d}\mu_m{}^2)^3 \\ & -(\mathbf{d}\mu_m{}^2)^2(3\mathrm{tr}A + a_{33}) \\ & +(\mathbf{d}\mu_m{}^2)(|A_{12}| + \textstyle\sum |A_{ij}| + (\mathrm{tr}A)^2 + a_{33}\mathrm{tr}A) \\ & +\Delta_2\end{aligned}$$

which is a cubic polynomial in $\mathbf{d}$. It can be solved by Cardan's formula, and for a negative discriminant there are three real roots. Note that the leading coefficient is positive and the value at $\mathbf{d} = 0$ is $\Delta_2 > 0$. One of the roots of this cubic polynomial is always real and negative. If the other two are complex or negative, no wave bifurcation will occur. But if they are positive real roots, and if

$$-\det\tilde{A}(\mu_m, \mathbf{d}, \mathbf{d}, 0) = -\det A + \mathbf{d}\mu_m{}^2(|A_{23}| + |A_{13}|) - \left(\mathbf{d}\mu_m{}^2\right)^2 a_{33} > 0$$

there will be a complex conjugate pair of eigenvalues of the full system crossing the imaginary axis for a critical diffusion coefficient $\mathbf{d}^*$. In CHAPTER 6 there is an example showing the desired linearization.

6 First Examples for Wave Bifurcation

For the semiphenomenological model of CO oxidation on platinum, the basic spatio-temporal solutions such as traveling waves, standing waves and target patterns, all have been observed experimentally as well as numerically. Recently LEVINE and ZOU [34] analyzed the modulated standing wave pattern, a standing wave superposed to homogeneous oscillations (see also CHAPTER 2). For the parameters in request, however, the homogeneous mode will always bifurcate first, as it would do for a two equations system. This is due to the fact that at its stable fixed point this model is not able to fulfill the conditions (C4) – (C6). It behaves like a two equations system to which it can be reduced as shown in CHAPTER 3.
Therefore the models which are analyzed here are essentially three equations systems in so far as the coupling of the kinetic system cannot be reduced to two equations by standard methods.

6.1 Example for Both Limiting Cases

To give a first example consider the following system together with Neumann boundary conditions.

$$\begin{aligned} \dot{u} &= d_1\Delta u && -\varepsilon u + \kappa\varepsilon v + 2\varepsilon w && -\kappa\lambda uvw \\ \dot{v} &= d_2\Delta v && +\frac{1}{\kappa}(1+2\varepsilon)u - (1+\varepsilon)v + \frac{1}{\kappa}(\varepsilon^2+6\varepsilon+1)w && -\lambda uvw \\ \dot{w} &= d_3\Delta w && +u - \kappa v + w && -u^3 \end{aligned}$$

It is a $\mathbf{Z}_2$-equivariant system having three fixed points. Obviously zero is one of them, and it is asymptotically stable in the space of constant functions. Its linearization fulfills all the conditions to get a wave bifurcation for $d_1 \neq 0$ as well as $d_1 = d_2 \neq 0$. The parameters κ, λ do not occur in any of the symmetric functions of the characteristic polynomial, since κ is canceled down and λ only occurs with higher order terms.

$$A|_{x=0} = \begin{pmatrix} -\varepsilon & \kappa\varepsilon & 2\varepsilon \\ \frac{1}{\kappa}(1+2\varepsilon) & -(1+\varepsilon) & \frac{1}{\kappa}(\varepsilon^2+6\varepsilon+1) \\ 1 & -\kappa & 1 \end{pmatrix}, \qquad \dot{x} = A\,x + o(|x|^2)$$

Computing (C1) – (C3) proves that all eigenvalues of A have negative real parts.

$$\begin{aligned} -\mathrm{tr}A &= 2\varepsilon &&> 0 \\ \Delta_2 &= \varepsilon^2 &&> 0 \\ -\det A &= 3\varepsilon^2 &&> 0 \end{aligned}$$

6.1.1 The Case of $d_1 \neq 0$

In the case of a diffusion term in a single equation the trace and determinant are decreased. It remains to show that $\tilde{\Delta}_2$ changes sign for a single mode m. The conditions (C4) – (C6) cannot be satisfied for diffusion terms in the second or third equation. But in case of $d_1 \neq 0$ and $d_2 = d_3 = 0$, it yields $-\mathrm{tr}(A_{23}) = \varepsilon > 0$, and as a first check $|A_{23}| = 5\varepsilon + \varepsilon^2$ is positive. Next (C5) evaluates to $-\varepsilon^2 + 3\varepsilon$ and (C6) is $(\varepsilon^2 - 3\varepsilon) - 4\varepsilon^3$ which is positive for $\varepsilon \in (0,1)$.

$$\begin{aligned} -\mathrm{tr}\tilde{A} &= 2\varepsilon + d_1{\mu_m}^2 &&> 0 \\ \tilde{\Delta}_2(\mu_m) &= \varepsilon^2 + d_1{\mu_m}^2(\varepsilon^2 - 3\varepsilon) + (d_1{\mu_m}^2)^2\varepsilon &&< 0 \\ -\det\tilde{A} &= 3\varepsilon^2 + d_1{\mu_m}^2(\varepsilon^2 + 5\varepsilon) &&> 0 \end{aligned}$$

As indicated above, $\tilde{\Delta}_2(\mu_m)$ can become negative for $0 < \varepsilon < 1$ and $\nu^- < d_1{\mu_m}^2 < \nu^+$ with

$$\nu^{\pm} = \frac{1}{2}\Big(3 - \varepsilon \pm \sqrt{(3-\varepsilon)^2 - 4\varepsilon}\Big)$$

(e.g. for $\varepsilon = 0.01$ it yields $\nu^{\pm} = \{0.3348231 \cdot 10^{-2}, 2.9866518\}$), whereas the $\mathrm{tr}\tilde{A}$ and $\det\tilde{A}$ do not change their signs for any μ_m. However, the constant zero is destabilized.
The system is implemented with the following set of parameters:

$$\varepsilon = 0.5,\ \kappa = 10.0,\ \lambda = 2.0,\ \text{and } d_1 = 0.1$$

Initial conditions for the straightforward algorithm are chosen at random around the zero solution with a maximal standard deviation of 0.001. As a result a first mode standing wave establishes itself in a spatially one-dimensional setting.
Computations in two spatial dimensions on a square domain result in a standing wave of the same mode. For illustration purposes see FIGURE 6.1. The zero solution is fixed in the center of the square and an s-shaped zero line rotates around for each of the three species.

6.1.2 The Case of $d_1 = d_2 \neq d_3 = 0$

In the case of $d_1 = d_2 \neq 0$ and $d_3 = 0$, and for the same $\varepsilon = 0.01$, i.e. for the same kinetic system as above, there are three real roots of $\tilde{\Delta}_2(\mu_m, d_1, d_1, 0) = 2d^3 + (6\varepsilon - 1)d^2 + 3\varepsilon^2 d + \varepsilon^2 = 0$ with $d := d_1{\mu_m}^2$. They can be computed to be about

$$\{-0.010050631, 0.010597026, 0.4694536\}.$$

The $\det\tilde{A}(\mu_m, d_1, d_1, 0) = 3\varepsilon^2 + d(2\varepsilon + \varepsilon^2) - d^2$ is positive for $d \in (-0.009975, 0.030075)$. So there is an overlap for the diffusion parameter where $\tilde{\Delta}_2(\mu_m)$ is negative and $\det\tilde{A}$ remains positive. Therefore one can imagine the wave bifurcation to hold for all intermediate parameters, i.e. $d_2 \in (0, d_1)$, so that THEOREM 5.5 holds (with additional hypotheses) for

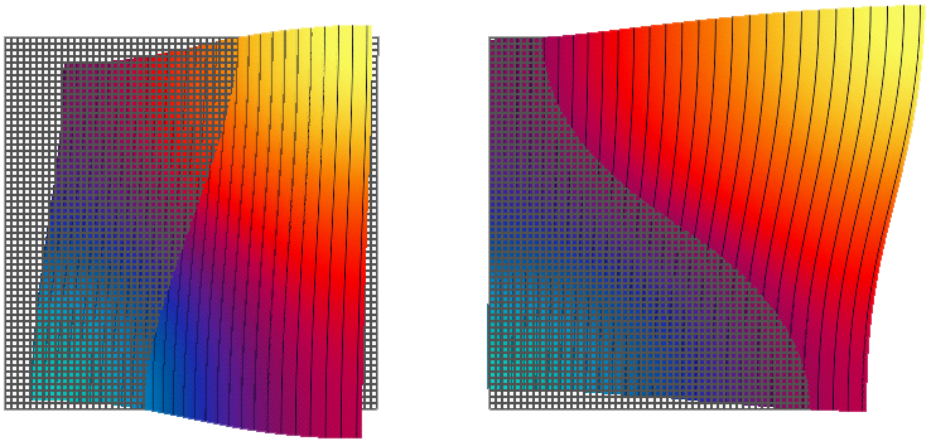

FIG. 6.1: The grid indicates the zero level in both pictures. On the left is shown the solution for the first equation, which is quite similar in shape to the second equation. On the right is shown the solution for the third equation. The color in both pictures indicates the third equation giving a cyan color to the minimum and marking its maximum with light yellow.
An animated sequence now shows a rotating wave where the maximum of the first equation (reddish lower right corner in the left picture) follows the maximum (yellow spot) of the third equation.

two parabolic equations coupled with a single ordinary equation, too. These conditions are quite ugly when extracted from Cardan's formula and should be left to the computer.

Nevertheless, with the straightforward algorithm no standing wave could be detected for $d_1 = d_2$. Instead there always develops a steady nonconstant solution that in shape strongly depends on the initial conditions. Presumably the wave bifurcation is no longer supercritical and therefore the wave solution does not exist for the indicated diffusion parameters.

6.2 Application to Autocatalytic Surface Reactions

The example of the previous section is constructed without an application in mind. The following system of three equations has a background as an autocatalytic reaction-diffusion system. It is derived with the help of stoichiometric network analysis (see EISWIRTH [11]). It may be interpreted to describe a surface reaction enhanced by a reconstruction process of the surface.

It has to be mentioned that the semi-phenomenological system of CHAPTER 2 is not of the form to be able to fulfill the conditions for the wave bifurcation. Whenever the kinetic parameters for the three variables system are chosen in a way which stabilizes a constant solution, condition (C5) is violated. There are of course standing wave solutions for this system as shown in CHAPTER 4. But it is not essential to argue with three equations. This justifies once more the elimination of the oxygen equation.

In the following network it is essential to have three equations. FIGURE 6.2 sketches a process in which a species w depends quadratically on itself and on an additional species v. While consuming two parts of w, there are four parts produced by the loop indicated by the parameter p_4.

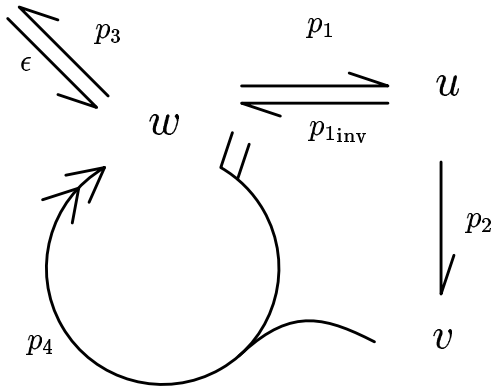

FIG. 6.2: This stoichiometric network sketches an autocatalytic process. Reaction kinetic parameters are written to the corresponding arrows which indicate the stoichiometry by the numbers of flags and feathers.

This network gives rise to the following differential equations with kinetic parameters p_1 to p_4, assuming a diffusion matrix with diagonal entries d_1 to d_3. The integer multiples come from the stoichiometry of the chemical network, so that all parameters can first be set identical one.
No flux boundary conditions on the cylinder $\partial\Omega \times (0,T]$ are considered.

$$\begin{aligned}
\dot{u} &= d_1\Delta u - p_{1_{\text{inv}}}u - 2p_2u + 3p_1w \\
\dot{v} &= d_2\Delta v + p_2u - p_4vw^2 && \text{in } \Omega \times (0,\mathrm{T}] \\
\dot{w} &= d_3\Delta w + p_{1_{\text{inv}}}u - 3p_1w - p_3w + 2p_4vw^2 + \epsilon
\end{aligned} \tag{6.1}$$

$$\frac{\partial}{\partial n}u = \frac{\partial}{\partial n}v = \frac{\partial}{\partial n}w = 0 \qquad \text{on } \partial\Omega \times (0,\mathrm{T}]$$

Solving the system for constant equilibria yields a single solution that requires

$$u = \frac{3\epsilon p_1}{(p_{1_{\text{inv}}} + 2p_2)p_3},\ v = \frac{3p_1p_2p_3}{(p_{1_{\text{inv}}} + 2p_2)\epsilon p_4},\ w = \frac{\epsilon}{p_3}.$$

Setting the parameters identical one yields an asymptotically stable equilibrium $E^* = (u^*, v^*, w^*)^t = (1,1,1)^t$. This equilibrium does not change when the paramters p_3 and ϵ are varied simultaneously such that $\epsilon/p_3 \equiv 1$.
The linearization at this point is

$$A|_{E^*} = \begin{pmatrix} -(p_{1_{\text{inv}}} + 2p_2) & 0 & 3p_1 \\ p_2 & -p_4(w^*)^2 & -2p_4 v^* w^* \\ p_{1_{\text{inv}}} & 2p_4(w^*)^2 & -3p_1 - p_3 + 4p_4 v^* w^* \end{pmatrix} = \begin{pmatrix} -3 & 0 & 3 \\ 1 & -1 & -2 \\ 1 & 2 & 1 - p_3 \end{pmatrix}$$

with the following set of eigenvalues

$$\left\{ -3,\ -\frac{1}{2}\left(p_3 - \sqrt{{p_3}^2 - 4p_3}\right),\ -\frac{1}{2}\left(p_3 + \sqrt{{p_3}^2 - 4p_3}\right) \right\}$$

indicating an asymptotically stable oscillatory fixed point.
Now the paramters p_3 and ϵ are varied simultaneously for small values of p_3.

A nonzero diffusion term in the v-equation can be ruled out as a source for the instability by a first check whether the submatrix is *stabilizing*: $|A_{13}| = -3(2-p_3)$ is negative for $p_3 < 2$.
Diffusion in the w-equation fails in principle for condition (C5), that is $-(|A_{23}| + |A_{13}| + \text{tr}(A_{12})\text{tr}A) = 8(1-p_3) - 17$ which is negative.
For a nonzero diffusion coefficient d_1 the condition (C5) is $-(|A_{12}| + |A_{13}| + \text{tr}(A_{23})\text{tr}A) = -{p_3}^2 - 6p_3 + 3$ which is positive for positive $p_3 < -3 + 2\sqrt{3}$.
To fulfill condition (C6) the parameter p_3 has to solve ${p_3}^4 - 4{p_3}^3 - 6{p_3}^2 - 36p_3 + 9 > 0$ and this expression is positive for $p_3 < 0.23904883974$. Note that the system gets singular for $p_3 \to 0$. For values of p_3 inbetween zero and its upper limit critical diffusion coefficients ${d_1}^*$ can be determined for each wavenumber up to the maximal wavenumber to be estimated with LEMMA 5.2. The closer p_3 gets to its upper limit, the bigger is this maximal number.
The conditions (C1) – (C6) are fulfilled for $d_1 \neq 0$ and $d_2 = d_3 = 0$. If the mobility of a single variable is considered as a source of a standing wave solution, only the u-species is able to destabilize the stable constant solution.

Existence of the solution is guaranteed via the asymptotic stability of E^*. This yields a neighborhood of the fixed point that is positively invariant such that the reaction diffusion system has a solution for all time if the initial data is within this neighborhood.
The numerical result of FIGURE 6.3 can be predicted.

Numerical Parameters

A sustained oscillation in space and time for the above model of an autocatalytic reaction can also be verified numerically. The discretized system of ordinary differential equations is solved with the LSODE package, using numerical estimates of the Jacobian matrix, and relative and absolute error tolerances as in CHAPTER 4. The space discretization is 300 gridpoints on a unit interval. Time discretization is done implicitly.

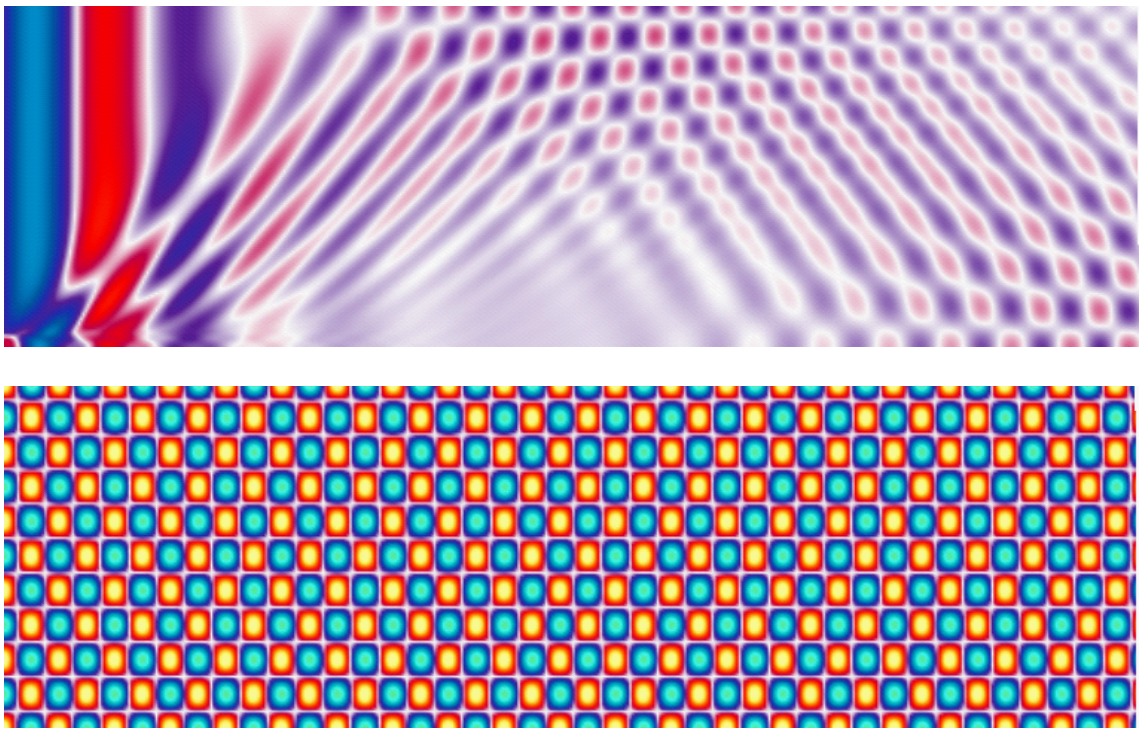

FIG. 6.3: The horizontal axis shows the temporal development, the vertical axis represents the spatial domain. The w-solution is displayed in color from a minimum of light blue to a maximum of light yellow. The asymptotically stable fixed point of the kinetic system is indicated in white. One-dimensional spatially nonuniform initial data (top, time steps 1-100) evolves into a standing wave pattern (bottom, time steps 4900-5000).

6.2.1 An Example from the Literature

ZHABOTINSKY et al. [46] also numerically show the phenomenon of wave bifurcation in a three variables system modelling cubic autocatalysis. Their kinetic system is coupled with the same simple diffusion terms and looks as follows:

$$\begin{aligned} \dot{u} &= d_1\Delta u + m\left(-uv^2 + w^2 - \frac{au}{g+u}\right) \\ \dot{v} &= d_2\Delta v + n(uv^2 - v + b) \qquad \text{in } \Omega \times (0,\mathrm{T}] \\ \dot{w} &= d_3\Delta w + u - w \end{aligned} \tag{6.2}$$

$$\frac{\partial}{\partial n}u = \frac{\partial}{\partial n}v = \frac{\partial}{\partial n}w = 0 \qquad \text{on } \partial\Omega \times (0,\mathrm{T}]$$

The authors use the same solver with the same tolerances and discretization schemes. They perform the simulations with zero diffusion coefficients in the first and second equa-

tion. Other parameters are $m=28$, $a=0.9$, $n=15.5$, $b=0.2$, $d_3=1$ and a length of the interval Ω of $L=20$ units. The initial conditions are chosen to be the stationary constant solution of approximately $(u,v,w)=(1.1308,0.5787,1.1308)$ where only a single one of the 300 gridpoints on the boundary of the domain is perturbed slightly. The standing wave result with a wavenumber of twelve can be reproduced easily. For further numerical experiments, they vary the length of the domain and the kinetic parameter m.

The same set of parameters as above but different initial data, as for instance a bigger part of the interval on which the stationary solution is perturbed or initial data which are perturbed randomly on every gridpoint in a neighborhood of the stationary solution, lead to a standing wave with a wavenumber of eleven. Since $d_3=1$ and a length of Ω of $L=20$ is equivalent to a diffusion coefficient $d_3=0.0025$ and $L=1$, this result can be interpreted with the help of FIGURE 6.4. The roots $\nu^{\pm}$ of the parabola of FIGURE 5.3 on page 58 which is used to illustrate THEOREM 5.5 provide a left and right critical diffusion coefficient for each mode. For the above system, the stationary solution is destabilized for perturbations of wavenumber eight up to fifteen.

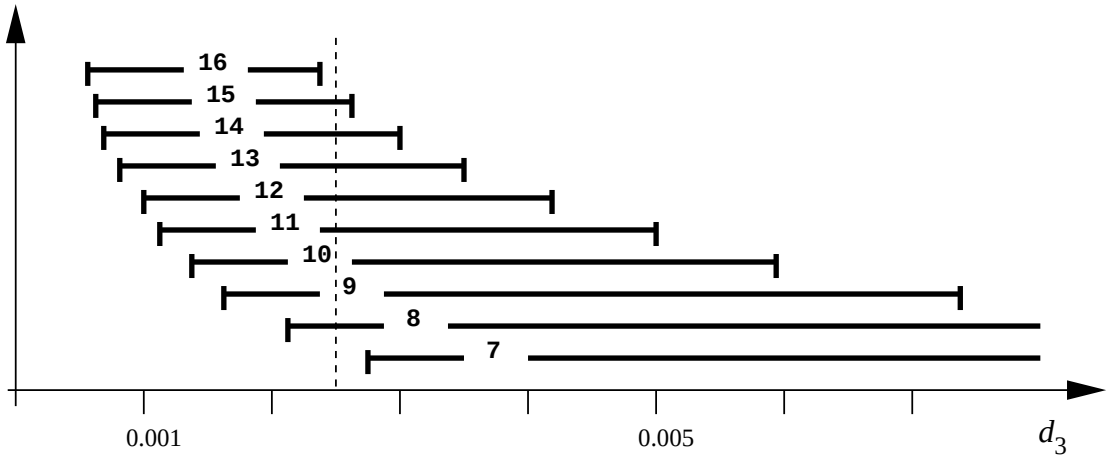

FIG. 6.4: For SYSTEM (6.2) with parameters $m=28$, $a=0.9$, $n=15.5$, $b=0.2$ the roots of approximately $\nu^-=1.3389$ and $\nu^+=5.8545$ give the above intervals of diffusion coefficients which destablize the constant solution with respect to the mode with the indicated wavenumber. The dashed line marks the diffusion coefficient $d_3=0.0025$. The modes which are destablized range from wavenumber eight to fifteen.

Increasing m slightly to a value of $m=28.56$ makes the roots $\nu^{\pm}$ move closer to each other so that the picking of a mode is more selective. For this kinetic parameter value the biggest wavenumber up to which the modes are well separated is fourteen (estimated with LEMMA 5.2). For $d_3=0.0025$ now only the standing wave of wavenumber twelve is destabilized. For m even bigger than 28.566616, the wave bifurcation is not possible any more. Decreasing m to a value less than 26.75 yields in a destabilization of also the zero

mode, i.e. the constant solution itself is not stable any more.

Discussion

The parameter m serves as the one to be varied for the different numerical tests in the paper of ZHABOTINSKY et al. [46]. With the help of the conditions for wave bifurcation of CHAPTER 5 an interval of $m \in (26.75, 28.567)$ is given for which standing wave solutions can be expected.
The bigger m is, the more selective is the parabola, and the more sensitive the system reacts on a change in the diffusion coefficient (or, equivalently, in the length of the domain). Changes in the initial data are not recognized by the final waveform as long as the wavenumber is below the estimated maximal number and the perturbations are within the wavelength.
For m nearer to the lower end of the interval the solutions depend even more on the initial data. If m gets even smaller the space-independent Hopf bifurcation occurs as well. Naturally, a straightforward integration of the initial value problem gives rise to quite different solutions, as the described *Standing Traveling Waves* in the above paper.

7 An Example from Biology

This three equations system is a nice example for wave bifurcation since the kinetic part will not show periodic solutions for any positive parameters. So it is sure that the system has no periodic solutions until a diffusion matrix with different coefficients for each equation is introduced. The conditions for the wave bifurcation now indicate which species has to have the biggest mobility.

7.1 A Model for Microbial Growth

The set-up of the kinetic system for growing cell cultures is derived from a chemostat model. Assume the microbes (algae or bacteria) to grow in a thin layer on top of an aggar (gel with nutrient) in a vessel while the nutrient is constantly supplied from below. Let $S:=S(x,t)$ be the concentration of the growth-limiting nutrient within the layer. The dynamic is determined by the concentration of the fast growing (and therefore fast consuming) cell population $u:=u(x,t)$, and the slow growing cells $v:=v(x,t)$. The concentrations are no longer constant but functions of space and time, since the model additionally considers a diffusion term for the cell movement. S^0 is the concentration of the limiting nutrient. For simplicity the dilution of the nutrient and the death rate of the cells have the same constant rate D. But it is only for the analysis that this assumption is required to have a conservation of mass equation. Computer algebra implementation of the equations show that this can be considerably weakened: Dilution and death rate can have different values without changing the qualitative behavior of the solution set.
In the standard Monod model the specific growth rate f depends on the amount of supplied nutrient. It is modeled by a Michaelis-Menten term $f(S)=mS/(a+S)$, where m is the maximum growth rate and a is the half-saturation constant.
Dividing the cell culture into two phases that have different metabolisms gives rise to two different growth rates $f_1(S)$ and $f_2(S)$. Again they may be considered to be of the form $m_1S/(a_1+S)$ and $m_2S/(a_2+S)$, respectively. These terms are used for numerical investigations, although for the analysis of the model, f_1 as well as f_2 can be more general functions (see [27] and the references therein).
Assume f_i, $i=1,2$ to be monotone increasing functions that saturate

(1) f_i are C^3 functions on an interval containing $[0,\infty)$.
(2) $f_i(0)=0$, $f_i(S)\to m_i<\infty$ as $S\to\infty$, $m_1>D>m_2$.
(3) $f_i'(S)>0$ on $[0,\infty)$.

The change in metabolism is modeled by nonnegative functions $\alpha(S)$ and $\beta(S)$, and it is sufficient if these functions are continuous and piecewise differentiable. It can be assumed that $\alpha(S)=0$ up to a threshold s_1 and that α is nondecreasing ($\alpha'(S)\geq 0$) for $S>s_1$. In contrast, β is nonincreasing ($\beta'(S)\leq 0$) for $0\leq S<s_2$ and can be considered $\beta(S)=0$ for $S\geq s_2$. Let α and β be piecewise linear functions of the form:

$$\alpha(S) = \begin{cases} 0 & 0 \le S < s_1 \\ K_1(S - s_1) \quad for & s_1 \le S < s_1 + \varepsilon_1 \\ K_1\varepsilon_1 & s_1 + \varepsilon_1 \le S \end{cases}$$

$$\beta(S) = \begin{cases} K_2\varepsilon_2 & 0 \le S < s_2 - \varepsilon_2 \\ K_2(S - s_2) \quad for & s_2 - \varepsilon_2 \le S < s_2 \\ 0 & s_2 \le S \end{cases}$$

with $K_1 > 0$ and $K_2 > 0$ positive constants.

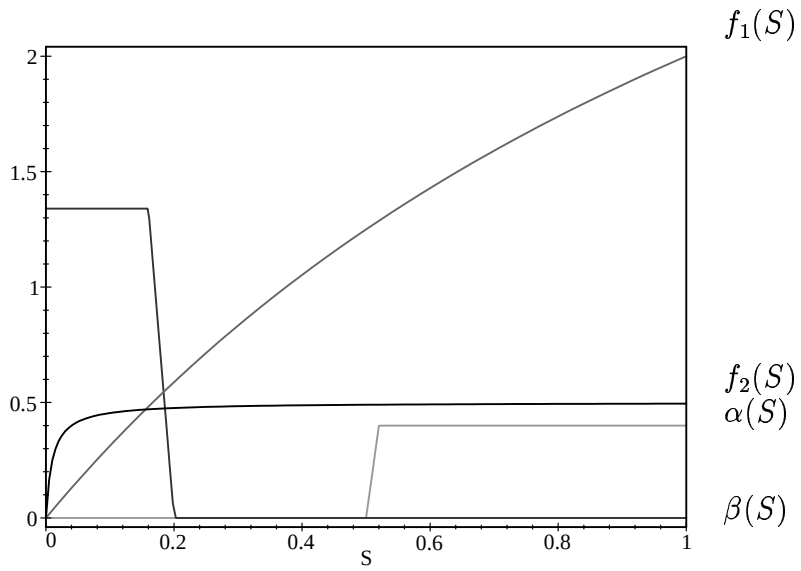

FIG. 7.1: The functions $\alpha(S)$, $\beta(S)$, $f_1(S)$, and $f_2(S)$ are positive functions depending on the amount of nutrient S. The piecewise linear functions α and β model the exchange between both cell populations and are well separated by a gap in S, where both functions are identically zero.

First assume that any of the variables may diffuse, but with different nonnegative diffusion coefficients d_i, $i = 1, 2, 3$. The topmost layer of the aggar in the vessel is considered to be a one or at most two-dimensional domain Ω with homogeneous Neumann, that is 'no flux', boundary conditions. The outer normal at the (smooth and convex) boundary of the domain is denoted by n.
This leads to the following model:

$$
\begin{aligned}
\text{[Nutrient]} \quad \frac{\partial S}{\partial t} &= d_1 \Delta S + (S^0 - S)D - f_1(S)u - f_2(S)v \\
\text{[Phase 1]} \quad \frac{\partial u}{\partial t} &= d_2 \Delta u + [f_1(S) - D - \beta(S)]u + \alpha(S)v \qquad \text{in } \Omega \times (0,\infty) \\
\text{[Phase 2]} \quad \frac{\partial v}{\partial t} &= d_3 \Delta v + [f_2(S) - D - \alpha(S)]v + \beta(S)u \\
\frac{\partial}{\partial n} S = \frac{\partial}{\partial n} u &= \frac{\partial}{\partial n} v = 0 \qquad \text{on } \partial\Omega \times (0,\infty)
\end{aligned}
\tag{7.1}
$$

with initial data (S_0, u_0, v_0) in $C(\Omega)$.
Existence of the solution for all time $t > 0$ results from bounded invariant rectangles, with the vector field of the kinetic equations at the boundary pointing strictly inwards (see for example SMOLLER [44], Chapter 14).
This model is biologically reasonable for the set of parameters consisting of positive constants. The analysis should be carried out for the whole range of positive parameters. The mathematical method of CHAPTER 5 can now be applied in SECTION 7.1.1 and SECTION 7.1.2.

7.1.1 Transient Oscillations for Nongrowing Second Phase

Requirements for the wave bifurcation include at least one stablizing and one destabilizing two-dimensional submatrix of the kinetic system. The spatial operator appears exactly in the equation that does not belong to the stabilizing submatrix.
Here this result is applied to a simpler model than SYSTEM (7.1) insofar as it lacks a growth rate function for the cells of the second phase.

$$
\begin{aligned}
\frac{\partial S}{\partial t} &= d_1 \Delta S + (S^0 - S)D - f(S)u \\
\frac{\partial u}{\partial t} &= d_2 \Delta u + [f(S) - D - \beta(S)]u + \alpha(S)v \\
\frac{\partial v}{\partial t} &= d_3 \Delta v + [\quad\quad - D - \alpha(S)]v + \beta(S)u
\end{aligned}
\tag{7.2}
$$

Investigating the kinetic system means neglecting any explicit spatial dependency, looking at a single point in the vessel without exchange with the neighborhood, or at a mean value in a stirred vessel (see [27] for a detailed analysis which is sketched in the following). It is easy to see that the phase space $\mathbb{R}^3_+$ is positively invariant under the solution map of the kinetic system. Moreover it can be shown that the simplex $\{(S,u,v) \in \mathbb{R}^3_+ | S+u+v \leq S^0\}$ is positively invariant. Introducing a variable $z(t) = S(t)+u(t)+v(t)$ yields the differential equation $z' = (S^0 - z)D$; hence $z(t) \to S^0$ as $t \to \infty$.

The set of equilibrium points and their local (and global) stability behavior is known. $E^0=(S^0,0,0)$ is an equilibrium point for all parameter values, and is globally stable in case of being the only fixed point of the system. E^0 becomes a saddle point as soon as a second equilibrium point comes into play. This second point is either $E^u=(S^u,S^0-S^u,0)$ or $E^*=(S^*,u^*,v^*)$ that now is locally stable. A Poincaré-Bendixson argument together with Markus' theorem (see in the appendix THEOREM A.1, and for the application of the argument see 7.1.2) state that there is no stable limit cycle and all trajectories are globally attracted by this second equilibrium except those on the boundary of the phase space.
The coexistence state of both cell populations in a stirred chemostat E^* is the only relevant equilibrium from which spatially nonconstant periodic solutions (standing waves) may bifurcate.
The Jacobian A at the stable equilibrium $E^*=(S^*,u^*,v^*)$ is given by

$$A|_{E^*} = \begin{pmatrix} -D-f'u^* & -f(S^*) & 0 \\ (f'-\beta')u^* & f(S^*)-D-\beta(S^*) & \alpha(S^*) \\ \beta'u^*-\alpha'v^* & \beta(S^*) & -D-\alpha(S^*) \end{pmatrix}$$

where $(\cdot)'$ denotes $\partial_S(\cdot)$ at E^*. Since E^* is an equilibrium point, and together with the conservation law $S^*+u^*+v^*=S^0$, this yields the following relations:

$$\begin{aligned} (u^*+v^*)D = (S^0-S^*)D = f(S^*)u^* \quad \Rightarrow \qquad v^*D &= (f(S^*)-D)u^* \\ [f(S^*)-D-\beta(S^*)]u^* &= -\alpha(S^*)v^* \\ [-D-\alpha(S^*)]v^* &= -\beta(S^*)u^* \end{aligned}$$

As a consequence, and since $v^*\neq 0$, $|A_{23}|=0$ for all parameter values.

$$\begin{aligned} |A_{23}| &= [f(S^*)-D-\beta(S^*)][-D-\alpha(S^*)]-\alpha(S^*)\beta(S^*) \\ &= (f(S^*)-D)[-D-\alpha(S^*)]+\beta(S^*)D \\ &= \frac{v^*D(-\beta(S^*))}{v^*}+\beta(S^*)D = 0 \end{aligned}$$

Next it can be deduced that $|A_{12}|>0$ for all parameter values.

$$|A_{12}| = \underbrace{(-D-f'(S^*)u^*)}_{<0}\underbrace{(f(S^*)-D-\beta(S^*))}_{\frac{-\alpha(S^*)v^*}{u^*}<0} + f(S^*)\underbrace{(f'(S^*)-\beta'(S^*))}_{>0}u^* > 0$$

Assuming f to be a nondecreasing function and α to be positive, $|A_{13}|$ is always positive. There is no wave bifurcation possible for any positive value of diffusion coefficients. And there also is no Turing instability since there is no activator or destabilizing submatrix even in a single equation.

As a conclusion, this model will not exhibit any nontransient spatial structure, neither stationary nor periodic, which bifurcates from a constant solution. Numerical tests for various initial conditions and parameters have shown that there is no evidence for any spontaneous bifurcation away from constant solutions.

7.1.2 Sustained Oscillations

The question now is, what is required for the model to be able to also describe sustained spatial structure of the solution? ROVINSKY, MENZINGER [42] analyze a three variables system with no activator submatrix but introduce a flow-induced instability for spatial effects. Since there is no transport by flow in the vessel, this idea cannot be used as an explanation.

Hence the destabilization should be inherent in the dynamics. This means that there should be a destabilizing submatrix (see REMARK 5.6). Any entry on the trace of the Jacobian is nonpositive and there is no biological reason why this should be altered. This means that there is no activator equation. Moreover, all two-dimensional submatrices have negative trace. Destabilizing two-dimensional submatrices therefore have to have negative determinants.

The model should be changed in a way to exhibit negative subdeterminants, but still biologically reasonable with growth rate functions that are positive as well as increasing, and with positive parameters.

The slope of β in E^* can possibly make $|A_{12}|$ negative. Consider a z-shaped relation instead of a piecewise linear function such that E^* does not change its position but $\beta'(S^*)>0$. Since α and β cannot be both nonzero, it follows that $\alpha(S^*)=0$ in this case. Then this change of the slope of β additionally affects the stability of E^*, because $-\det A = -(-D)|A_{12}|<0$. A negative subdeterminant yields a positive determinant and an essential condition, namely the stability of the equilibrium, is violated.

Slow Growing Second Phase

In SECTION 7.1.1 there is no growth rate function for the cells of the second phase, making some of the computations a bit easier. In fact introducing a positive growth rate for this phase, too, yields the possibility of negative $|A_{13}|$ without changing any of the qualitative results yet known about the chemostat model. SYSTEM (7.3) is the kinetic part of SYSTEM (7.1) and can be analyzed with the same methods as sketched in the previous section. This kinetic model came up in discussions with Betty Tang in 1992 during her visit in Heidelberg.

$$\begin{aligned} \frac{\partial S}{\partial t} &= (S^0 - S)D - f_1(S)u - f_2(S)v \\ \frac{\partial u}{\partial t} &= [f_1(S) - D - \beta(S)]u + \alpha(S)v \\ \frac{\partial v}{\partial t} &= [f_2(S) - D - \alpha(S)]v + \beta(S)u \end{aligned} \tag{7.3}$$

Note that introducing a variable $z(t) = S(t) + u(t) + v(t)$ yields the differential equation $z' = (S^0 - z)D$; hence $z(t) \to S^0$ as $t \to \infty$. There are at most two equilibrium points which are called E^0 and either E^u, if the latter is a pure fast growing cell culture, or E^*, if it is a coexistence state.
They are found when solving the right-hand side of SYSTEM (7.3) to be zero. This is equivalent to solving the following equations using the conservation law. Looking mainly for the coexistence state, it is the solution of

$$\begin{aligned} (S^0 - S)D - f_1(S)(S^0 - S - v) - f_2(S)v &= 0 \\ (f_2(S) - D - \alpha(S))v + \beta(S)(S^0 - S - v) &= 0 \end{aligned}$$

with $v^* > 0$. Eliminating v from the equations yields

$$(S^0 - S)\left((D - f_1(S)) + \frac{(f_1(S) - f_2(S))\beta(S)}{D + \beta(S) - f_2(S)}\right) = 0$$

which then can be solved for S^*. Since $S^0 > S^*$, this is equivalent to solving $H(S^*) = 0$ with

$$H(S) := \begin{cases} \dfrac{(D - f_2(S))(D + \beta(S) - f_1(S))}{D + \beta(S) - f_2(S)} & \text{if} \quad 0 < S < s_2 \\ D - f_1(S) & \text{if} \quad S \geq s_2 \quad (\Leftrightarrow \beta(S) \equiv 0). \end{cases}$$

To avoid any unnecessary difficulties, in the following always assume $f_2(S) < D$. This also excludes the case that $S^* \geq s_2$ as a by-product, because for nonzero v^* and $\beta(S^*) = 0$, the term $f_2(S) - D - \alpha(S)$ has to be zero to solve the equation, and that is not possible.
The uniqueness of S^* (if it exists) is a consequence of the monotonicity of $D + \beta(S) - f_1(S)$.
Again the set of equilibrium points consists of either solely $E^0 = (S^0, 0, 0)$, or $\{E^0, E^u\}$, or $\{E^0, E^*\}$, respectively. E^0 is globally stable as long as it is the only attractor of the system. It becomes a saddle point when a second equilibrium occurs. In general the Jacobian is

$$A = \begin{pmatrix} -D - f_1'u^* - f_2'v^* & -f_1(S^*) & -f_2(S^*) \\ (f_1' - \beta')u^* + \alpha'v^* & f_1(S^*) - D - \beta(S^*) & \alpha(S^*) \\ (f_2' - \alpha')v^* + \beta'u^* & \beta(S^*) & f_2(S^*) - D - \alpha(S^*) \end{pmatrix}$$

and evaluated at E^0 it yields

$$A|_{E^0} = \begin{pmatrix} -D & -f_1(S^0) & -f_2(S^0) \\ 0 & f_1(S^0) - D - \beta(S^0) & \alpha(S^0) \\ 0 & \beta(S^0) & f_2(S^0) - D - \alpha(S^0) \end{pmatrix}.$$

The functions α and β cannot be both nonzero, so in either case ($\alpha=0$ or $\beta=0$) the eigenvalues of E^0 are just the entries on the diagonal

$$\{-D,\ f_1(S^0) - D - \beta(S^0),\ f_2(S^0) - D - \alpha(S^0)\}.$$

If there exists either E^u or E^* then $f_1(S^0)-D-\beta(S^0)$ is positive. This is because in either case $D+\beta(S)-f_1(S)=0$ can be solved for $S^*<S^0$. For E^u it follows that $\beta(S^u)=0$, for E^* it follows that $\beta(S^*)\neq 0$. Since β is nonincreasing and f_1 is strictly increasing it yields

$$D + \beta(S^0) \leq D + \beta(S^*) = f_1(S^*) < f_1(S^0)$$

and E^0 has one positive eigenvalue.
Now concentrate on E^* and its asymptotic stability. Therefore the symmetric functions are computed from the Jacobian at E^* where $\alpha(S^*)=0$.

$$A|_{E^*} = \begin{pmatrix} -D - f_1'u^* - f_2'v^* & -f_1(S^*) & -f_2(S^*) \\ (f_1' - \beta')u^* & 0 & 0 \\ f_2'v^* + \beta'u^* & \beta(S^*) & f_2(S^*) - D \end{pmatrix}$$

It is easy to see that $\mathrm{tr}A<0$, $\sum|A_{ij}|>0$, and $\det A<0$. In detail

$$\begin{aligned} |A_{23}| &= 0 \\ |A_{12}| &= f_1(S^*)(f_1' - \beta')u^* > 0 \\ |A_{13}| &= (-D - f_1'u^* - f_2'v^*)(f_2(S^*) - D) + f_2(S^*)(f_2'v^* + \underbrace{\beta'u^*}_{<0}) \end{aligned}$$

and in the sum $\sum|A_{ij}|$ the only negative term $f_2(S^*)\beta'u^*$ is compensated by $f_1(S^*)(-\beta'u^*)$ of $|A_{12}|$. Finally every term in the determinant is negative

$$\det A = -f_2(S^*)(f_1' - \beta')u^*\beta(S^*) - \Big(-f_1(S^*)(f_1' - \beta')u^*(f_2(S^*) - D)\Big) < 0.$$

Therefore E^* is always a stable equilibrium point, if $-\mathrm{tr}A\sum|A_{ij}|>-\det A$, that is (C3). Since the computation now involves too many terms, there is an easier way to derive the asymptotic stability of E^* as a by-product of the next paragraph.

Asymptotic Behavior

The qualitative behavior of SYSTEM (7.3) can be deduced from a planar autonomous system, so that any kind of chaotic behavior can be excluded. Moreover, limit cycles can be excluded by a Poincaré-Bendixson argument. The idea is as follows: SYSTEM (7.3) is equivalent to a nonautonomous system

$$\begin{aligned} \frac{\partial S}{\partial t} &= (S^0 - S)D - f_1(S)u - f_2(S)(z(t) - S - u) \\ \frac{\partial u}{\partial t} &= [f_1(S) - D - \beta(S)]u + \alpha(S)(z(t) - S - u) \end{aligned} \tag{7.4}$$

where $z(t)$ is the solution of $z' = (S^0 - z)D$. Since $z(t) \to S^0$ as $t \to \infty$, SYSTEM (7.4) is asymptotically autonomous, with SYSTEM (7.5) being the limit autonomous system.

$$\begin{aligned} \frac{\partial S}{\partial t} &= F_1(S,u) = (S^0 - S)D - f_1(S)u - f_2(S)(S^0 - S - u) \\ \frac{\partial u}{\partial t} &= F_2(S,u) = [f_1(S) - D - \beta(S)]u + \alpha(S)(S^0 - S - u) \end{aligned} \tag{7.5}$$

SYSTEM (7.5) is analyzed first. The triangular region $\Delta := \{(S,u) \in \mathbb{R}^2_+ \mid S + u \leq S^0\}$ is positively invariant. Equilibrium points are solely $\bar{E}^0 = (S^0, 0)$ or $\{\bar{E}^0, \bar{E}^u\}$ or $\{\bar{E}^0, \bar{E}^*\}$ with $\bar{E}^u = (S^u, S^0 - S^u)$ on the boundary of Δ and $\bar{E}^*$ inside.
Next it can be proven that $\bar{E}^0$ is a saddle whenever a second equilibrium exists. Therefore compute the Jacobian

$$J = \begin{pmatrix} -D - f_1' u^* - f_2'(S^0 - S^* - u^*) + f_2(S^*) & -f_1(S^*) + f_2(S^*) \\ (f_1' - \alpha' - \beta')u^* + \alpha'(S^0 - S^* - u^*) - \alpha(S^*) & f_1(S^*) - \alpha(S^*) - \beta(S^*) - D \end{pmatrix}$$

and evaluate it at $\bar{E}^0$:

$$J|_{\bar{E}^0} = \begin{pmatrix} -D + f_2(S^0) & -f_1(S^0) + f_2(S^0) \\ -\alpha(S^0) & f_1(S^0) - \alpha(S^0) - \beta(S^0) - D \end{pmatrix}$$

In case of $\alpha(S^0) = 0$ the eigenvalues are the entries on the diagonal. Since α is nondecreasing, $\alpha(S^*) = 0$ in this case, so that the same estimate holds as in the case of SYSTEM (7.3), and the second entry on the diagonal is positive.

$$D + \beta(S^0) \leq D + \beta(S^*) = f_1(S^*) < f_1(S^0).$$

In case of $\alpha(S^0) \neq 0$ it follows that $\beta(S^0) = 0$ and the eigenvalues compute to

$$\lambda_{1,2} = -D + \frac{1}{2}(f_1 - f_2 - \alpha) \pm \frac{1}{2}\sqrt{f_1^2 + 2(\alpha f_1 + f_1 f_2 - 3 f_2 \alpha) + \alpha^2 + f_2^2}.$$

If $f_2=0$ these are the eigenvalues already given in [27], namely $\{-D+f_1,-D-\alpha\}$ and it is obvious that the first one is positive. However, it only grows as long as $2f_1-6\alpha+f_2>0$ because the expression under the square root is

$$(f_1+\alpha)^2+f_2(2f_1-6\alpha+f_2) > (f_1+\alpha)^2$$

and the positive eigenvalue only increases when introducing a positive f_2.
The eigenvector of the stable manifold of $\bar{E}^0$ does not intersect the triangular region and the positive invariance guarantees that the ω-limit set of this region is either the other equilibrium or the union of the point and limit cycle(s).
By a Poincaré-Bendixson argument, the case of a limit cycle can be excluded. In short, any limit cycle of a planar system contains an equilibrium point of opposite asymptotic stability properties inside. Because of the positive invariance of the triangular region a limit cycle of SYSTEM (7.5) has to lie around the inner equilibrium E^*. Moreover, any limit cycle, if it exists, has to be stable. This can be shown when evaluating the divergence of the vector field along a periodic solution $\phi(t)=(S(t),u(t))$ of SYSTEM (7.5) with $\phi(0)=\phi(T)$, and $T>0$ as the minimal period. The second equation of this system can be rewritten as $f_1-D-\beta=\dfrac{\partial_t u-\alpha(S^*-S-u)}{u}$, and integration by time is always negative.

$$\begin{aligned}\int_0^T\left(\frac{\partial F_1(\phi(t))}{\partial S}+\frac{\partial F_2(\phi(t))}{\partial u}\right)dt &= -\int_0^T\Big(D-f_2(S(t))\Big)\,dt\\ &\quad -\int_0^T\Big(f_1'(S(t))u(t)+f_2'(S(t))(S^0-S(t)-u(t))\Big)\,dt\\ &\quad -\int_0^T\frac{\alpha(S(t))(S^0-S(t))}{u(t)}\,dt \;+\; \log\frac{u(T)}{u(0)}\\ &< 0\end{aligned}$$

If $\bar{E}^*$ is asymptotically stable, no limit cycle can occur, since at least one unstable cycle has to be inside Δ. To see the asymptotic stability of $\bar{E}^*$ first realize that $\alpha(S^*)=0$. Assuming $\alpha(S^*)\neq 0$ it follows that $\beta(S^*)=0$ and from $F_2(S,u)=0$ it follows $(f_1-D)u=-\alpha(S)(S^0-S-u)$. This leads to a contradiction when solving $F_1(S,u)=0$

$$\begin{aligned}&(S^0-S-u)D+uD-f_1u-f_2(S^0-S-u)=0\\ \Leftrightarrow\quad &-(f_1-D)u=(f_2-D)(S^0-S-u)\end{aligned}$$

since f_1-D cannot be negative and positive. So $f_1=D$ and $\alpha(S^*)=0$.
Knowing that $\alpha(S^*)=0$ (but in fact $\beta(S^*)\neq 0$ and $f_1(S^*)-\beta(S^*)-D=0$), it is easy to verify the stability of $\bar{E}^*$, since $J|_{\bar{E}^*}$ has negative trace and positive determinant.
Now Markus' theorem (see in the appendix THEOREM A.1) can be applied showing immediately that every trajectory of the nonautonomous system with initial value inside Δ asymptotically approaches $\bar{E}^*$. Finally all trajectories of SYSTEM (7.3) approach an equilibrium point E^0, E^u or E^* since it is equivalent to the nonautonomous system as can be seen with the help of the conservation law.

Requirements for Wave Bifurcation

There is no difference in the global behavior of the solution map of a three variables chemostat model with or without a growth rate function $f_2(S)$ as can be seen from the study of the asymptotic behavior of SYSTEM (7.3). But the Jacobian at E^* now has a destabilizing two-dimensional submatrix. Recall that $|A_{13}|$ includes a negative term, namely $\beta' u^*$. Using the computer algebra program *Maple* gave a first hint that there exists a stable equilibrium point E^* with a negative $|A_{13}|$. Since $|A_{12}|$ remains positive for all parameter values, applying REMARK 5.6 identifies the third variable to be the diffusive species. Recall the formal limit (EQUATION (5.4)) but with the nonzero diffusion coefficient in the third variable.

$$\tilde{\Delta}_2(\mu_m, 0, 0, d_3) \;=\; -\mathrm{tr}(A_{12})(d_3{\mu_m}^2)^2 + (|A_{13}| + |A_{23}| + \mathrm{tr}(A_{12})\mathrm{tr}A)d_3{\mu_m}^2 + \Delta_2$$

With the appropriate cyclic changes the requirements for the kinetic system are as follows:

(C4) $-\mathrm{tr}(A_{12}) > 0$

(C5) $-(|A_{13}|+|A_{23}|+\mathrm{tr}(A_{12}))\mathrm{tr}A) > 0$

(C6) $(|A_{13}|+|A_{23}|+\mathrm{tr}(A_{12})\mathrm{tr}A)^2+4\mathrm{tr}(A_{12})\Delta_2 > 0$

Then it is possible that the parabola is negative for some d_3, that is $\tilde{\Delta}_2(d_3{\mu_m}^2) < 0$. Spatial inhomogeneities in the initial conditions now give rise to time-periodic nonconstant solutions such as standing waves. The solution branches for the various spatial wavelengths bifurcate from the stable constant solution for critical diffusion parameters that can be determined by LEMMA 5.2. So the system may have two (or more) stable attractors, namely a constant steady state and a nonconstant time-periodic solution.

Steady State Turing Patterns

The second variable has to be the diffusive species for steady nonconstant solutions as can be seen from EQUATION (5.6) adapted to the case of diffusion in the second variable.

$$-\det\tilde{A}(\mu_m, 0, d_2, 0) \;=\; |A_{13}|d_2{\mu_m}^2 - \det A$$

Again this limit can be negative for some $d_2\mu_m$. In this case the spatial inhomogeneities of the initial conditions give rise to patches where either phase 1 or phase 2 of the cell culture predominates.

Recall the case of a two variables *activator-inhibitor* system, where (c3) guarantees the existence of an activator, but the inhibitor has to diffuse faster. It can be observed that for three variables and in the formal limit with only one nonzero diffusion coefficient, the now two-dimensional submatrix is a destabilizing activator system and the remaining inhibitor equation includes the spatial operator.

7.2 Computational Results

A sustained oscillation in space and time for SYSTEM (7.1) can also be verified numerically. First of all the stable equilibrium point E^* has to be detected. For the following set of parameters

$$S^0 = 1.0,\ D = 0.5,\ m_1 = 5.0,\ m_2 = 0.5,\ a_1 = 1.5,\ a_2 = 0.01,$$
$$K_1 = 20.0,\ K_2 = 33.5,\ s_1 = 0.5,\ s_2 = 0.2,\ \varepsilon_1 = 0.02,\ \varepsilon_2 = 0.04$$

the equilibrium point $(S^*,u^*,v^*) \approx (0.19755, 0.18241, 0.62003)$ satisfies (C1) – (C3) and is therefore an asymptotically stable constant solution. The conditions (C4) – (C6) are also fulfilled for these parameters. With LEMMA 5.2 the maximal wavenumber can be estimated to be either seven or eight. Critical diffusion coefficients for the seventh mode are about $d_{3_{7_l}} = 0.001514$ and $d_{3_{7_r}} = 0.0018998$ and for the eighth mode $d_{3_{8_l}} = 0.001159$ and $d_{3_{8_r}} = 0.001455$. The destabilization of the ninth and tenth mode overlap, since the diffusion coefficient lies in $d_{3_9} \in (0.000917, 0.001149)$ and $d_{3_{10}} \in (0.000742, 0.000931)$, respectively.
The discretized system of ordinary differential equations is solved with the LSODE package, using numerical estimates of Jacobian matrix and the same relative and absolute error tolerances as in the previous computations. Time discretization is done implicitly with a maximal step size of $t = 0.01$. With the above considerations a diffusion coefficient $d_3 = 0.001$ destabilizes the ninth mode but not yet the tenth. To guarantee the spatial step size to be of the appropriate order of magnitude, i.e. $h^2 \sim t$, the space discretization is 300 gridpoints on a unit interval, so $h^2 = {d_3}^{-1}(300)^{-2} \sim 0.01$.
The initial data is taken close to E^* with an inhomogeneous perturbation within the spatial wavelength and an amplitude of approximately 0.01 as a single peak in each equation at the same place but arbitrarily located on the grid. Homogeneous Neumann conditions serve as boundary conditions.
It can be observed that the small initial peak grows to a peak of considerable height before the diffusion broadens it. This maximal amplitude is used for scaling purposes over the whole time scale. The wave pattern travels to the boundary, is reflected and decreases in amplitude. But finally, when the predicted stable pattern is approximately reached, the waves grow again in amplitude. The computed result shows the predicted standing wave pattern of wavenumber 9 (see FIGURE 7.2).
Qualitatively the same attractor results from randomly disturbed initial data having mean value at the constant solution E^*.

Discussion

The modified Monod model of [27] turns out to be very robust against changes that allow for spatially nonuniform perturbations. The local and global solution set cannot be altered in their asymptotic behavior although the transient growth dynamics gains complexity.
The standing wave solution will not be there until the quiescent cells have a growth rate modeled by a positive increasing function $f_2(S)$. Now the two-dimensional submatrix of

the Jacobian consisting of the derivatives of nutrient and of these slow growing cells is destabilizing. Adding a diffusive term to this third equation of cells of phase 2 folds up a periodic nonconstant solution. For the vessel, no flux boundary conditions might be most appropriate, so the initial wave gets reflected at the boundary and a standing wave solution is established.
Numerically the only asymptotically (or orbitally) stable solutions to be found are the constant E^* and this standing wave solution. If the initial data stimulates a wavelength bigger than the predicted one, the smoothening effect of the diffusion is responsible for the constant solution E^* which is asymptotically attractive.
Note here that without diffusion no such periodic solution exists. That means stirring the reactor will always lead to a constant steady solution of either no surviving cells, a pure fast growing cell culture, or a coexistence state.

If the experiment shows sustained spatio-temporal oscillations, the mathematical model should contain a growth rate function smaller than the death rate D for the cells of the second phase. These cells should have the property to diffuse through the medium (gel) in the vessel. The result can be interpreted in the way that the cells do not only change their metabolism but also change their mobility for example by shrinking to a size that allows for diffusion, whereas the fast growing cells stick to their places and are immobile.
If the experiment shows a patchiness, the same mathematical model can be used but here the fast growing cells should have the greater mobility.
To model transient oscillations, there is the need of separating the cells into active and quiescent ones. For sustained oscillations it is now required that the cells of phase 2, which have the smaller growth rate, can diffuse. This is sufficient for a stable standing wave that will disappear again in case the vessel is stirred.

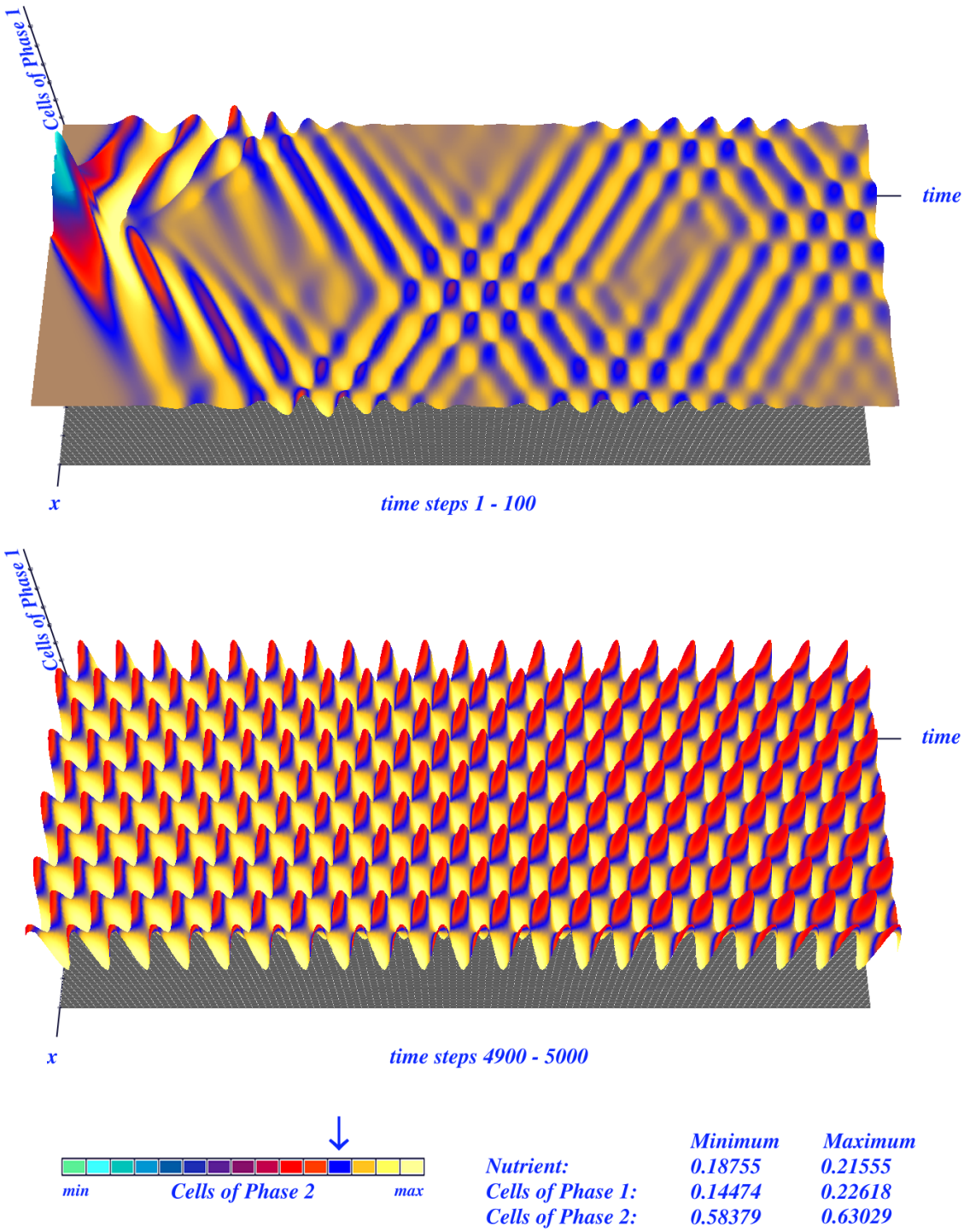

FIG. 7.2: The temporal evolution of a one-dimensional spatially nonuniform initial data (above, time steps 1-100) results in a standing wave pattern (below, time steps 4900-5000). The concentration of slow growing but mobile cells is mapped in color to the profile of fast growing and immobile cells. The value for the constant solution of slow growing cells v^* is marked with dark color (see arrow).

A Theorems

The theorems which are used in the argumentation without being essential to the proofs in the various contexts are listed here. For their proofs see the papers cited below.

A.1 Nonautonomous Systems

For a comparison of the asymptotic behavior of the solutions of a nonautonomous differential system to critical points and periodic solutions of a limiting autonomous system the following definition and theorem are used.

Definition A.1 *Let* $S:\dot{x}_i=f_i(x_i,t)$ *be a real first order nonautonomous ordinary differential system, and let* $S_\infty:\dot{x}_i=f_i(x,t)$ *be an autonomous system for each* $x\in\theta\subset\mathbb{R}^n$ *open.* S *is* asymptotic *to* S_∞ $(S\to S_\infty)$ *if for each compact set* $K\subset\theta$ *and each* $\varepsilon>0$ *there is a* $T=T(K,\varepsilon)>t_0$ *such that* $|f_i(x,t)-f_i(x)|<\varepsilon$ *for all* $i=1,\cdots,n$, *all* $x\in K$ *and all* $t>T$.

Theorem A.1 (Markus) *Let* $S\to S_\infty$ *in* θ *and let* P *be a critical point of* S_∞. *Assume that the variational equation of* S_∞ *based on* P *has characteristic values with negative real parts. Then there is a neighborhood* N *of* P *and a time* T *such that* $\mathrm{S}_+=\mathrm{P}$ *for every solution* $\mathrm{S}(t)$ *of* S *intersecting* N *at a time later than* T.

See the Contributions to the Theory of Nonlinear Oscillations by MARKUS [36].

A.1.1 Perturbation of Planar Homoclinic Orbits

Let $\dot{x}=f(x)$ be a Hamiltonian vector field defined on (a subset of) $\mathbb{R}^2$ and $H(x)$ its Hamilton function. Let $\varepsilon g(x,t,\lambda)$, $\lambda\in\mathbb{R}$ be a small parameterized perturbation that is periodic in t. The following conditions hold for the unperturbed system $(\varepsilon=0)$:

(1) The system possesses a homoclinic orbit $q^0(t)$ to a hyperbolic saddle point.

(2) Let $\Gamma^0=\{q^0(t)|t\in\mathbb{R}\}\cup\{p_0\}$. The interior of Γ^0 is filled with a continuous family of periodic orbits $q^\alpha(t)$, $\alpha\in(-1,0)$. In other words, for $d(x,\Gamma^0):=\inf_{q\in\Gamma^0}|x-q|$ it yields $\lim_{\alpha\to 0}\sup_{t\in\mathbb{R}}d(q^\alpha(t),\Gamma^0)=0$.

(3) Let $h_\alpha=H(q^\alpha(t))$ and T_α be the period of $q^\alpha(t)$. Then T_α is a differentiable function of h_α and $dT_\alpha/dh_\alpha>0$ inside Γ^0.

Lemma A.1 *For* ε *sufficiently small, the perturbed system has a unique hyperbolic periodic orbit* $\gamma_\varepsilon^0(t)=q^0(t)+O(\varepsilon)$. *Correspondingly, the Poincaré map* $P_\varepsilon^{t_0}$ *has a unique hyperbolic saddle point.*

Definition A.2 *The Melnikov function is defined as*

$$M(t_0,\lambda) := \int_{-\infty}^{\infty} f\big(q^0(t-t_0)\big) \wedge g\big(q^0(t-t_0),t,\lambda\big)\ dt$$

for a time as well as parameter dependent perturbation $g(x,t,\lambda)$. If g is not explicitly time dependent, this reduces to

$$M(\lambda) = \int_{-\infty}^{\infty} f\big(q^0(t)\big) \wedge g\big(q^0(t),\lambda\big)\ dt = \int_{-\infty}^{\infty} (f_1 g_2(\lambda) - f_2 g_1(\lambda))\ dt.$$

Theorem A.2 *Consider the parameterized family $\dot{x} = f(x) + \varepsilon g(x,t,\lambda)$, $\lambda \in \mathbb{R}$ with the assumptions above. If the Melnikov function $M(t_0,\lambda)$ has simple zeros independent of ε, then, for ε sufficiently small, the unstable and the stable manifold of the perturbed saddle point $p_\varepsilon^{t_0}$ of Γ, i.e. $W^u(p_\varepsilon^{t_0})$ and $W^s(p_\varepsilon^{t_0})$, intersect transversely. If $M(t_0,\lambda)$ remains away from zero then $W^u(p_\varepsilon^{t_0}) \cap W^s(p_\varepsilon^{t_0}) = \emptyset$. If the Melnikov function is not explicitly time dependent and $M \equiv 0$, then the homoclinic orbit is preserved in the perturbed system.*

For a brief overview of Melnikov Theory see for instance GUCKENHEIMER, HOLMES [19].

A.2 Normal Forms

The idea of normal forms is to transform a system such that it finally has as few nonzero terms as possible. There is a formal way to proceed in successive steps described in the proof of the following theorem. The procedure is by no means unique since the complementary space $\mathcal{G}_k$ can be spanned by different basis vectors.

Theorem A.3 (Poincaré-Birkhoff Normal Form Theorem) *Let $\dot{u} = f(u)$ be a system with*

$$f(0) = 0$$
$$Df(0)u = \mathrm{L}$$

Let $\mathcal{H}_k$ be the space of homogeneous polynomials of degree k with $\mathcal{H}_k = \mathrm{ad}\,\mathrm{L}(\mathcal{H}_k) \oplus \mathcal{G}_k$. Then there exists a polynomial change of coordinates of degree k such that the system $\dot{u} = f(u)$ then has the form

$$\dot{v} = g(v) = g^{(1)}(v) + g^{(2)}(v) + \cdots + g^{(r)}(v) + o(|v|^r)$$

with $\mathrm{L} = g^{(1)}(v)$ and $g^{(k)}(v) \in \mathcal{G}_k$ for $2 \le k \le r$.

For a detailed proof see GOLUBITSKY, STEWART, SCHAEFFER [21], p. 285.

A.3 Bifurcation Theory

Most of the bifurcation problems can to some extend be reduced to a finite dimensional setting by projection methods. So for example the Hopf theorem of SECTION A.3.2 is an extension for the application in the theory of semilinear parabolic operators (see also HENRY [22]).
The idea of bifurcation to steady states or periodic solutions is already contained in the finite dimensional case. It has to deal with the spectrum of the linearization of the right-hand side of a system of differential equations. If such an eigenvalue is a simple real zero this is a necessary condition for a bifurcation to a steady state solution. Depending on the codimension of the problem (that is the number of parameters which are needed to reveal the complete dynamical behavior in a neighborhood of the bifurcation point, see for instance GOLUBITSKY, SCHAEFFER [20]) this can be a limit point, a transient bifurcation, a hysteresis point or a pitch fork, just to mention some of the possibilities which arise for low (especially finite) codimension.
A simple pure imaginary eigenvalue in the linearization of a system of differential equations over the real field occurs together with its complex conjugate. If it crosses the imaginary axis transversally when varying the bifurcation parameter, and if there is no resonance (i.e. no integer multiple of this eigenvalue lies in the spectrum), there is bifucation to a time periodic solution. This is the so called *Hopf bifurcation.*
It can be *subcritical*, which means that the bifurcating periodic solution is unstable, or *supercritical*, that is when the bifurcating solution is stable. This can be decided on a sign condition (see THEOREM A.7).
In the case that the sign condition fails, there is no exchange of asymptotic stability between the constant and the periodic solution. This can be an indicator that there exists a coordinate change such that the Ljapunov Center THEOREM A.4 can be applied.

A.3.1 Bifurcation in Finite Dimensions

Theorem A.4 (Ljapunov Center Theorem) *Let $U \subset \mathbb{R}^{2n}$ be open and $H \in C^k(U,\mathbb{R})$, $k \geq 3$ be a Hamilton function. Then $H' := DH$ is the gradient and $H'' := D^2H$ the Hessian of H, and z_0 is a critical point of H. Let $i\omega$ for $\omega > 0$ be a simple eigenvalue of $JH''(z_0)$ with $J \in \mathcal{L}(\mathbb{R}^n \times \mathbb{R}^n)$ the symplectic normal form, and*

$$\operatorname{spec}(JH''(z_0)) \cap i\omega\mathbb{Z} = \{\pm i\omega\}.$$

Then the Hamiltonian system

$$\dot{z} = JH'(z)$$

possesses a one parametric set of noncritical periodic orbits $\{\gamma(s) | 0 < s < \varepsilon\}$ in a neighborhood of z_0.
That means there are C^{k-2} functions

$$z(\cdot) : (-\varepsilon, \varepsilon) \to U, \quad T(\cdot) : (-\varepsilon, \varepsilon) \to \mathbb{R}_+$$

with

$$z(0) = z_0 \quad \textit{and} \quad T(0) = 2\pi/\omega,$$

such that $\gamma(s) := \gamma(z(s))$ *for* $0 < |s| < \varepsilon$ *is a noncritical* $T(s)$ *periodic orbit through* $z(s) \in U$. *For* $0 < s_1 < s_2$ *the orbits* $\gamma(s_1) \neq \gamma(s_2)$, *and in a neighborhood of* z_0 *every periodic orbit belongs to the family* $\{\gamma(s) | 0 \leq s < \varepsilon\}$.

The following theorem and THEOREM A.7 give concrete formulas for the stability of periodic orbits either bifurcating from a homoclinic orbit or from a steady state.

Theorem A.5 (Stability Formula in Case of a Homoclinic Orbit) *Consider a system of differential equations* $\dot{x} = f(x, \lambda)$; $x \in \mathbb{R}^2$, $\lambda \in \mathbb{R}$, *such that the following conditions hold:*

(1) *When* $\lambda = \lambda_0$, *there is a hyperbolic saddle point* p_0 *and a homoclinic orbit (saddle-loop)* $\gamma_0 \subset W^u(p_0) \cap W^s(p_0)$. *Let* $q \neq p_0$ *be a point on* γ_0.

(2) *Let* M *be a one-dimensional transversal section to* γ_0 *at* q. *Let* $I = [\lambda_0 - \varepsilon, \lambda_0 + \varepsilon]$ *be an interval in parameter space. As* λ *varies, let* $p_\lambda = p(\lambda)$ *be the curve of saddle points with* $p(\lambda_0) = p_0$, *and let* $u(\lambda)$, $s(\lambda)$ *be smooth curves in* $\mathbb{R}^2 \times \mathbb{R}$ *contained in* $(M \times I) \cap W^u(p_\lambda)$ *and* $(M \times I) \cap W^s(p_\lambda)$. *Assume* $(d/d\lambda)(u(\lambda) - s(\lambda)) \neq 0$ *at* $\lambda = \lambda_0$.

(3) *For* $\lambda = \lambda_0$, $\mathrm{tr}[Df(p_0)] < 0$ *(resp.* > 0*)*.

Then there is a family Γ *of stable (resp. unstable, depending on* $\mathrm{sgn}(\mathrm{tr}[Df(p_0)])$*) periodic orbits in* (x, λ)*-space for the systems* $\dot{x} = f(x, \lambda)$, *whose closure contains* $\gamma_0 \times \{\lambda_0\}$. *The periods of these periodic orbits are unbounded as* $\lambda \to \lambda_0$. *There is an* ε *close to 0 such that if* $\lambda \in [\lambda_0, \lambda_0 + \varepsilon]$ *(or* $\lambda \in [\lambda_0 - \varepsilon, \lambda_0]$*), then* $\dot{x} = f(x, \lambda)$ *has exactly one periodic orbit in the family of* Γ.

A.3.2 Hopf Bifurcation in Infinite Dimensions

The most general result on the existence of periodic solutions in infinite dimensions for equations of the form

$$\frac{du}{dt} + Lu + f(\mu, u) = 0$$

is gained by CRANDALL and RABINOWITZ [10]. They work in a real Banach space X with complexification $X_c = X + iX$ and L is the densely defined linear operator on X (and on its complexification X_c). The Banach spaces $X_\alpha \subset X$ with the norms $||\cdot||_\alpha$ are defined by

$$\begin{aligned} X_\alpha &= D((L + rI)^\alpha) \\ ||\cdot||_\alpha &= ||(L + rI)^\alpha x|| \qquad \text{for} \quad x \in X_\alpha, \end{aligned}$$

where $||\cdot||$ is the norm in X and $r > -\mathrm{Re}\lambda$ for all $\lambda \in \mathrm{spec}(L)$ such that the fractional powers $(L + rI)^\alpha$ are defined for $\alpha \geq 0$.

(HL) (i) $-L$ is the infinitesimal generator of a strongly continuous semigroup $T(t)$ on X,

(ii) $T(t)$ is a holomorphic semigroup on X_c,

(iii) $(\lambda I - L)^{-1}$ is compact for λ in the resolvent set of L,

(iv) i is a simple eigenvalue of L,

(v) $ni \notin \mathrm{spec}(L)$ for $n = 0,2,3,\ldots$.

(Hf) There is an $\alpha \in [0,1)$ and a neighborhood Ω of $(0,0)$ in $\mathbb{R} \times X_\alpha$ such that $f \in C^2(\Omega, X)$. Moreover $f(\mu,0) = 0$ and $f_x(0,0) = 0$ if $(\mu,0) \in \Omega$.

(Hβ) $\mathrm{Re}\beta'(0) \neq 0$.

The fraction α is fixed at the value given by (Hf) where $f_x(\mu,x)$ denotes the Frechét derivative of f with respect to x. This is a bounded linear operator from $X_\alpha \to X$ (and a fortiori from $X_1 \to X$). By (HL)(iv) i is an I-simple eigenvalue of L regarded as a mapping of X_{1c} into X. The general definition of K-simple eigenvalues is given below.

Definition A.3 *Let $B(X,Y)$ denote the set of bounded linear maps of real Banach spaces X into Y. Let L, $K \in B(X,Y)$, N denotes the null space and R the range of the respective operators. Then $\mu \in \mathbb{R}$ is a* K-simple *eigenvalue of L if*

(i) $\dim N(L - \mu K) = \mathrm{codim} R(L - \mu K) = 1$ *and,*

(ii) *if* $N(L - \mu K) = \mathrm{span}\{x_0\}$, *then* $Kx_0 \notin R(L - \mu K)$.

This definition is needed here for complex Banach spaces (the complexifications are N_c and R_c) and with $K = I$.
Hence if $x_0 \in N_c(L - iI) \setminus \{0\}$, then there are continuously differentiable functions $x(\mu)$, $\beta(\mu)$ defined for small $|\mu|$ such that

$$(L + f_x(\mu, 0))x(\mu) = \beta(\mu)x(\mu)$$

$$x(0) = x_0, \quad \beta(0) = i.$$

So $\beta(\mu)$ is the unique continuation of the purely imaginary eigenvalue and (Hβ) is the transversality condition of the classical Hopf theorem.
Now $\mathcal{F}$ can be define as a mapping of a subset of $\mathbb{R} \times \mathbb{R} \times C_{2\pi}(\mathbb{R}, X_\alpha)$ into $C_0([0,2\pi], X_\alpha)$

$$\mathcal{F}(\rho, \mu, u)(\tau) := u(\tau) - T(\rho\tau)u(0) + \rho \int_0^t T(\rho(\tau - \xi)) f(\mu, u(\xi)) d\xi$$

and the infinite dimensional version of the Hopf theorem can be stated.

Theorem A.6 (Hopf Bifurcation in Infinite Dimensions) *Let* $(\mathrm{H}L)$, $(\mathrm{H}f)$, *and* $(\mathrm{H}\beta)$ *be satisfied. Then there are positive numbers* ε, η *and continuously differentiable functions* $(\rho,\mu,u):(-\eta,\eta)\to\mathbb{R}\times\mathbb{R}\times C_{2\pi}(\mathbb{R},X_\alpha)$ *with the following properties:*

(a) $\mathcal{F}(\rho(s),\mu(s),u(s))=0$ *for* $|s|<\eta$

(b) $\mu(0)=0$, $u(0)=0$, $\rho(0)=1$, *and* $u(s)\neq 0$ *if* $0<|s|<\eta$

(c) *If* $(\mu_1,u_1)\in\mathbb{R}\times C(\mathbb{R},X_\alpha)$ *is a solution of* $u_t+Lu+f(\mu,u)=0$ *of period* $2\pi\rho_1$, *where* $|\rho_1-1|<\varepsilon$, $|\mu_1|<\varepsilon$, *and* $||u||_\alpha<\varepsilon$, *then there exist numbers* $s\in[0,\eta)$ *and* $\theta\in[0,2\pi)$ *such that* $u_1(\rho_1\tau)=u(s)(\tau+\theta)$ *for* $\tau\in\mathbb{R}$.

Moreover, if $f\in C^{k+1}(\Omega,X_\alpha)$ *or if* f *is real analytic, then the functions* $(\rho(s),\mu(s),u(s))$ *are respectively of class* C^k *or real analytic.*

The Hopf bifurcation theorem can be extended to a version with a concrete stability formula as is given below. In the following N_c denotes the complement of the null space and f comprehends the right-hand side, i.e. the vector field, and not only the nonlinear part without linear components as in the previous setting. Furthermore ρ is the continuation of the purely imaginary eigenvalue, and the bifurcation parameter is called λ.

Theorem A.7 (Stability Formula for the Hopf Bifurcation) *Let* $\Lambda\subset\mathbb{R}$ *open and let* X *be an open subset of some Banach space* E. *The vector field* $f\in C^3(\Lambda\times X,E)$ *has* $f(\,\cdot\,,0)=0$. *For* $\lambda_0\in\Lambda$ *it yields*

(i) $\{\pm i\omega_0\}$ *are simple eigenvalues of* $D_xf(\lambda_0,0)=\tilde{A}$, *where* $\omega_0>0$,

(ii) *there are no eigenvalues of the form* $ik\omega_0$ *for* $k\in\mathbb{Z}\setminus\{\pm 1\}$ *and*

(iii) $D_\lambda\mathrm{Re}\rho(\lambda_0)>0$, *where* $\rho(\lambda)$ *is the unique continuation of the eigenvalue of* $\tilde{A}$ *for* λ *in a neighborhood of the critical* λ_0 *satisfying* $\rho(\lambda_0)=i\omega_0$.

Then there are C^1*-functions* $(x,T,\lambda):(-\varepsilon,\varepsilon)\to X\times\mathbb{R}^+\times\Lambda$ *with the properties that for each* $s\in(0,\varepsilon)$ *there is a noncritical* $T(s)$*-periodic orbit* $\gamma(s):=\gamma(x(s))$ *through* $x(s)$ *solving* $\dot{x}=f(\lambda(s),x)$, $\gamma(s)\neq\gamma(t)$ *for* $0<s<t<\varepsilon$, *and there are no other noncritical periodic orbits of* $\dot{x}=f(\lambda,x)$ *in a neighborhood of* $(0,2\pi/\omega_0,\lambda_0)\in X\times\mathbb{R}^+\times\Lambda$.

If $\mathrm{Re}\Big(\mathrm{spec}(\tilde{A})\setminus\{\pm i\omega_0\}\Big)<0$ *and* $s\dot{\lambda}(s)>0$ *for a parameterization* $|s|>0$ *of the branch of noncritical peridic orbits* $\gamma(s)$, *then the bifurcation is* supercritical *and* $\gamma(s)$ *is orbitally stable.*

If $s\dot{\lambda}(s)<0$ *for* $|s|>0$, *the bifurcation is* subcritical *and the branch of noncritical peridic orbits* $\gamma(s)$ *is orbitally unstable.*

With

$$\mathrm{sgn}\Big(s\dot{\lambda}(s)\Big)\;=\;\mathrm{sgn}\Big(\gamma(s)\Big)\;=\;\mathrm{sgn}\left(-\frac{3\pi}{4\omega^2}\delta\right)$$

it is necessary that $\delta<0$ *for a* supercritical *bifurcation. A* subcritical *bifurcation is equivalent to* $\delta>0$.

The Stability Criterion. *Let* $\varphi(\xi,\eta,\zeta) := f(\lambda_0,\xi,\eta,\zeta)$ *with components*

$$\varphi = \left(\varphi^1, \varphi^2, \varphi^3\right)$$

be the vector field according to the coordinates (ξ,η) *of* N *and* ζ *of* N_c *with* $(\varphi^1,\varphi^2)\in N$ *and* $\varphi^3\in N_c$ *and*

$$N \oplus N_c = ker D\varphi \oplus N_c$$

such that

$$D\varphi|_N = \begin{pmatrix} 0 & -\omega_0 \\ \omega_0 & 0 \end{pmatrix}.$$

The value of δ *can be computed with*

$$\begin{aligned}\delta \;=\; & \omega_0(\varphi^1_{111}+\varphi^1_{122}+\varphi^2_{112}+\varphi^2_{222}) \\ & -\varphi^1_{11}\varphi^1_{12}+\varphi^1_{11}\varphi^2_{11}-\varphi^1_{12}\varphi^1_{22}-\varphi^1_{22}\varphi^2_{22}+\varphi^2_{11}\varphi^2_{12}+\varphi^2_{12}\varphi^2_{22}+\tilde{\delta}\end{aligned}$$

where the subscripts of φ *denote the respective derivatives, namely,* $\varphi_1 := D_1\varphi(0)$, $\varphi_{11} := D_1^2\varphi(0)$ *etc.*

If $\varphi^3_{11}=0$ *then* $\tilde{\delta}=0$, *otherwise*

$$\tilde{\delta} = -\frac{4\omega_0^2}{\pi}\langle \xi', D^2g(0)[\zeta,\xi]\rangle$$

and

$$\zeta := -[Dg(0)|_{N_c}]^{-1}PD^2g(0)[\xi]^2$$

where g *is the Poincaré map* $g(x_0) := x_0 - u(2\pi\omega_0, x_0)$ *for the global solution* $u(\cdot,x_0)$ *of the initial value problem* $\dot{x}=f(x)$, $x(0)=x_0$.

For the stability criterion see Amann [1] or Marsden, McCracken [37].

A.4 Routh-Hurwitz Theory

Finally here is a survey of the formulas used from the theory of matrices.

Theorem A.8 (Routh-Hurwitz) *The number k of roots of the real polynomial $f(z)=a_0z^n+b_0z^{n-1}+a_1z^{n-2}+b_1z^{n-3}+\cdots \quad (a_0\neq 0)$ which lie in the right half plane is given by the formula*

$$k = V\left(a_0, \Delta_1, \frac{\Delta_2}{\Delta_1}, \frac{\Delta_3}{\Delta_2}, \cdots, \frac{\Delta_n}{\Delta_{n-1}}\right)$$

or equivalently

$$k = V(a_0, \Delta_1, \Delta_3, \cdots) + V(1, \Delta_2, \Delta_4, \cdots)$$

with Δ_i, $i=1,\cdots,n$ the successive principal minors of a square matrix H of order n, and V the number of changes of sign of adjacent members in a finite sequence.

The Routh-Hurwitz Criterion. In order for all roots of the real polynomial $f(z)=z^N+\cdots \quad (a_0=1>0)$ to have negative real parts it is necessary and sufficient that the inequalities

$$\Delta_1 > 0, \Delta_2 > 0, \cdots, \Delta_N > 0$$

hold.

Vice versa the Hurwitz determinants can be computed out of the roots of the poynomial with the help of **Orlando's Formula:**

$$\Delta_{N-1} = (-1)^{\frac{N(N-1)}{2}} \prod_{i<k}^{1\ldots N} (\lambda_i + \lambda_k)$$

See the book of GANTMACHER [17] for a comprehensive survey.

B On Specific Systems

B.1 Planar Systems of Van der Pol Type

From the theory of electric circuits is known the following second order ordinary differential equation

$$\varepsilon\ddot{x} + \lambda f'(x)\dot{x} + x + \alpha(t) = 0$$

where via $\alpha(t)$ a periodic forcing can be added to the nonlinear equation known as Van der Pol oscillator (with $\alpha \equiv 0$). Consider λ to be a parameter of the system. Typically f is the integral of a quadratic polynomial such that it is a cubic-like function with humps. For instance, take $f'(x) = x^2 - 1$, such that $f = x^3/3 - x$. Setting $\dot{y} = \varepsilon\ddot{x} + \lambda f'\dot{x}$ yields a system

$$\begin{aligned} \varepsilon\dot{x} &= y - \lambda f(x) \\ \dot{y} &= -(x + \alpha) \end{aligned}$$

with just a single fixed point in zero. Its stability behavior depends on the trace of the linearization that is λ/ε. The first equation is a quasi steady state and $\lambda f(x)$ represents the slow manifold for ε small. Small perturbations lead to trajectories making big excursions which have the shape of a duck. Recent work on such *phantom ducks* was done by Braaksma [4] merely with a polynomial of the form $f'(x) = x^2 - x$ and making use of different time scales.
Independent of ε there occurs a Hopf bifurcation for $\lambda = 0$ and the above system is purely linear. For $\varepsilon = 1$ it already is in normal form and the branch of periodic solutions can be parametrized in a way that $\lambda(s) \equiv 0$. The Hopf bifurcation is neither subcritical nor supercritical and the period of the bifurcating solution grows from 2π to ∞. This resembles the case of System (3.11) although for the Van der Pol oscillator there is no homoclinic orbit that bounds the amplitude.
Now consider the special *Liénard equation* with $f'(\lambda, x) = x^2 - \lambda$

$$\ddot{x} + (x^2 - \lambda)\dot{x} + x = 0.$$

Tranformed to a planar system it has the same linearization in zero as the above system such that a Hopf bifurcation occurs for $\lambda = 0$. It is already in normal form and the stability criterion easily computes to $\delta = 2\pi\varphi^1_{111} = -4\pi$. The bifurcating branch is supercritical. A change in sign of the polynomial f, i.e. $f'(x) = \lambda - x^2$, gives a positive $\delta = 2\pi\varphi^1_{111} = 4\pi$ and the branch is subcritical.

Adding diffusion terms (and appropriate boundary conditions) yields the following system.

Example B.1 (Van der Pol Oscillator with Diffusion)

$$\begin{aligned} \varepsilon\dot{x} &= d_1\Delta x + y - f(\lambda, x) \\ \dot{y} &= d_2\Delta y - x \end{aligned}$$

When the zero solution is stable there is no activator present in this system (conditions (c1) – (c3) cannot be satisfied, diffusion cannot destabilize the constant zero solution). No homoclinic orbit and no saddle point occurs for the kinetic system. The possible limit sets are the constant zero and (a) limit cycle(s).
The wave bifurcation is not applicable since it does in principle not occur for planar systems. The conclusion is that this system cannot be treated with the methods introduced in the present work.

B.2 Fitz-Hugh–Nagumo

This system is considered to be a model for the Hodgkin–Huxley equations describing the physiological phenomenon of signal transmission across nerve axons. The difference to the previous example is that it has multiple steady states.

Example B.2 (Fitz-Hugh–Nagumo) *Let $f(v)$ be a cubic polynomial with negative leading coefficient and three real roots at $0 < v_1 < v_2$. Let δ/γ be small enough that $f(v) - (\delta v)/\gamma$ still has three real roots.*

$$\begin{array}{rcl} \dot{u} &=& \delta v - \gamma u \\ \dot{v} &=& v_{xx} + f(v) - u \end{array} \qquad \text{on } |x| < L \in \mathbb{R},\ t > 0$$

with homogeneous Neumann boundary conditions

$$v_x(\pm L, t) = 0, \quad \text{for } t > 0.$$

Theorem B.1 *Every nonconstant steady state solution of the F-H–N system is unstable.*

Sketch of the Proof (after SMOLLER [44]): A steady state solution satisfies the scalar problem

$$v_{xx} + f(v) - \frac{\delta v}{\gamma} = 0, \quad v_x(\pm L) = 0$$

since u can be eliminated from $v_{xx} + f(v) - u = 0$ by the unique solution of $\delta v - \gamma u = 0$. The linearized operator of the F-H–N system at the nonconstant steady state solution $(\delta v(x)/\gamma, v(x))$ contains an element with positive real part in its spectrum. With this linearized operator $A(\lambda)(\,\cdot\,)$ defined by $A(\lambda)w := w_{xx} + \left(f'(v) - \dfrac{\delta v}{\lambda+\gamma}\right)w$ the eigenvalue problem reads

$$A(\lambda)w = \lambda w, \quad w_x(\pm L) = 0.$$

It has to be shown that there is an eigenfunction $w \not\equiv 0$ with $\lambda > 0$. Let $\mu(\lambda)$ and $\nu(\lambda)$ denote the supremum of the sectrum of $A(\lambda)$ with homogeneous Neumann or Dirichlet boundary conditions, respectively. Let $v(x)$ be a nonconstant solution, then it follows that $v_x(x) \not\equiv 0$. Now v_x serves as eigenfunction of $A(0)$ with homogeneous Dirichlet boundary

condition corresponding to the eigenvalue $\lambda=0$. The Sturm comparison theorem gives $\mu(\lambda)>\nu(\lambda)$ and especially $\mu(0)>\nu(0)\geq 0$. Writing $\mu(\lambda)$ in a variational form

$$\mu(\lambda) = \sup_{w\in W^2,\ ||w||_{L^2}=1} \langle A(\lambda)w, w\rangle < c$$

it can be shown that $\mu(\lambda)$ is bounded from above uniformly in λ. This together with $\mu(\lambda)$ being a continuous function yields the existence of a $\bar{\lambda}>0$ which solves $\mu(\bar{\lambda})=\bar{\lambda}$ such that there is a $\bar{w}\not\equiv 0$ with

$$A(\bar{\lambda})\bar{w} = \mu(\bar{\lambda})\bar{w} = \bar{\lambda}\bar{w}, \quad \bar{w}(\pm L) = 0.$$

□

Note that this argumentation fails in case of a diffusion term in that equation of the system which has no unique solution. Therefore nonconstant steady states could be observed for the models of the present work (see CHAPTER 4).

The F-H−N system is the example most cited for periodic traveling waves. In a limiting case for $\delta=\gamma=0$ the variable u is a quasi steady state. With new coordinates $\xi=x+\theta t$ and then investigating the case of wave velocity $\theta=0$ where $(\ \cdot\ )'$ denotes $d/d\xi$ it reads

$$v' = w, \qquad w' = u - f(v)$$

and with $F(v)$ being the integral of f, it has the Hamiltonian

$$H(v,w) = \frac{w^2}{2} + F(v) - uv.$$

In the case of $u=0$, the system has a homoclinic orbit and for a certain $\tilde{u}$, it has two heteroclinic orbits connecting the outer fixed points. The existence of traveling wave trains is proved by isolating blocks which can be constructed about the limiting orbits for small δ (see CONLEY [9]).

It is tempting to think of the Hamiltonian of CHAPTER 3 to bring on a similar result in the case of the CO-oxidation with hysteresis in the phase transition. In this chapter the Hamiltonian was not received by a transformation to traveling wave coordinates but by neglecting the spatial operator and transforming solely the kinetic system. Without hysteresis one can follow the F-H−N approach (see FLACKE et al. [15]) but this is not possible if a unique quasi steady state for the equation of the phase transition cannot be assumed.
Nevertheless in either case the periodical spatio-temporal solutions can be observed numerically.

B.3 Field–Noyes

These equations serve as a model for the Belousov-Zhabotinsky reaction and have the form:

Example B.3 (Field–Noyes)

$$\begin{aligned} \dot{u} &= \varepsilon_1 \Delta u + \alpha(v - uv + u - \beta u^2) \\ \dot{v} &= \varepsilon_2 \Delta v + \alpha^{-1}(\gamma w - v - uv) \\ \dot{w} &= \varepsilon_3 \Delta w + \delta(u - w) \end{aligned}$$

Their kinetic part is also known as Oregonator and there is a whole chapter in the book of MURRAY [38] describing the relaxation oscillation detected for this system. As is shown in SMOLLER [44], the domain $\sum = \{(u,v,w) : 0 \le u \le a, 0 \le v \le b, 0 \le w \le c\}$ with $a > \max(1, \beta^{-1})$, $c > a$, $b > \gamma c$ is positively invariant for this system with positive parameters.

It will not show a wave bifurcation, as can easily be seen with the following computations. Linearization at the zero solution yields $-\det A = -(\delta + \gamma\delta) < 0$ such that (C3) $-\det A > 0$ is always violated for positive parameters.
The only other positive equilibrium has coordinates

$$u_s = w_s,\ v_s = \frac{\gamma u_s}{1+u_s},\ u_s = \frac{1}{2}\left(\frac{1-\beta-\gamma}{\beta} + \sqrt{\left(\frac{1-\beta-\gamma}{\beta}\right)^2 + 4\frac{1+\gamma}{\beta}}\right)$$

and the Jacobian

$$A|_{(u_s,v_s,w_s)} = \begin{pmatrix} \alpha(1 - v_s - 2\beta u_s) & \alpha(1-u_s) & 0 \\ -\alpha^{-1} v_s & -\alpha^{-1}(1+u_s) & \alpha^{-1}\delta \\ \delta & 0 & -\delta \end{pmatrix}.$$

The entries of this matrix have the following signs

$$\begin{pmatrix} - & \pm & 0 \\ - & - & + \\ + & 0 & - \end{pmatrix}, \text{ thereby } \begin{aligned} |A_{12}| &= -(1 - v_s - 2\beta u_s) + v_s - u_s + 2\beta {u_s}^2 \overset{?}{\lessgtr} 0 \\ |A_{13}| &= -\alpha\delta(1 - v_s - 2\beta u_s) > 0 \\ |A_{23}| &= \alpha^{-1}\delta(1 + u_s) > 0 \end{aligned}$$

Even if (u_s, v_s, w_s) is a stable fixed point, (C5) is always violated for positive parameters as can be seen when plotting the conditions as functions of the parameters.
A short note on where to look: It can be excluded that $\varepsilon_3 \neq 0$ causes a wave bifurcation, because the only indefinite subdeterminant is $|A_{12}|$ with its only negative term $-u_s$. To

fulfill (C5) for either $\varepsilon_1 \neq 0$ or $\varepsilon_2 \neq 0$ this term $-u_s$ has to compensate for all the other positive terms which is only possible for $\beta << 1/2$. But before that, Δ_2 gets negative. No wave bifurcation can be detected in the B-Z reaction. Since this oscillating system serves as a model for homogeneous catalysis, this result is not astonishing. In a fluid phase the mobility of the different chemical reactants will not differ so much, and they should not be regarded as the cause of spatio-temporal patterns.

C Notations

C.1 Chemical Constants and Units

1 atm	=	760 Torr	=	1.01325×10^5 Nm^{-2}		Pressure
1 bar	=	10^5 Pa	=	10^5 Nm^{-2}		
1 Torr	=	133.322 Pa	=	1.33322 mbar		
1 cal	=	4.1868 J				Energy

Tab. C.1: Physical and chemical units after ATKINS [2].

R	=	$8.31441 \frac{\text{J}}{\text{mol} \cdot \text{K}}$	Ideal gas constant
L	=	6.02205×10^{23} mol^{-1}	Avogadro constant

Tab. C.2: Some constants after ATKINS [2].

C.2 Mathematical Abbreviations

$$
\begin{aligned}
d_{im} &:= d_i {\mu_m}^2, \; i = {}_{1,\cdots,N} \\
\mathrm{tr}(A_{i_1 i_2}) &:= a_{i_1 i_1} + a_{i_2 i_2} \\
|A_{i_1 i_2}| &:= a_{i_1 i_1} a_{i_2 i_2} - a_{i_1 i_2} a_{i_2 i_1} \\
\tilde{A}(\mu_m) &:= A - D(\mu_m) = (a_{ij})_{i,j \in \{1,\cdots,N\}} - diag(d_1 {\mu_m}^2, \cdots, d_N {\mu_m}^2) \\
V(a,b) &:= \begin{cases} 0 & \text{for } ab > 0, \\ 1 & \text{for } ab < 0 \end{cases} \\
V(a_1, a_2, \cdots) &:= \sum V(a_i, a_{i+1}) \\
k &:= V(a_0, \Delta_1, \Delta_3, \cdots) + V(1, \Delta_2, \Delta_4, \cdots) \\
k_m &:= V(1, \tilde{\Delta}_1(d\mu_m), \tilde{\Delta}_3(d\mu_m), \cdots) + V(1, \tilde{\Delta}_2(d\mu_m), \tilde{\Delta}_4(d\mu_m), \cdots) \\
\tilde{k} &:= \textstyle\sum_{m=0}^{\infty} k_m
\end{aligned}
$$

List of Figures

List of Tables

Bibliography

[1] H. Amann, Gewöhnliche Differentialgleichungen, de Gruyter, 1983.

[2] P. W. Atkins, Physical Chemistry, Oxford University Press, 2nd edition, 1982.

[3] R. I. Bogdanov, Versal Deformation of a Singular Point of a Vector Field on the Plane in the Case of Zero Eigenvalues, Func. Anal. Appl. **9**, 144 - 145, (1975).

[4] B. Braaksma, Critical Phenomena in Dynamical Systems of Van der Pol Type, D. thesis, Utrecht, 1993.

[5] M. Bär, N. Gottschalk, M. Eiswirth, G. Ertl, Spiral waves in surface reactions: Model calculations, J. Chem. Phys. **100** (2), 1206 - 1214, (1994).

[6] M. Bär, S. Nettesheim, H.-H. Rotermund, M. Eiswirth, G. Ertl, Transition between Fronts and Spiral Waves in a Bistable Surface Reaction, Phys. Rev. Let. **74** (7), 1246 - 1249, (1995).

[7] M. Bär, Ch. Zülicke, M. Eiswirth, G. Ertl, Theoretical modeling of spatiotemporal self-organization in a surface catalyzed reaction exhibiting bistable kinetics, J. Chem. Phys. **96** (11), 8595 - 8604, (1992).

[8] F. Behrendt, O. Deutschmann, B. Ruf, R. Schmidt, J. Warnatz, Simulation of Heterogeneous Reaction Systems, Gas Phase Chemical Reaction Systems, ed.: J. Wolfrum, H.-R. Volpp, R. Rannacher, J. Warnatz, Springer Series in Chemical Physics **61**, Springer, 1996.

[9] C. Conley, On travelling wave solutions of nonlinear diffusion equations, Dynamical Systems, Theory and Applications, Lecture Notes in Physics **38**, Springer-Verlag, 1975.

[10] M. Crandall, P. Rabinowitz, The Hopf Bifurcation Theorem in Infinite Dimensions, Arch. Rational Mech. Anal. **67**, 53 - 72, (1977).

[11] M. Eiswirth, Instability and Oscillations in Chemistry, Suri Kagaku **372**, 59 - 64, (1994).

[12] W. Engel, M. Kordesch, H.-H. Rotermund, S. Kubala, A. von Oertzen, A UHV-compatible photoelectron emission microscope for applications in surface science, Ultramicroscopy **36**, 148, (1991).

[13] M. Eiswirth, P. Möller, K. Wetzl, R. Imbihl, G. Ertl, Mechanisms of spatial self-organization in isothermal kinetic oscillations during the catalytic CO oxidation on Pt single crystal surfaces, J. Chem. Phys. **90**, 510, (1989).

[14] G. Ertl, Oscillatory Kinetics and Spatio-Temporal Self-Organization in Reactions at Solid Surfaces, Science **254**, 1750 - 1755, (1991).

[15] M. Flacke, M. Bär, H. Engel, M. Eiswirth, Traveling waves in the CO oxidation on Pt(110): Theory, J. Chem. Phys. **97** (6), 4555 - 4563, (1992).

[16] H. Fujii, M. Mimura, Y. Nishiura, A Picture of the Global Bifurcation Diagram in Ecological Interacting and Diffusing Systems, Physica 5D, 1 - 42, (1982).

[17] F. R. Gantmacher, Applications of the Theory of Matrices, Interscience Publishers, Inc., New York, 1959.

[18] R. P. H. Gasser, E. B. Smith, A Surface Mobility Parameter for Chemisorption, Chem. Phys. Lett. **1**, 457, (1967).

[19] J. Guckenheimer, P. Holmes, Nonlinear Oscillations, Dynamical Systems, and Bifurcations of Vector Fields, Appl. Math. Sci. **42**, Springer-Verlag, 1983.

[20] M. Golubitsky, D. G. Schaeffer, Singularities and Groups in Bifurcation Theory, Vol. I, Appl. Math. Sci. **51**, Springer-Verlag, 1985.

[21] M. Golubitsky, I. Stewart, D. G. Schaeffer, Singularities and Groups in Bifurcation Theory, Vol. II, Appl. Math. Sci. **69**, Springer-Verlag, 1988.

[22] D. Henry, Geometric Theory of Semilinear Parabolic Equations, Lecture Notes in Mathematics **840**, Springer-Verlag, 1980.

[23] A. C. Hindmarsh, ODEPACK, A Systemized Collection of ODE Solvers, Scientific Computing, North-Holland, Amsterdam, 55 - 64, (1983).

[24] R. Imbihl, M. P. Cox, G. Ertl, H. Müller, W. Brenig, Kinetic oscillations in the catalytic CO oxidation on Pt(100): Theory, J. Chem. Phys. **83** (4), 1578, (1985).

[25] R. Imbihl, The Study of Kinetic Oscillations in the Catalytic CO-Oxidation on Single Crystal Surfaces, Manuscript, (1989).

[26] S. Jakubith, H. H. Rotermund, W. Engel, A. von Oertzen, G. Ertl, Spatiotemporal Concentration Patterns in a Surface Reaction: Propagating and Standing Waves, Rotating Spirals, and Turbulence, Phys. Rev. Let. **65** (24), 3013 - 3016, (1990).

[27] W. Jäger, S. Krömker, B. Tang, Quiescence and Transient Growth Dynamics in Chemostat Models, Math. Biosciences **119**, 225 - 239, (1994).

[28] N. Kopell, L. N. Howard, Plane wave solutions to reaction diffusion equations, Stud. Appl. Math. **12**, 291 - 328, (1973).

[29] K. Krischer, Nichtlineare Dynamik zweier Grenzflächenreaktionen, Dissertation, Freie Universität Berlin, 1990.

[30] K. Krischer, M. Eiswirth, G. Ertl, Oscillatory CO oxidation on Pt(110): Modeling of temporal self-organization, J. Chem. Phys. **96** (12), 9161 - 9172, (1992).

[31] S. Krömker, Analyse eines Differentialgleichungsmodells zur Beschreibung der CO-Oxidation an Platin, Diplomarbeit, Fakultät für Mathematik, Universität Heidelberg, 1990.

[32] S. Krömker, The Graphics Program *cnom2.0*, User Manual, IWR Preprint 95 - 32, Universität Heidelberg, (1995).

[33] N. Lakoš, D. Terman, Stable Steady-State Pattern Formation on Isothermal Catalyst Surfaces, Arch. Rational Mech. Anal. **121**, 377 - 399, (1993).

[34] H. Levine, X. Zou, Catalysis at single-crystal Pt(110) surfaces: Global coupling and standing waves, Phys. Rev. E **48** (1), 50 - 64, (1993).

[35] K. Maginu, Reaction-Diffusion Equation Describing Morphogenesis, I. Waveform Stability of Stationary Wave Solutions in a One Dimensional Model, Math. Biosciences **27**, 17 - 98, (1975).

[36] L. Markus, Asymptotically Autonomous Differential Systems, Contributions to the Theory of Nonlinear Oscillations, Vol. III, ed. Lefschetz, Princeton University Press, 17 - 29, 1956.

[37] J. E. Marsden, M. McCracken, The Hopf Bifurcation and Its Applications, Appl. Math. Sci. **19**, Springer-Verlag, 1976.

[38] J. D. Murray, Mathematical Biology, Biomathematics **19**, Springer-Verlag, 2nd print, 1990.

[39] Y. Nishiura, Global Structure of Bifurcating Solutions of some Reaction-Diffusion Systems, SIAM J. Math. Anal. **13** (4), 555, (1982).

[40] S. Nettesheim, A. v. Oertzen, H.-H. Rotermund, G. Ertl, Reaction diffusion patterns in the catalytic CO-oxidation on Pt(110): Front propagation and spiral waves, J. Chem. Phys. **98** (12), 9977 - 9985, (1993).

[41] A. v. Oertzen, A. Mikhailov, H.-H. Rotermund, G. Ertl, Subsurface oxygen formation on the Pt(110) surface: experiment and mathematical modeling, Surface Science **350**, 259 - 270, (1996).

[42] A. B. Rovinsky, M. Menzinger, Differential Flow Instability in Dynamical Systems without an Unstable (Activator) Subsystem, Phys. Rev. Let. **72** (13), 2017, (1994).

[43] H.-H. ROTERMUND, Raumzeitliche Musterbildung bei Oberflächenreaktionen untersucht von Ultrahochvakuum bis zu Atmosphärendrücken, Talk given at the Physikalisch-Chemisches Institut der Universität Heidelberg, (7.2.1997).

[44] J. SMOLLER, Shock Waves and Reaction-Diffusion Equations, A Series of Comprehensive Studies in Mathematics **258**, Springer-Verlag, 1983.

[45] A. M. TURING, The Chemical Basis of Morphogenesis, Philos. Trans. R. Soc. London, Ser. B **237**, 37 (1952).

[46] A. M. ZHABOTINSKY, M. DOLNIK, I. R. EPSTEIN, Pattern formation arising from wave instability in a simple reaction-diffusion system, J. Chem. Phys. **103** (23), 10306 - 10314 (1995).

Man könnte die Menschen in zwei Klassen abteilen; in solche, die sich auf eine Metapher und 2) in solche, die sich auf eine Formel verstehen. Deren, die sich auf beides verstehen, sind zu wenige, sie machen keine Klasse aus.

H. von Kleist
Kleine Schriften

Thanks to you all

This work is dedicated to my grandmother.

The rest of my family was helpful as well. Bernhard Przywara always encouraged me and finally also discussed some mathematical aspects, although ramification is not bifurcation and braids are not always out of hair.
My brother showed me the first real LEED picture I ever saw (and the last since then in the lab in Mainz). My mother never asked how long it will take till I finish, and my father always asked and then promised to write a letter to me (by hand) when I finish.

And the scientific family now follows in alphabetical order: Markus Eiswirth pushed me through explaining to him my ideas on wave bifurcation on the telephone and via e-mail. Steffen Heinze was always helpful with mathematical advice and encouraged me to continue. My advisor Professor Jäger gave me the freedom for real research in a vivid field of interdisciplinary atmosphere. Markus A. Kirkilionis (among others) shared an office with me and a preference for philosophy and social sciences. Heike Lischke reminded me of modeling the dirty facts and observations and not playing around with abstract but nice and clean models (not to forget the canoe trips she organized). Elke Pietschmann read the manuscript and shared the other sports activities to care for the body behind the mind. Stefan Schnadt had to listen when I was revealing my ideas to him loosely. Angela Stevens is now at Stanford University, expecting me to come over (for a vacation). Edda Turri-Seibert brought a modern spirit to the life at the institute.

And finally thanks to all the people at the *Institut für Angewandte Mathematik* and the *Interdisziplinäres Zentrum für Wissenschaftliches Rechnen* who lived with me through this time.

Curriculum Vitae

	Susanne Krömker
20. April 1964	geboren in Osnabrück als Tochter von Werner Krömker und Sophie Krömker, geborene Heilshorn
Aug 1970	Einschulung in die Diesterweg Grundschule, Osnabrück
Aug 1974	Besuch des Käthe-Kollwitz-Gymnasiums, Osnabrück
Mai 1983	Abitur
Okt 1983	Diplomstudium Mathematik an der Universität Osnabrück, Nebenfach Betriebswirtschaft
Okt 1983 – März 1989	Stipendium der Studienstiftung des deutschen Volkes
Okt 1984	Studienortwechsel an die Ruprecht-Karls-Universität, Heidelberg; Nebenfachwechsel zur Chemie
Dez 1985	Vordiplom
Okt 1987 – Juli 1989	Wissenschaftliche Hilfskraft am Mathematischen Institut; Programmentwicklung zur Visualisierung reaktiver Strömungen
Aug 1990	Diplomarbeit: Analyse eines Differentialgleichungsmodells zur Beschreibung der CO-Oxidation an Platin, Betreuer: Prof. W. Jäger, Dr. B. Fiedler
Apr 1991	Abschluß des Studiums
Mai – Aug 1991	Buchübersetzung aus dem Amerikanischen, Thomas F. Banchoff: Beyond the Third Dimension; Geometry, Computer Graphics, and Higher Dimensions, dt. Titel: Dimensionen, 31. Bd. der Bibliothek Spektrum der Wissenschaft
Okt 1991 – Dez 1992	Wissenschaftliche Mitarbeiterin am Sonderforschungsbereich 123: *Stochastische Mathematische Modelle*
seit Jan 1993	Wissenschaftliche Mitarbeiterin am Sonderforschungsbereich 359: *Reaktive Strömungen, Diffusion und Transport*
Apr 1994 – März 1997	Mitglied des Graduiertenkollegs am Interdisziplinären Zentrum für Wissenschaftliches Rechnen der Universität Heidelberg (IWR): *Modellierung und Wissenschaftliches Rechnen in Mathematik und Naturwissenschaften*
seit Okt 1994	Wissenschaftliche Mitarbeiterin am IWR
	Ich bin ledig und besitze die deutsche Staatsangehörigkeit.